Unclassified

REPORT DOCUMENTATION PAGE		READ INSTRUCTIONS BEFORE COMPLETING FORM
1. REPORT NUMBER CONTRACT REPORT ARBRL-CR-00364	2. GOVT ACCESSION NO.	3. RECIPIENT'S CATALOG NUMBER
4. TITLE (and Subtitle) EFFECTS OF TERRAIN ON BLAST PREDICTION METHODS AND PREDICTIONS		5. TYPE OF REPORT & PERIOD COVERED. Final
		6. PERFORMING ORG. REPORT NUMBER SSI 7636-1
7. AUTHOR(s) Kenneth Kaplan		8. CONTRACT OR GRANT NUMBER(s) DAAD05-77-C-0721
9. PERFORMING ORGANIZATION NAME AND ADDRESS Scientific Service, Inc. 1536 Maple Street Redwood City, CA 94063		10. PROGRAM ELEMENT, PROJECT, TASK AREA & WORK UNIT NUMBERS 1L162118AH75
11. CONTROLLING OFFICE NAME AND ADDRESS. US Army Armament Research & Development Command US Army Ballistic Research Laboratory Aberdeen Proving Ground, MD 21005		12. REPORT DATE JANUARY 1978
		13. NUMBER OF PAGES . 105
14. MONITORING AGENCY NAME & ADDRESS(if different from Controlling Office). US Army Harry Diamond Laboratories 2800 Powder Mill Road Adelphi, Maryland 20783		15. SECURITY CLASS. (of this report) Unclassified
		15a. DECLASSIFICATION/DOWNGRADING SCHEDULE

16. DISTRIBUTION STATEMENT (of this Report)

Approved for public release; distribution unlimited.

17. DISTRIBUTION STATEMENT (of the abstract entered in Block 20, if different from Report)

18. SUPPLEMENTARY NOTES

19. KEY WORDS (Continue on reverse side if necessary and identify by block number)

Blast Waves   Small Charges
Diffraction   Terrain Effects
Non-Ideal Blast
Reflection

20. ABSTRACT (Continue on reverse side if necessary and identify by block number)
The design of a small charge experiment based on real terrain is given.
The model simulates a 125 kt weapon burst at a height of 300m over the
prototype terrain. Predictions are shown for the effects of the terrain on
the blast wave profile as a function of rising and falling slopes.

DD FORM 1473 EDITION OF 1 NOV 65 IS OBSOLETE   Unclassified

SUMMARY

BRL has undertaken a program to investigate the adequacy of methods currently available for predicting the effects of topographic features on the blast wave from nuclear weapons. As part of that program, under Contract No. DDAD05-77-C-0721, Scientific Service, Inc. (SSI) was requested to aid in the design of a model based on real terrain, and to make predictions of the effects of this model terrain on blast waves generated by 454 gm high explosive (HE) charges. The size of the HE charges, and their height of burst over the model (0.6 m) were chosen to simulate the burst of a 125 kt weapon at a height of 300 m over prototype terrain.

The work undertaken by SSI included an extensive review of the more than 15 years of research work on which the current prediction methods are based. This review, and the subsequent application of currently available prediction techniques, led to the following conclusions:

● There are unresolved differences between two techniques for predicting shock front overpressures as affected by terrain, both of which at one time or another had been recommended for field use.
● Certain terrain features can generate transients of very short duration which place severe requirements on the time response of the systems for measuring the blast pulses from small HE charges. (These transients can be important in full-scale situations.)
● No techniques were available for predicting the effects of terrain on pressure behind the shock front in complex terrain. A new method was devised to do this.
● In certain situations, maximum pressures can occur behind the front of the blast wave, and these can differ substantially from shock front pressures, which are usually thought to be maximum.
● Errors in the current prediction curves were found and corrected. Because of the severe requirements placed on the pressure recording systems, the model study may not answer all unresolved questions.

TABLE OF CONTENTS

5

TABLE OF CONTENTS

LIST OF ILLUSTRATIONS

LIST OF ILLUSTRATIONS

LIST OF TABLES

I. INTRODUCTION

The characteristics of a blast wave propagating along the ground surface change when it encounters a topographic feature: pressures in the pulse generally increase when the wave encounters a rising slope or proceeds down the axis of a valley with parallel or converging sides; pressures generally decrease when the wave encounters a falling slope. Under certain conditions, these changes in pressure can be significant.

Techniques were developed some years ago for predicting these terrain-related changes, and a few tests confirming their accuracy were conducted. Recently, however, questions arose about the adequacy of the techniques, that is, whether they could deal with the practical problems that might be encountered in the field.

For this reason, BRL has undertaken a program aimed at evaluating the adequacy of currently available techniques. The basic plan for this evaluation is quite straightforward. Predictions would first be made of the characteristics of blast waves from 454 gm charges exploded over a small scale model containing topographic features resembling those of real terrain. (Burst locations and heights would be based on a prototype full-scale situation involving weapon yields of 125 kt and burst heights of 300 m.) Tests would then be conducted, and the experimental results would be compared with the predictions. Both predictions and experimental measurements would be restricted to blast overpressures.

As part of this program, BRL awarded Contract DAAD05-77-C-0721 to Scientific Service, Inc. (SSI) to: design the model; select locations for the pressure transducers in the model; make recommendations about instrumentation; and, finally, to make predictions of complete pressure-time histories for the burst conditions and transducer locations selected. This report summarizes these activities. It describes the techniques now available to make predictions of blast wave pressure changes caused by terrain features; discusses the reasons for choosing a particular model and measuring station layout; and applies the prediction techniques to the particular situtations to be tested.

II. PREDICTION METHODS

A. Background

Methods currently available for predicting the effects of terrain on air blast stem from programs, begun in the early 1950's and extending for some 15 years, involving theoretical analyses, and experiments with nuclear weapons, shock tubes and small high explosive charges.

The program was initiated after some terrain effects were noted during early weapons tests (Ref. 1) and experiments using simple (constant slope)

11

terrain models and small high explosive charges, were conducted to investigate the magnitude of the effects (Refs. 2, 3, 4). The information from these experiments was used to establish methods for predicting changes in overpressure at and behind the front of shock waves as a function of incident overpressure, slope angle (the angle of steepest ascent), and azimuth angle (the angle between the direction of shock propagation and a line drawn perpendicular to the slope contours).

These methods were then used to make predictions of effect in two complex terrain models (Ref. 5) and in real terrain (Ref. 6). There was close correlation between measured and predicted results in the terrain models. On the full scale test on real terrain, rising slope terrain effects were masked by the presence of precurser phenomena, in which interaction between the thermal pulse from the burst and the ground surface caused the blast wave to develop an irregular configuration generally characterized by a rounded front and by higher than normal dynamic pressures. On those terrain features (mostly falling slopes) which did not see the thermal pulse, predictions compared well with measurements (Ref. 7).

Subsequent to the full-scale test, theoretical work was undertaken to develop techniques for predicting terrain effects on dynamic pressure (Refs. 8, 9). As a by-product of this work, an analytic approach to predicting shock front overpressure (Ref. 10) was found to agree remarkably well with the results of an earlier extensive series of shock tube measurements (Ref. 11). Because of its sound theoretical basis and good agreement with measurement, a prediction technique based on this approach supplanted the earlier one based on measurements from tests with small charges. Generally the two techniques yield essentially the same results at higher incident overpressures, but at lower incident overpressures the analytic technique predicts higher pressures on rising slopes, and lower pressures on falling slopes than does the technique based on small-charge tests.

The special problem of channeling -- in which a shock wave propagates along the axis of a valley with parallel or converging sides -- was then studied both theoretically and experimentally with charges weighing 110 gm, and a method for predicting channeling effects was developed (Ref 12). Finally, methods for dealing with a variety of real terrain features were developed (Ref. 13), and now form the basis for the techniques suggested for general use (Ref 14).

B. General Considerations

When a blast wave propagating over the ground surface encounters a negative or falling slope, it undergoes a phenomenon known as diffraction.* The wave

---

* In general discussions of gas dynamics, the term "diffraction" is most frequently used to refer to effects of any slope change, negative or positive. Less confusion results if the term is used to describe effects of negative slope changes only, and the term "reflection" used to describe effects of positive slope changes.

expands to stay in contact with the slope, becomes curved, and pressures at and behind the shock front decrease. A typical shock pattern after diffraction is sketched in Fig. 1A. If the blast wave encounters a positive or rising slope, it undergoes reflection*, which can be of two types. A steep slope causes "regular reflection" (also known as "two-shock" reflection), in which a single reflected shock forms behind the incident shock as shown in Fig. 1B. A shallower slope causes "Mach reflection" in which a third shock, the Mach stem, forms between the ground surface and the conjunction of incident and reflected shocks producing a pattern like that of Fig. 1C. The demarcation between conditions that cause regular Mach reflection is not sharp; indeed, there are certain conditions under which both types of reflection can occur. In either case, however, pressures in the shock wave at the ground surfaces are greater than they are in the incident shock wave.

When a blast wave propagates down the axis of a valley with either parallel or converging sides, (that is, undergoes channeling) it is confined by the valley walls and pressures within the wave become greater than they would be if it were propagating over flat terrain.

The changes a wave undergoes when it encounters a slope change are dependent on the strength of the shock (i.e., overpressure behind the shock front relative to ambient pressure ahead of the front), and the angle of the slope change or slope angle.* This angle would be the angle θ_S in Fig. 1, if the direction of propagation of the shock in the three sketches of Fig. 1 were normal to the slope contours. In the general case, where the direction of propagation is not normal to the slope contours, an "effective slope angle" θ is used, defined as

$$\sin \theta = (\sin \theta_S) (\cos \phi) \tag{1a}$$

where ϕ is the angle between the direction of shock propagation and the normal to the slope contours. The angle ϕ is shown in the inset to Fig. 2, a plot relating θ, θ_S, and ϕ.

In the following, prediction graphs for various types of interaction are given. The most common shock-terrain interactions are those involving Mach reflection and diffraction. These are discussed first, and are followed by more limited discussions of regular reflection and channeling. The section closes with material describing how the prediction graphs are to be used, that is, how to make predictions of topographic effects.

C. Prediction Graphs

   1. Mach Reflection and Diffraction. Methods in current use for predicting

---

* Alternatively, the angle between a normal to the shock front and a normal to the slope contours, termed the "angle of incidence" is frequently used when discussing shock waves encountering slopes. This angle equals 90° minus the slope angle. For discussing topographic effects, the slope angle is more convenient to use since it can be derived directly from topographic maps.

Incident Wave →

θ s

A. Falling Slope - - Diffraction

Incident Wave →

Reflected
Wave

Rarefaction

θ s

B. Rising Slope - - Regular Reflection

Incident
Shock →

Bow
Shock

Mach Stem

Slip
Stream

θ s

C. Rising Slope - - Mach Reflection
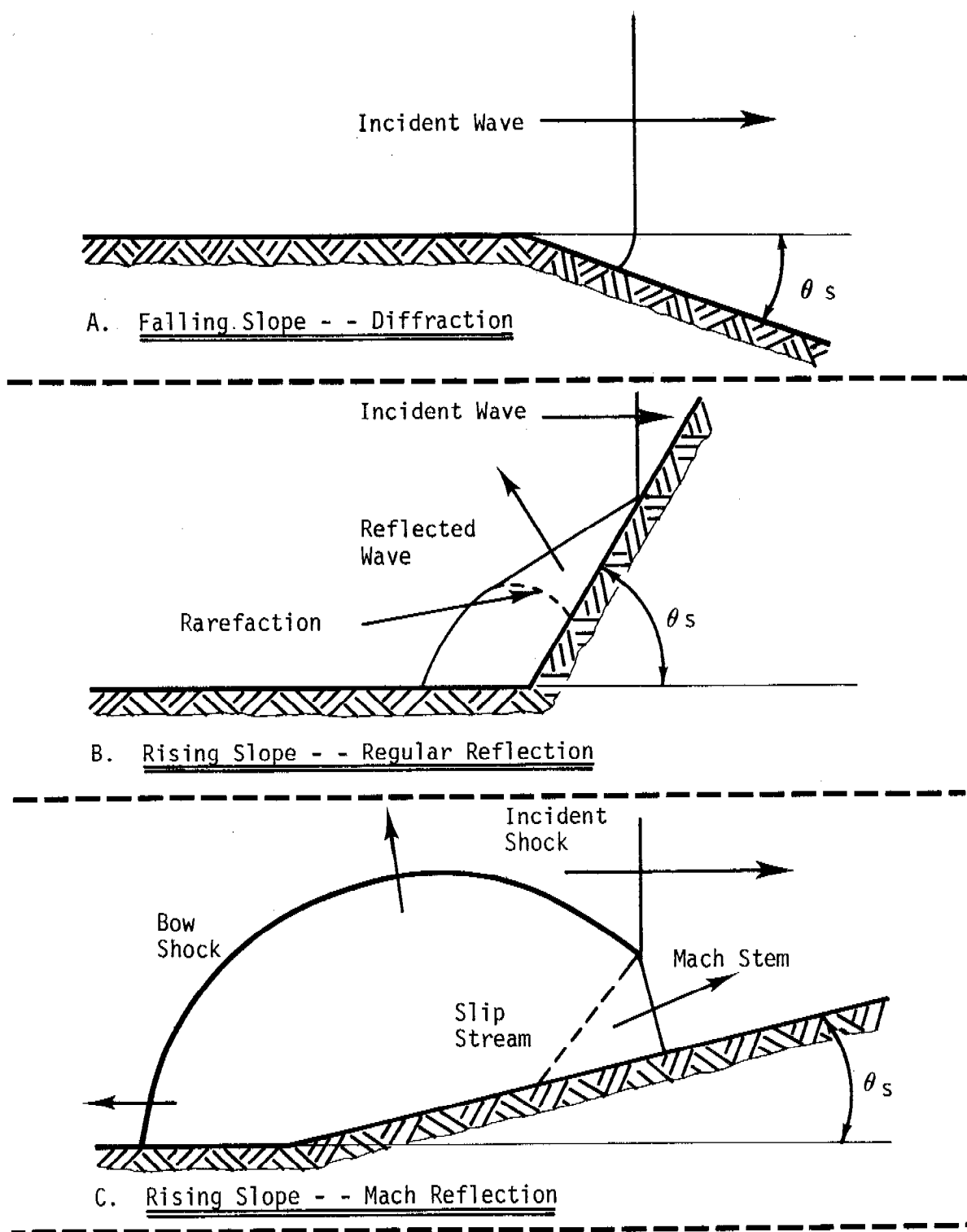
Fig. 1. Changes in Shock Wave Patterns Caused by Changes in Terrain.
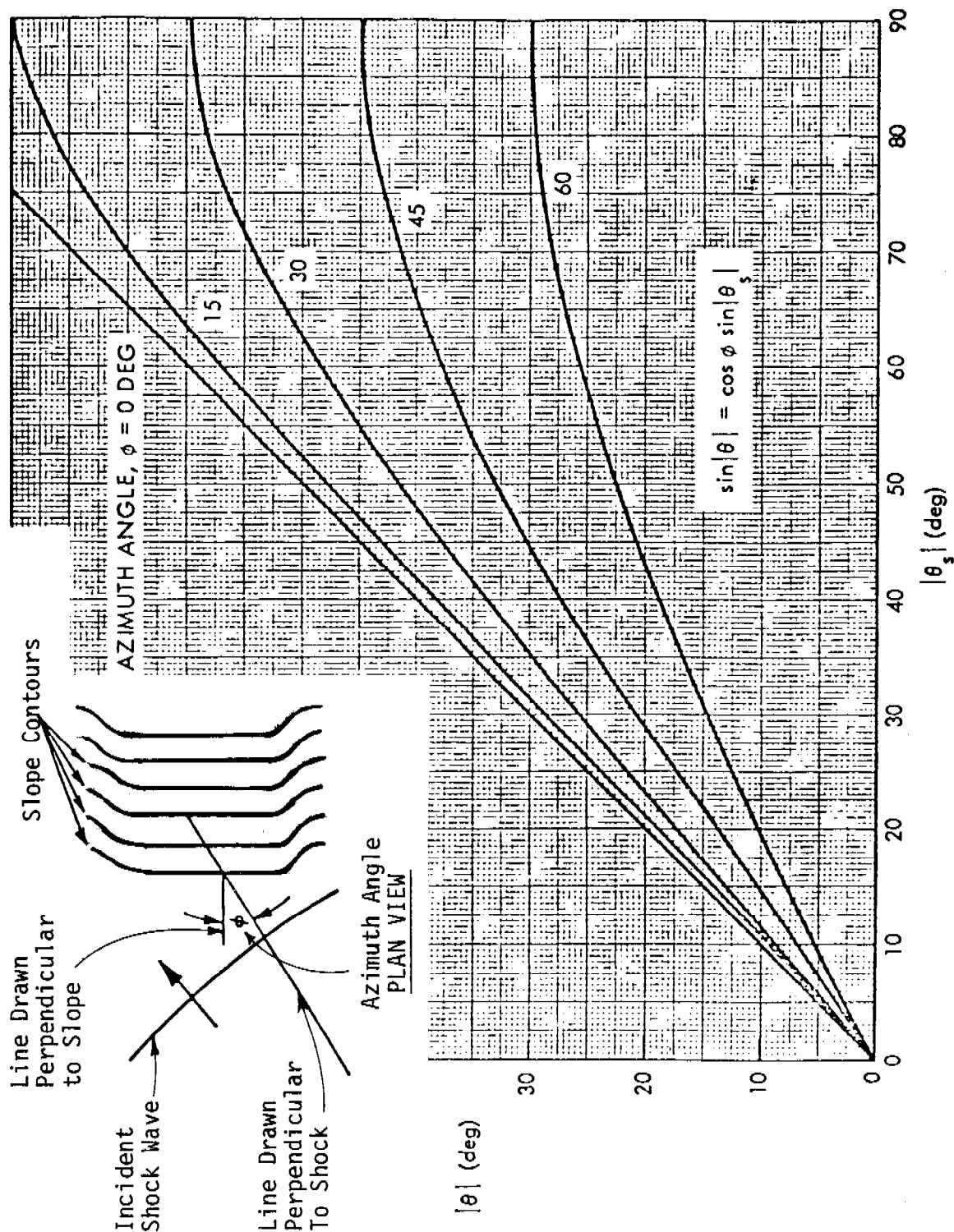
Fig. 2. Effective Slope Angle θ as a Function of Slope Angle θ_s for Various Azimuth Angles φ.

15

the effects of Mach reflection and diffraction are based on an approximate theory developed by Whitham (Ref. 10). In that theory it is assumed that the paths of air particles remain perpendicular to the shock wave even when it is being distorted by reflection or refraction. While the Whitham theory is thus only approximate, the excellent agreement between its predictions of shock strengths and White's measurements of shock strength in a shock tube (Ref. 11), shown in Fig. 3, indicate that the theory has wide applicability.

The theory involves a function w defined by

$$w = \int_{1}^{M} \left\{ \frac{2}{(M^2 - 1)K} \right\}^{1/2} dM \qquad (2)$$

where   M = the Mach number of the shock
        = the shock propagation velocity/speed of sound

$$K = 2\left\{ \left[1 + \left(\frac{2}{\gamma + 1} \right) \left(\frac{1 - \mu^2}{\mu} \right) \right] \left[2\mu + 1 + M^{-2} \right] \right\}^{-1}$$

$$\mu = \frac{(\gamma - 1) M^2 + 2}{2\gamma M^2 - (\gamma - 1)}$$

and γ = the ratio of specific heats of a gas at constant pressure and volume. For air, $\gamma = 1.4$

The Whitham function w was integrated by numerical methods especially for this program and is shown in Fig. 4, along with the Mach number M, both as functions of shock wave pressure.* The change in shock front pressure caused by a change in slope angle θ is derived by finding the value of w for a particular value of incident shock pressure p_i from the graph of Fig. 4; adding θ (in radians) to w; then using Fig. 4 again to find a value of pressure corresponding to the value of $w + \theta$. Note that θ may be either positive or negative depending on whether the shock wave encounters a rising or a falling slope.

Curves more convenient than those of Fig. 4 for anyone making predictions of the effects of topography, are shown in Figs. 5 and 6. These curves directly relate overpressure at the shock front (also called "zero-time" overpressure) on a terrain

_____

* In this report, the term "pressure" when referring to a shock wave will be used interchangeably with the term "overpressure", that is, the pressure behind a shock front in excess of ambient pressure ahead of the front. Thus, the "pressure" of a weak shock wave approaches zero.

16
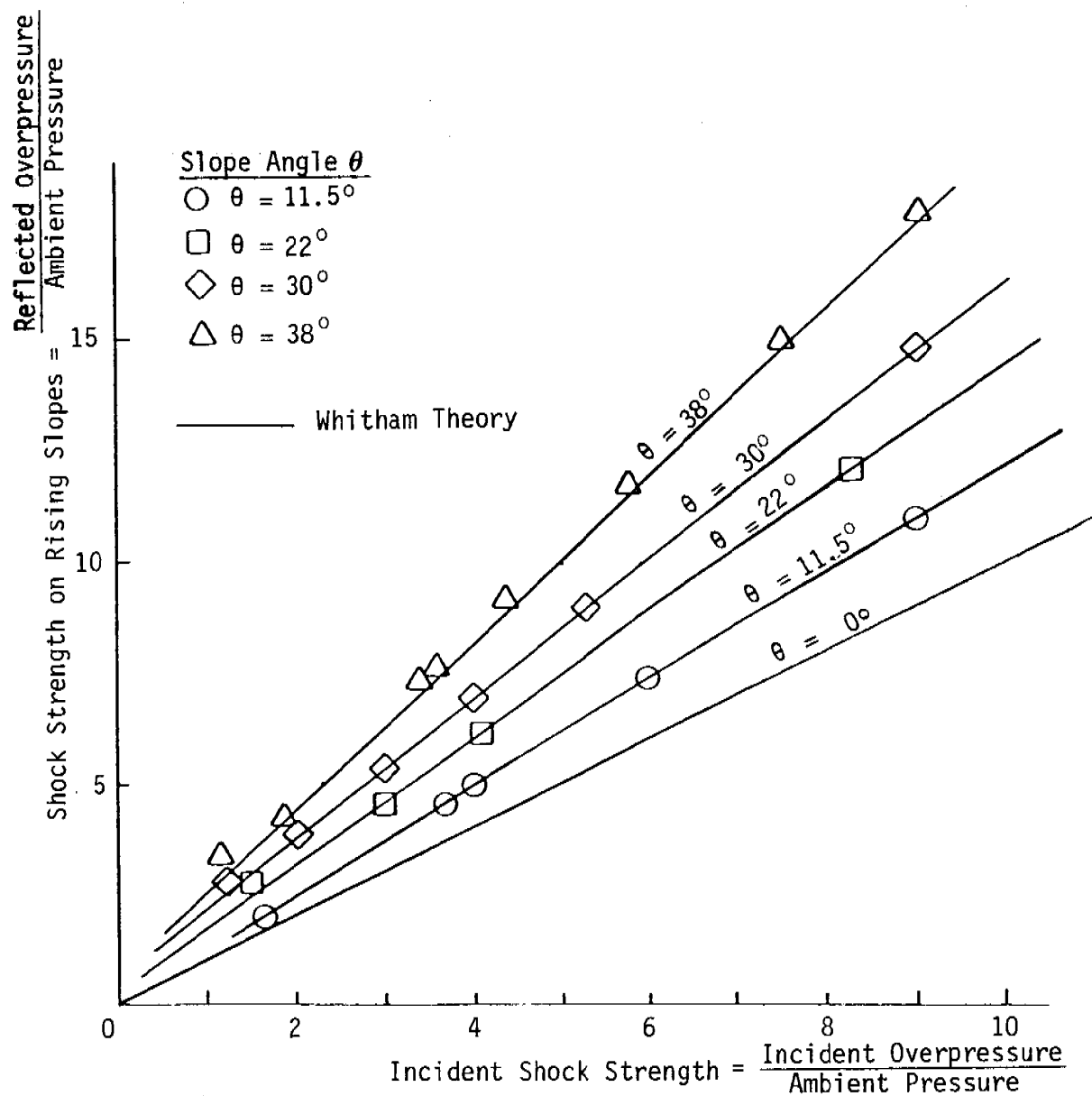
Fig. 3. Comparison of Predictions of Shock Strengths on Rising Slopes from Whitham's Theory with White's Shock Tube Measurements.

17
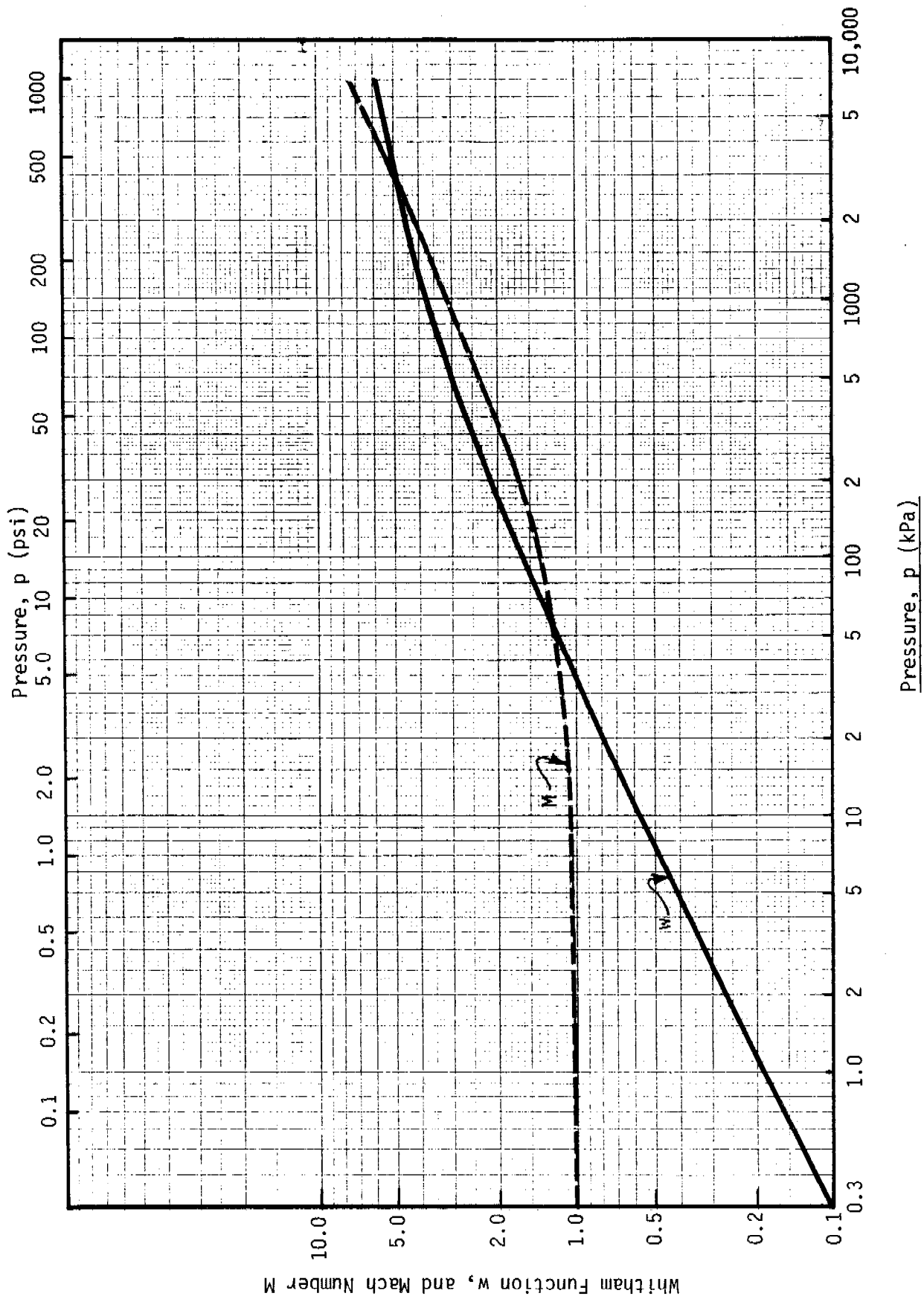
Fig. 4. Whitham Function w (Eq 2) and Mach Number M vs Shock Wave Overpressure.

18

Fig. 5. Overpressure at the Shock Front on a Rising Slope (Reflected Overpressure) vs Peak Incident Overpressure for Shock Waves Undergoing Mach Reflection. From Whitham Theory.

Note: Numbers in parenthesis identify extreme (limit) slope angles along the "Limit for Mach Reflection" line. Other numbers on the figure identify the slope angles to which each curve applies.

Fig. 6. Overpressure at the Shock Front on a <u>Falling Slope</u> (Diffracted Overpressure) vs Peak Incident Overpressure. From Whitham Theory.

Note: Numbers on the figure identify the slope angles to which each curve applies.

feature to peak incident overpressure for various slope angles.*

Note on Fig. 5, the line labelled "Limit for Mach Reflection". Generally, for a given incident overpressure if the slope angle is greater than the slope angle values on the line, regular (two-shock) reflection would occur.

The prediction curves based on experiments with small HE charges which the Whitham curves supplanted are shown in Figs. 7 and 8. The Whitham theory curves and the small charge curves are in generally good agreement at incident pressure levels greater than 70 kPa with rising slopes, and about 150 kPa with falling slopes. With lower incident pressure levels, the Whitham curves yield higher values of pressure on rising slopes, and lower values on falling slopes.

The small charge studies showed that peak overpressure did not always occur at the shock front on a rising slope. This had also been observed in White's earlier shock tube work and led to the generation of curves for predicting changes in pressure behind the shock front. Prediction curves developed for both rising and falling slope angles of 10, 20, and 30 deg. are shown in Figs. 9 and 10.** Note that the ordinate for these curves is "pressure ratio" (pressure on a slope divided by incident pressure) not reflected pressure itself as in Figs. 5 through 8.

The abscissas of these curves are values of the ratio t/L, where t is time after passage of the shock front over a point of measurement, and L is the distance of that point from the location upstream at which the slope changed. The units (ms/s or s/km) indicate that a shock wave on a slope follows the "self similar principle", that is, it grows similar to itself in time from the point of slope change. As an illustration of the principle, the pressure ratio in a shock wave on a slope at a time 0.1 msec after its passage over a point 1 m from the start of the slope (t/L = 0.1 ms/m) will be the same as the pressure ratio 0.5 msec after passage of the same shock wave over a point 5 m from the start of the slope (t/L = 0.5/5 = 0.1 ms/m). The principle, which holds strictly for two dimensional shock waves with constant pressure behind the shock front, was also shown to hold approximately for three dimensional blast waves with decreasing pressures behind the front (Ref. 3).

Figs. 9 and 10 show directly what the pressure pattern of a two dimensional, constant pressure (flat-topped) shock wave would look like as a function of time

---

* These are similar to the curves given in Ref. 14 with some corrections and additions. The rising slope (reflected pressure) curves, and the "Limit for Mach Reflection" line, required correction at incident overpressure values of less than about 20 kPa; the falling slope (diffracted pressure) curves required correction over much of their range. In addition, for purposes of this program, the falling slope curves have been extended to diffracted pressure values less than 7 kPa.

** The curves of Figs. 9 and 10 were derived for equal increments of pressure in psi rather than kPa. Limits on both time and funds on this project did not permit rederivation of the curves for equal pressure increments in kPa.
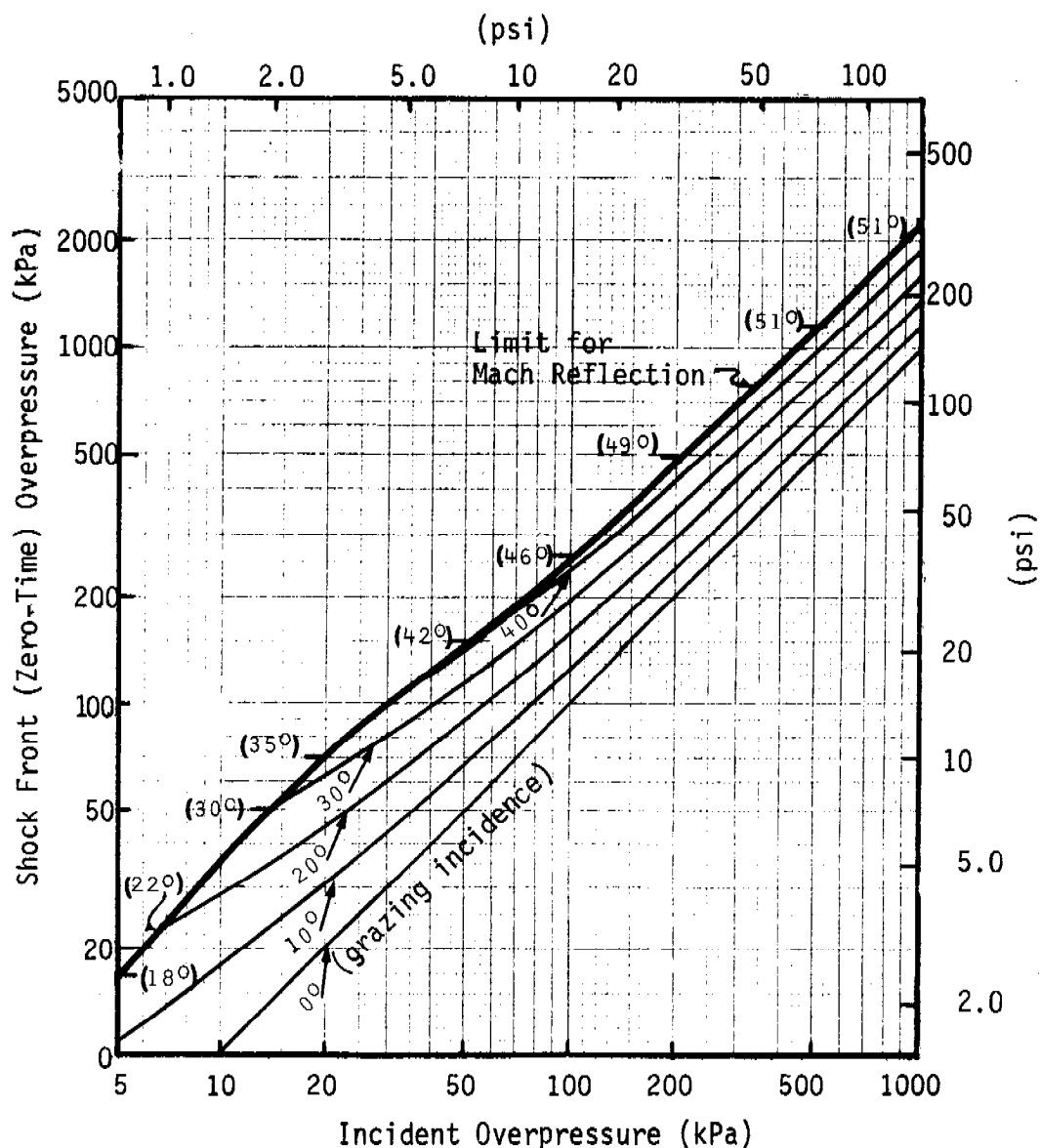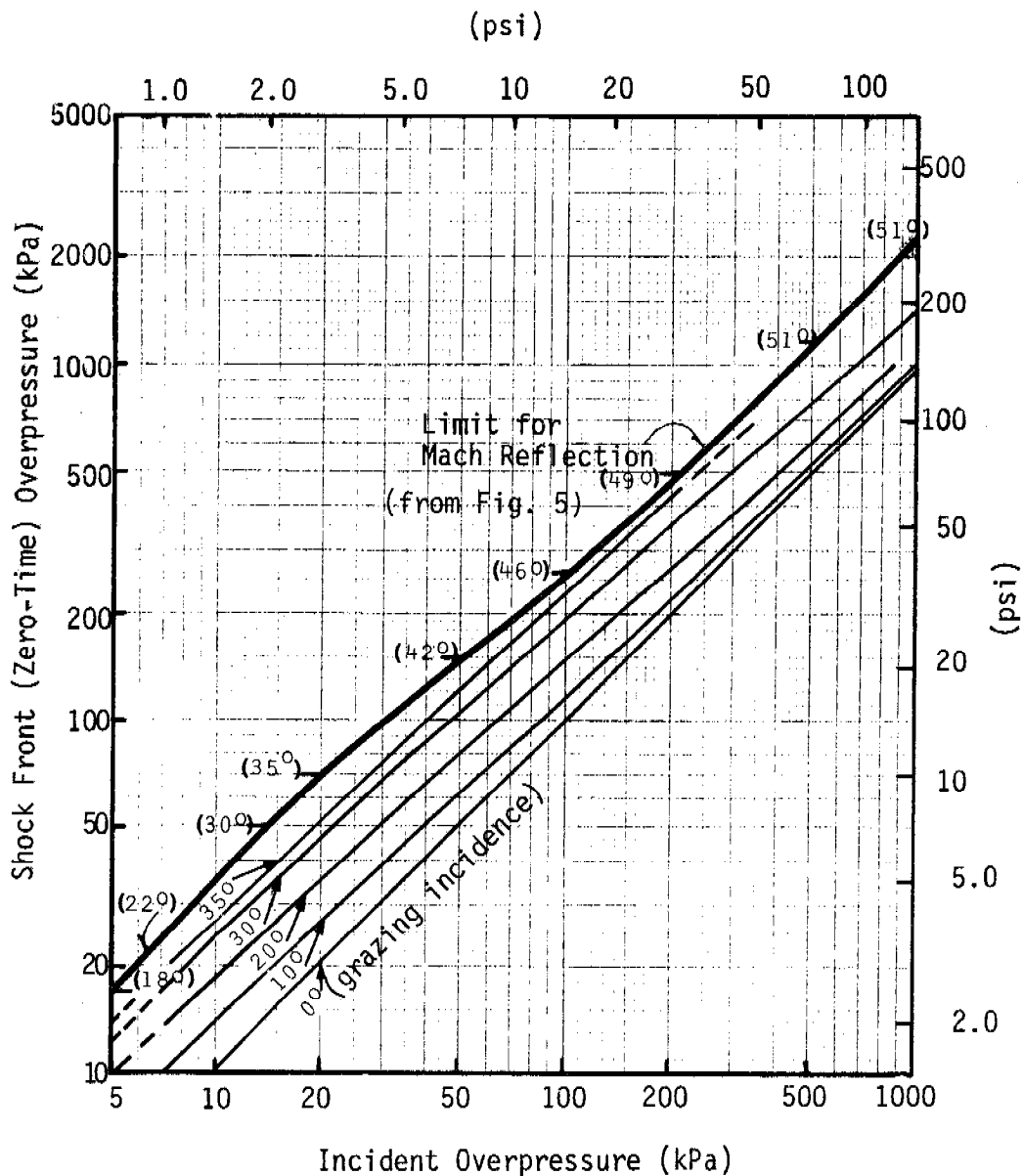
Fig. 7. Overpressure at the Shock Front on a Rising Slope (Reflected Overpressure) vs Peak Incident Overpressure for Shock Waves Undergoing Mach Reflection. From Small Charge Studies.

Note: Numbers in parenthesis identify extreme (limit) slope angles along the "Limit for Mach Reflection" line. Other numbers on the figure identify the slope angles to which each curve applies.
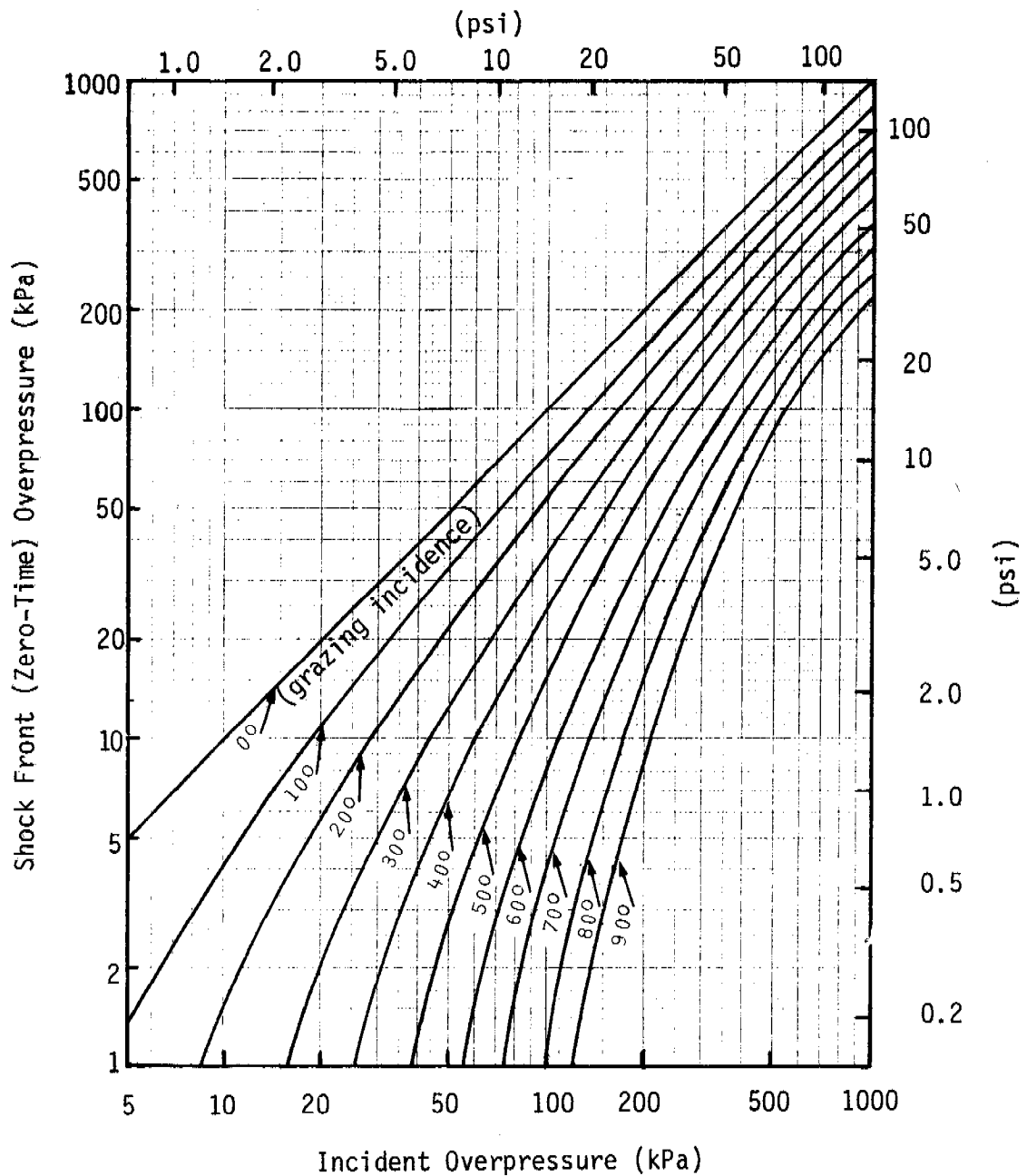
Fig. 8. Overpressure at the Shock Front and Falling Slope (Diffracted Over-pressure) vs Peak Incident Overpressure. From Small Charge Studies.

Note: Numbers on the Figure identify the slope angles to which each curve applies.
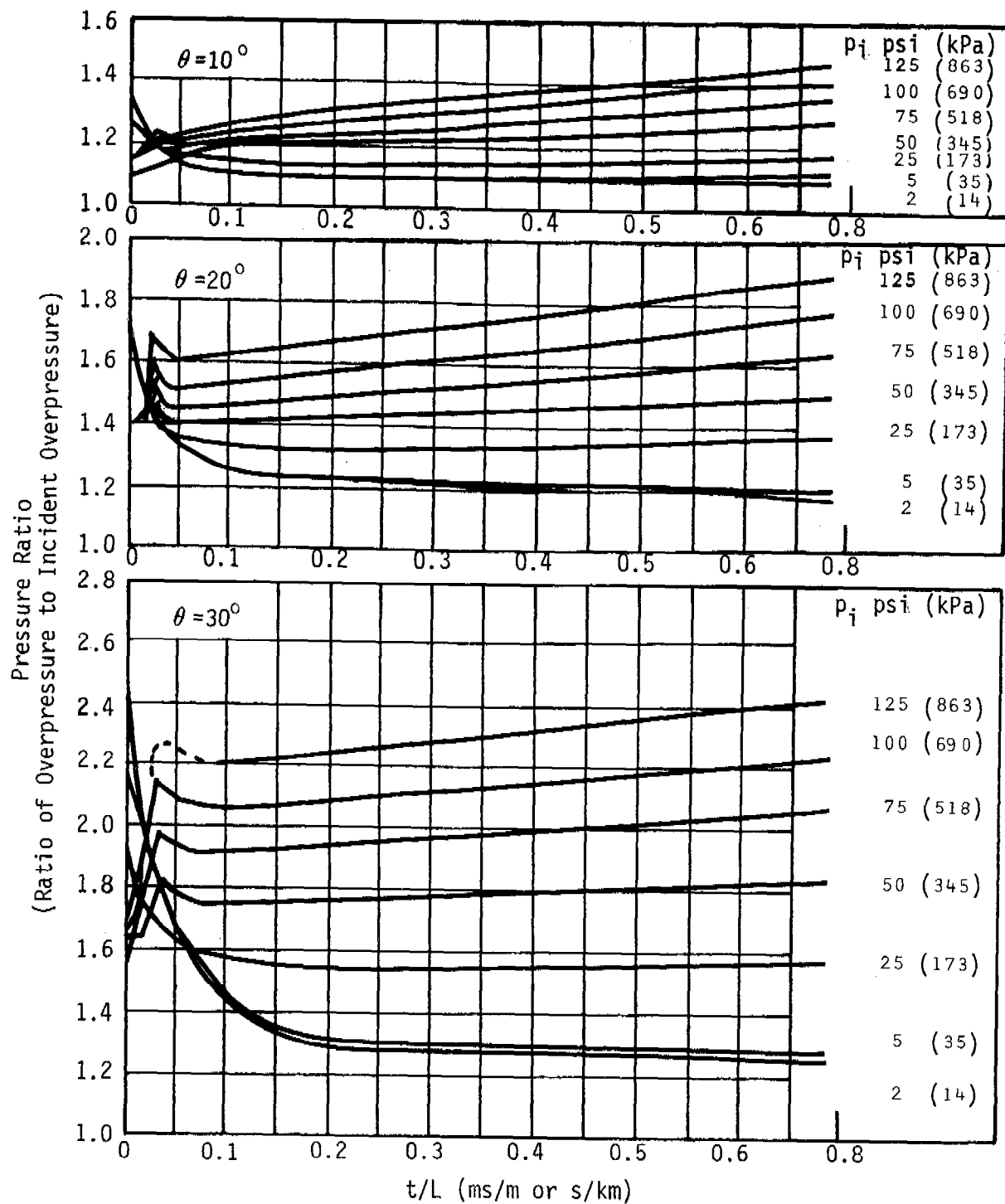
Fig. 9. Rising Slope Pressure Ratios as Functions of t/L for Various Incident Peak Pressures p_i, and for Slope Angles θ of 10, 20, and 30 Degrees.
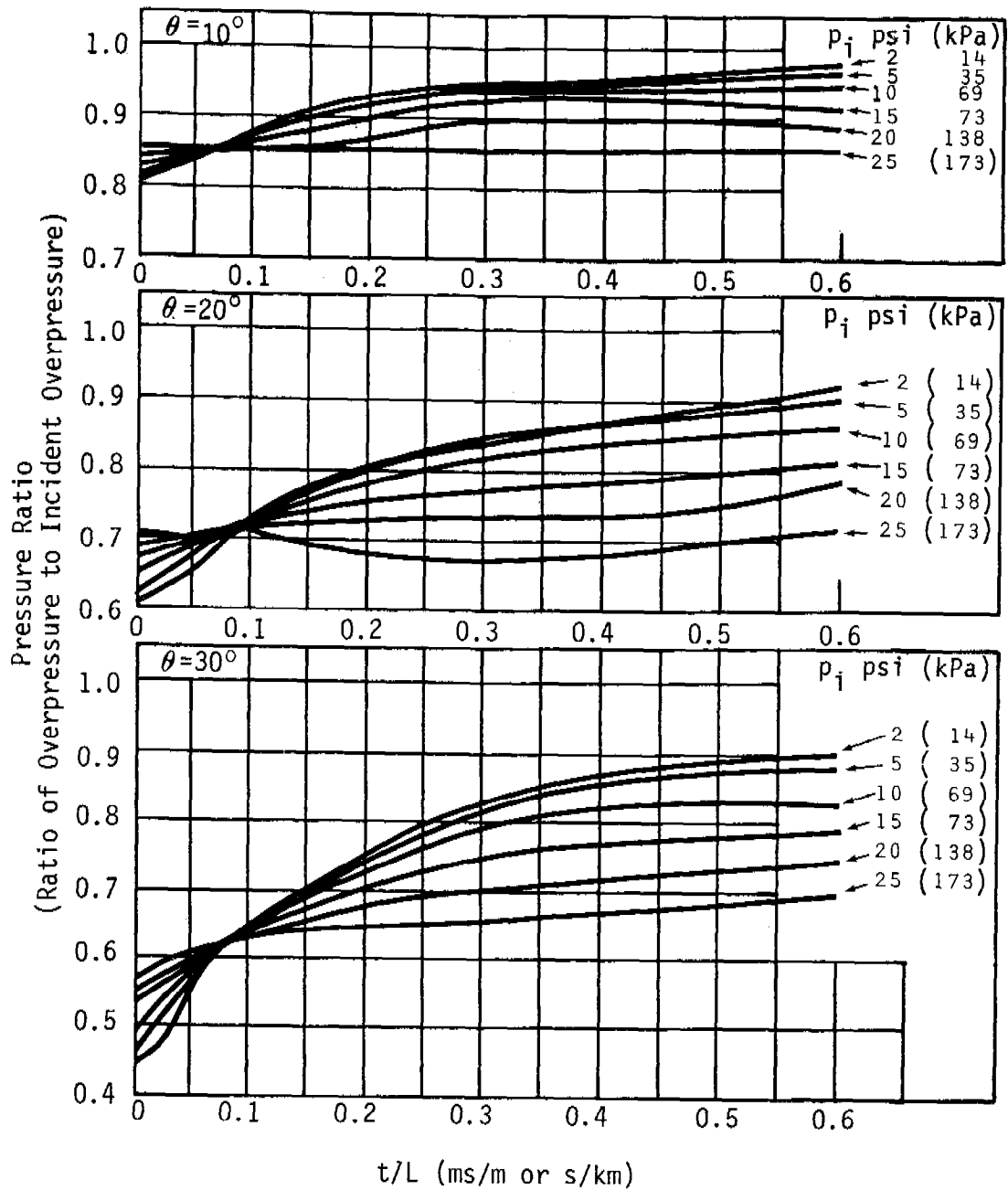
Fig. 10. Falling Slope Pressure Ratios as Functions of t/L for Various Incident Peak Overpressures p_i, and for Slope Angles θ of 10, 20, and 30 Degrees.

25

after it encounters a slope. For example, on a 30 deg. rising slope (Fig. 9) a 14 kPa (2 psi) incident shock wave would become strongly peaked. Pressure at the front would be about 36 kPa or 5.2 psi (pressure ratio = 2.6) and it would decrease by about 50% at t/L of about 0.2 ms/m. In contrast, a 690 kPa (100 psi) incident wave would have a pressure ratio at the shock front of about 1.7. This would first increase by over 25% at t/L ≃ 0.03 ms/m and then stay relatively constant.

Though not apparent, the curves imply that pressure changes caused by a sudden slope change spread out in time as the shock wave propagates up a slope. (The further up the slope a measurement is made, the later in the pulse will a particular effect be noticed.) This phenomenon can substantially alter a pressure pulse as it moves over a terrain feature, as can be seen in the three examples of Fig. 11. The first two examples are for 30 deg. rising slopes; the third is for a 30 deg. falling slope. The basic time scales on the figure are for a nuclear burst with a yield of 1 kt, although additional labelling has been added to show anticipated effects for nuclear bursts with a yield of 1 Mt, as well as high-explosive (TNT) bursts from charges weighing 1 lb (454 gm).

In each example, four pulses are shown. The dotted line is the incident pulse, i.e., the pulse that would be at the measuring station in the absence of a terrain feature. For illustrative purposes, peak incident pressure for Fig. 11A was chosen as 690 kPa (∿100 psi); for Figs. 11B and 11C, as 35 kPa (∿5 psi). For clarity, (because the high-pressure pulse is of relatively short duration) the time scale of Fig. 11A is five times those of Figs. 11B and 11C.

The incident pulse for Fig. 11A is from Ref. 15; for Figs. 11B and 11C the incident pulse shown is calculated from the modified exponential relationship given later in this report in the section on predictions.

The other three curves in each example show the pulses from a burst with a yield of 1 kt that would be measured at 1 m, 10 m, and 100 m from the start of each slope. (For a 1 Mt yield, the distances would be 10 m, 100 m, and 1 km; for a 1 lb HE charge they would be 1 cm, 10 cm, and 1 m.)

In the first case, (rising slope, incident pressure = 690 kPa) the pressure peak at the station closest to the start of the slope is behind the shock front and is about 20% greater than that at the other two stations.

In the second case (rising slope, incident pressure = 35 kPa) the values of pressure at the peaks (the shock fronts) are the same at the three stations, but the pulse at the closest station has a very sharp spike.

In the last case (falling slope, incident pressure = 35 kPa) three different pressure maxima would be observed. The maximum at the middle station would be about 30% greater than that at the furthest station; the maximum at the closest station, about 75% greater.

2. Regular Reflection. As already noted, for a given incident pressure, if the slope angle is greater than the values along the lines labelled "Limit for
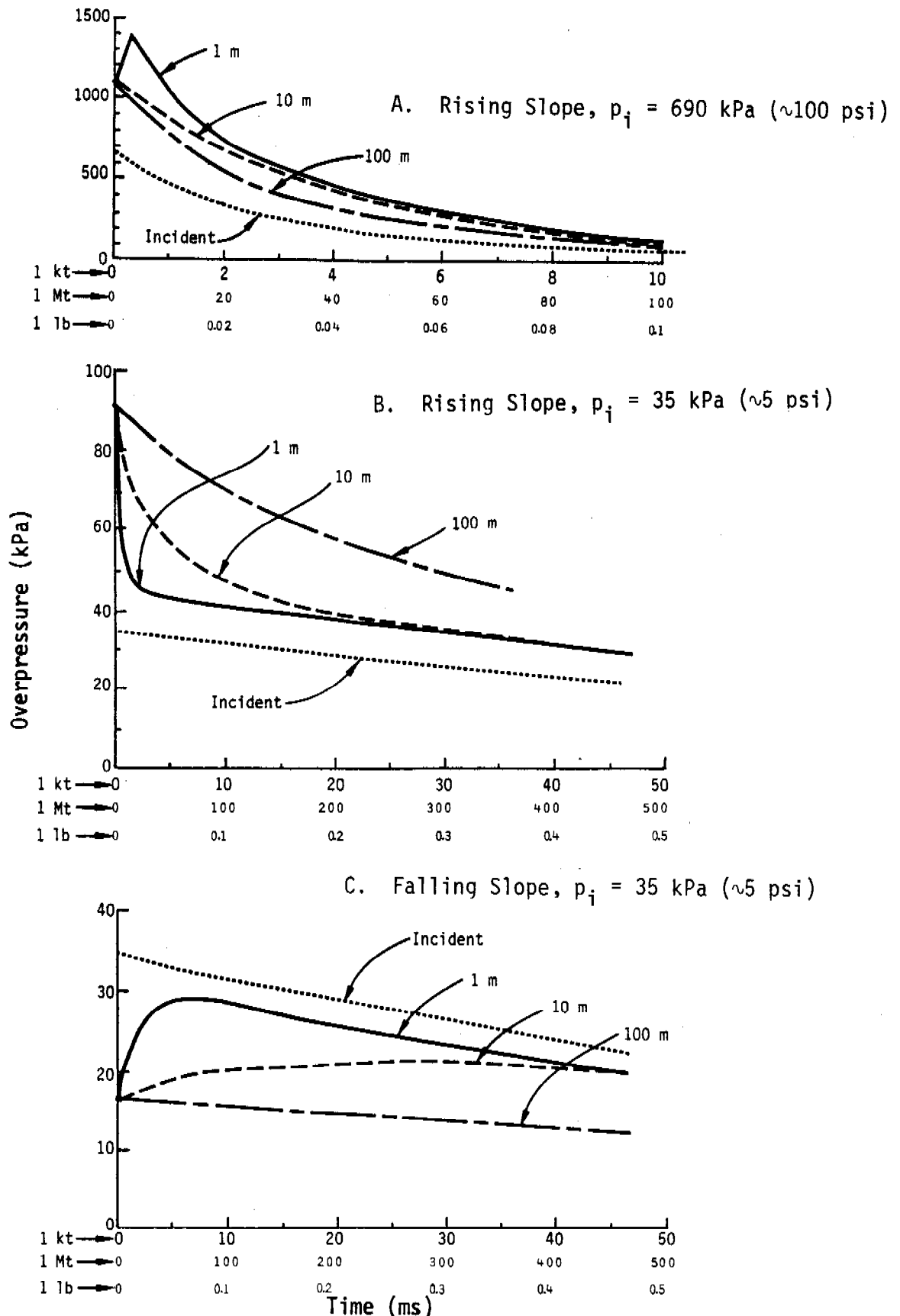
Fig 11.   Three Examples of Changes in Blast Wave Characteristics at Different Places on 30 Degree Slopes for Various Values of Peak Incident Overpressure, p_i.

Mach Reflection" in Figs. 5 and 7, regular (two-shock) reflection generally takes place. (See Fig. 1.) A plot of shock pressure after regular reflection vs incident pressure for various values of slope angle is shown in Fig. 12. The curves were derived from Ref. 16. They correct and extend the range of the regular reflection curves of Ref. 14, and are somewhat more convenient to use since reflected pressure can be read directly.

In general, reflected pressures decrease as slope angles increase up to about 55 deg. At incident pressures below about 100 kPa reflected pressures are essentially constant for all values of slope angles between 55 and 90 deg. At incident pressures greater than about 100 kPa, however, reflected pressures increase as slope angles increase above 55 deg. Thus, at incident pressures below about 100 kPa, the curves labelled 55 deg. and 90 deg. are merged; at incident pressures greater than about 100 kPa, the 90 deg. curve lies above the 55 deg. curve.

The line labelled "Limit for Regular Reflection" serves the same purpose as the similar line of Figs. 5 and 7.* In this case, for a given incident overpressure, if the slope angle is smaller than the slope angle values on the line, Mach reflection will generally take place.

3. Channeling. The last subject dealt with in the small charge studies was "channeling" in which a shock wave proceeds along a valley with parallel or converging walls. When this happens, the shock waves moving along the valley side walls reinforce each other, increasing pressure near the axis of the valley. Flat bottom, "V" bottom, and converging valleys were studied, and in Ref. 12, simple relationships between pressure ratio and the slope angles of the valley side walls were developed. These relationships are shown in Fig. 13. The slope angles of importance are identified in the inserts on the figure.

D. Techniques for Making Predictions

1. Shock Front Pressures. The curves and plots relating overpressures on a slope and in channeling situations to various terrain and blast parameters all deal with a single topographic feature: a single change of slope from the terrain over which a shock wave is propagating, or a single elongated valley for channeling. But real terrain generally differs from this model, with rising slopes succeeding falling slopes, and valley and hill characteristics constantly changing. For this reason, in Ref. 13, techniques were developed for making predictions of at least peak overpressure in real terrain, and many of these techniques were incorporated in Ref. 14 now in general use.

Two initial steps must be taken to make predictions with shock waves encountering

---

* Because the demarcation between regular and Mach reflection is not sharp, the limit lines in Figs. 5 and 12 are not identical. The Mach reflection limit line (Fig. 5) lies above the regular reflection limit line (Fig. 12) at values of incident pressure less than about 50 kPa, and below that line at higher values of incident pressure. Values of reflected pressure from Figs. 5 and 12 differ somewhat for these conditions.

28
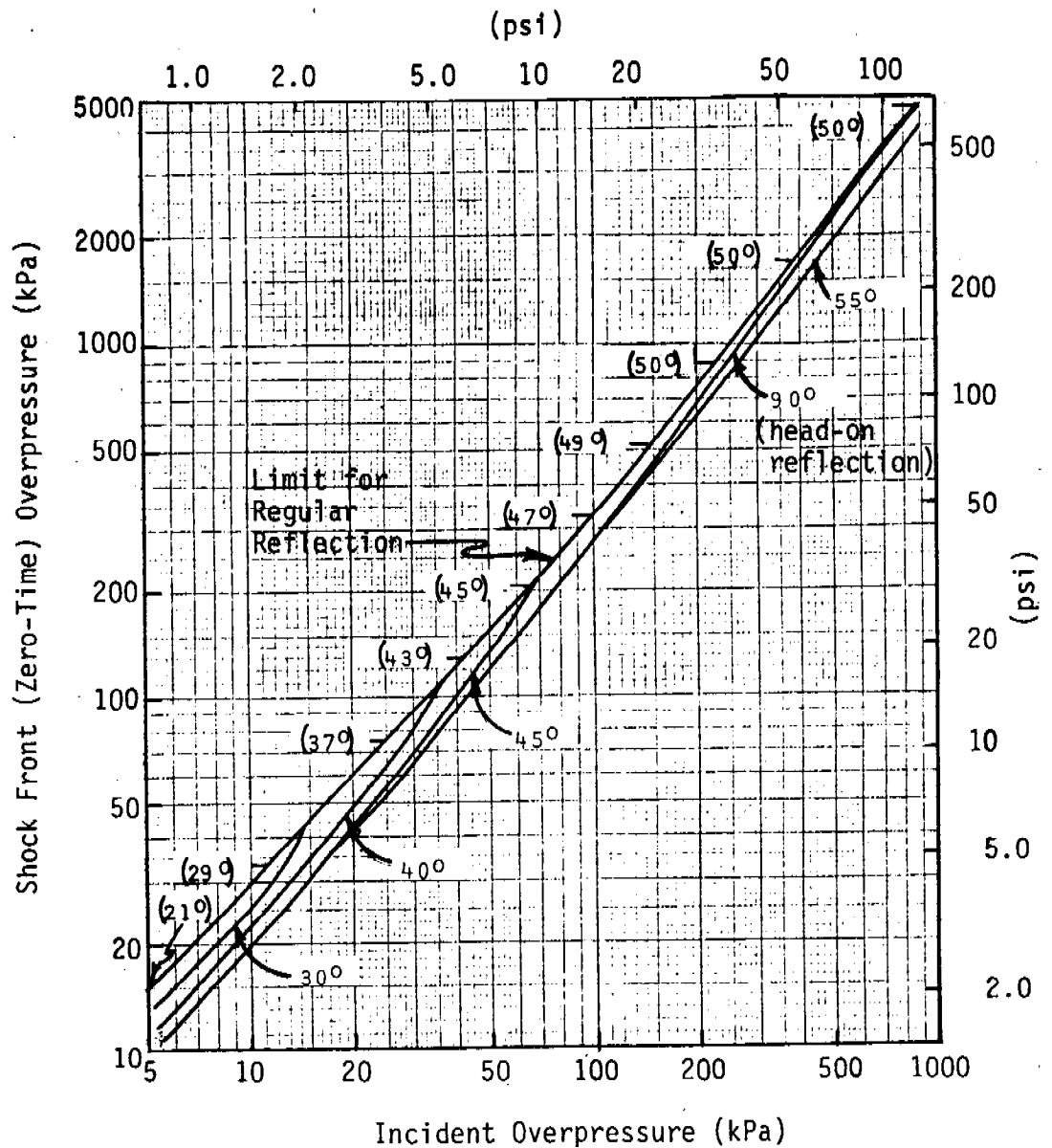
Fig. 12. Overpressure at the Shock Front on a Rising Slope (Reflected Over-
pressure) vs Peak Incident Overpressure for Shock Wave Undergoing
Regular Reflection.

Note: Numbers in parenthesis identify extreme (limit) slope
angles along the "Limit for Regular Reflection" line. Other numbers
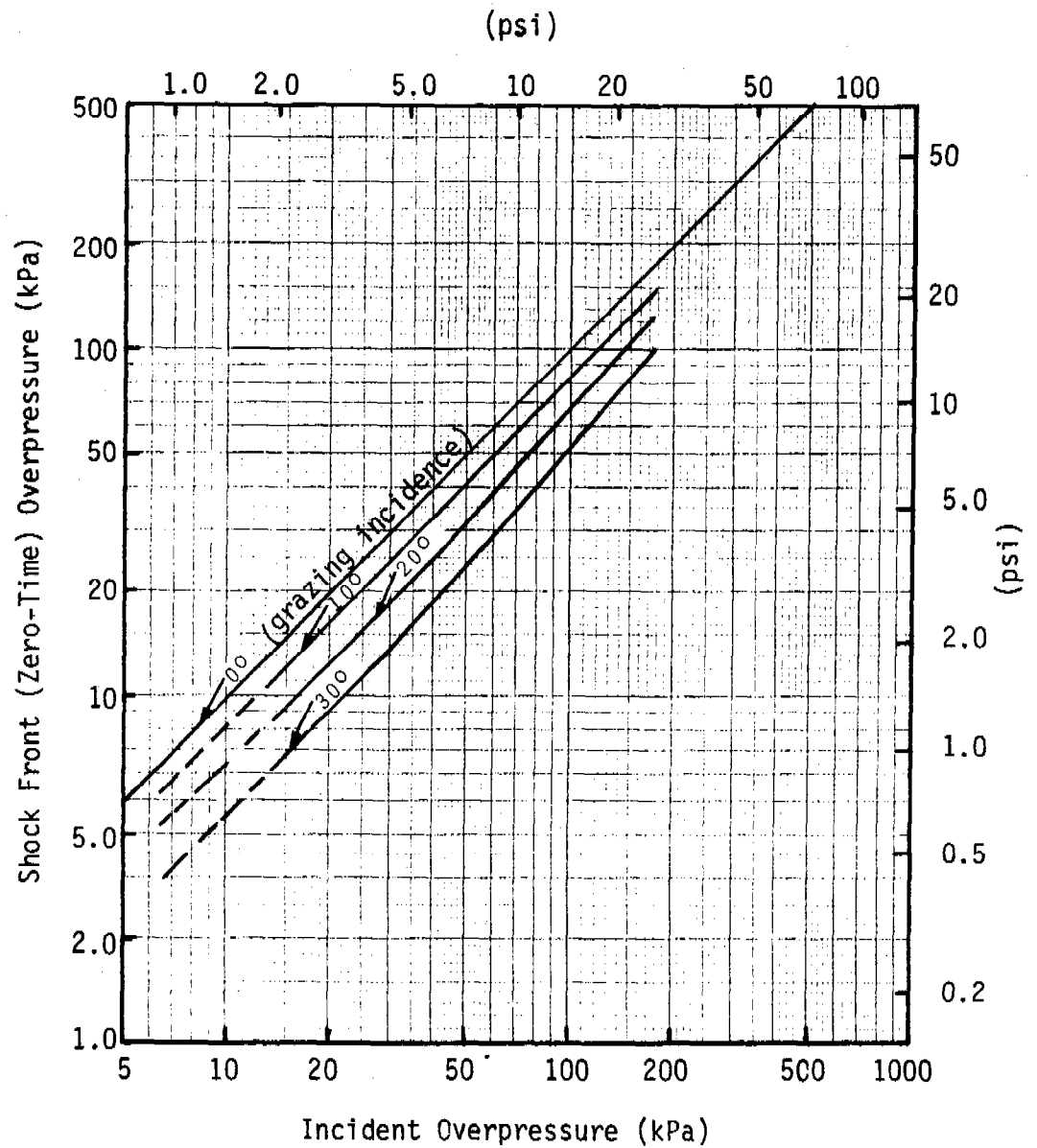on the figure identify the slope angles to which each curve applies.
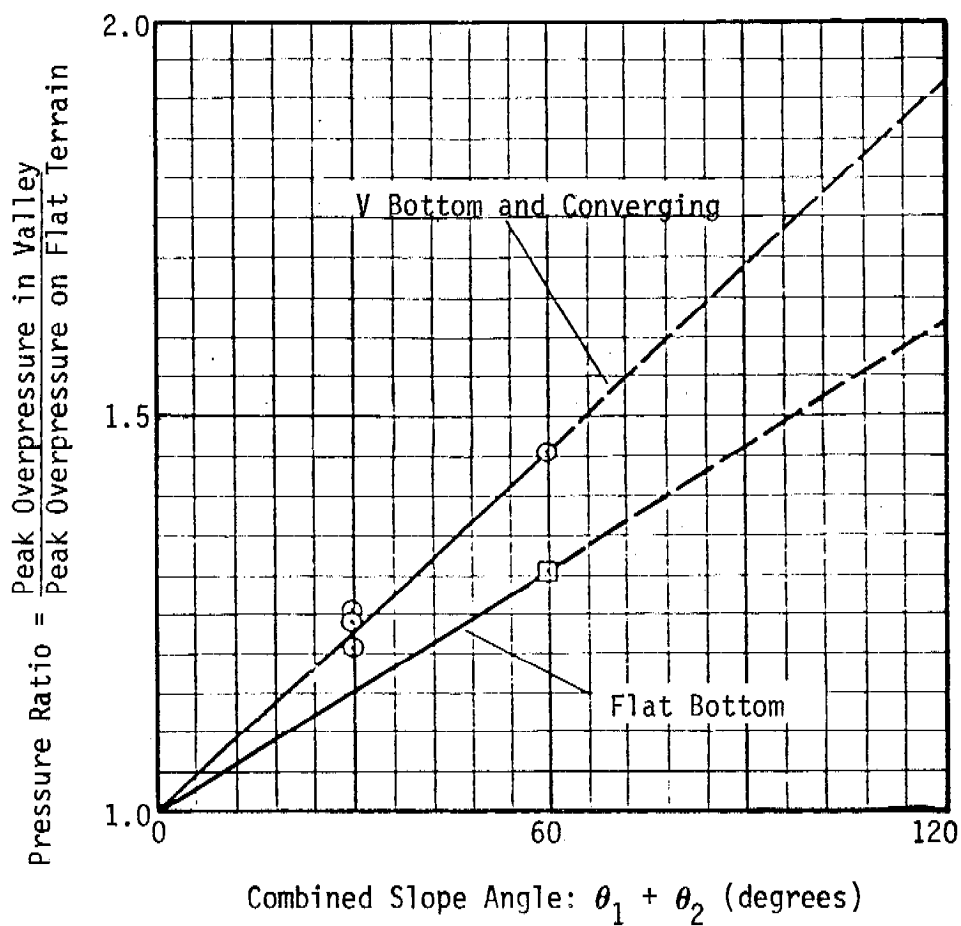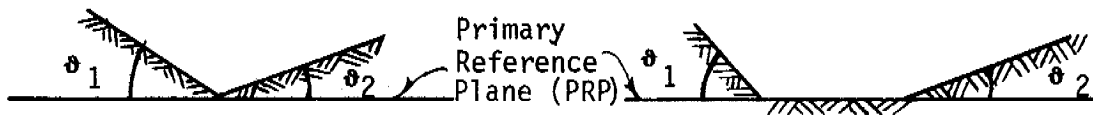
Fig. 13. Average Peak Pressure Ratio at the Bottom of Valleys as a Function of Combined Slope Angle.

slopes. First, a so-called "primary reference plane" (PRP), must be established; second the effective slope angle θ (relative to the PRP) at a point for which predictions are to be made (a target) must be determined. The PRP is actually any convenient ground surface area over which shock wave characteristics can be determined, between ground zero and a target. (The area where a Mach stem from an above surface burst first forms, for example, could constitute a PRP.)

The effective slope angle θ at a target may be determined most directly, as shown in the sketch, by drawing a line on a plan view of an area of interest which connects GZ with the target.

Line drawn perpendicular
to contours at Target

Target

φ

GZ
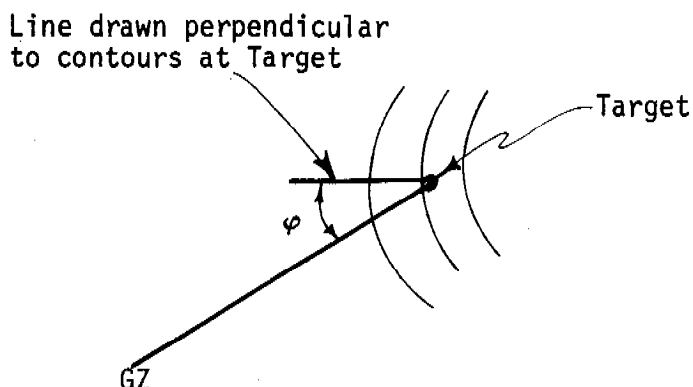
The angle between this line and a perpendicular to the contours of the target is the angle φ. The modified effective slope angle θ', derived from a sectional view along this line is related to the nominal slope angle θ_s by:

$$\tan \theta' = (\tan \theta_s)(\cos \phi) \tag{1b}$$

The angle θ_s can be calculated from this relationship, and used in Eq. 1a to calculate the effective slope angle θ.

For most topographic conditions that might be encountered, however, the angle θ' is very close to θ, and can be used in its place (thus avoiding all calculations except the initial determination of θ' from the sectional view). It is only when both the angles θ_s and φ are large that the more complex procedure might be used. Table 1 illustrates these points.

Once θ is determined, Figs. 5 and 6 (based on Whitham theory) or Figs. 7 and 8 (based on small charge work) can be used to determine shock front pressure on a slope, using as incident pressure the value of peak pressure at the target location determined as if there were only flat terrain between GZ and the target.

In channeling situations the prediction graph (Fig. 13) requires knowledge of the slope angles of the valley sides relative to the PRP, to be determined as is shown in the insets to the figure. If the direction of propagation of the shock wave is not within about 20 deg to the axis of the valley, the topographic situation should be treated as a series of slopes with a shock wave

31

Table 1

Comparisons of Modified Effective Slope Angle θ' With
Effective Slope Angle θ, for Various
Values of Slope Angle θ_s and Azimuth Angle φ

Slope Angle θ_s (deg.)	Azimuth Angle φ (deg.)	Modified Effective Slope Angle θ' (deg.)	Effective Slope Angle θ (deg.)
10	20	9.4	9.4
	40	7.7	7.6
	60	5.0	5.0
20	20	18.9	18.8
	40	15.6	15.2
	60	10.3	9.9
30	20	28.5	28.0
	40	23.9	22.5
	60	16.1	14.5
40	20	38.3	37.2
	40	32.7	29.5
	60	22.8	18.8

traversing them at a large azimuth angle, instead of a valley in which channeling occurs.

The characteristics of a shock wave after it has traversed a number of topographic features is actually determined by its successive responses to each feature between GZ and the target area. It was shown in Ref. 25, however, (and in the current version of that document, Ref. 7) that for determining the pressure at the front of a shock wave at a target, a "local slope" approach could be used. In this approach, the shock front pressure is determined solely from the effective slope angle at the target relative to the PRP, that is, as if the PRP was the slope immediately preceding that at the target. The general rationale for this approach is that effect of positive and negative slopes of equal angle essentially compensate for one another, so that pressure at the front of a shock wave moving over terrain features would be determined by the sum of the angles (positive and negative), of the slopes over which it had passed.

The Whitham theory provides some support for this approach. In its application, the theory implies use of the approach, with θ -- again either positive or negative -- being added to the Whitham theory function w to determine pressure at the shock front on a slope.

It was noted in Ref. 14 that techniques which appear to be more rigorous (in which an attempt is made to follow a shock wave through a series of slope changes) would themselves only yield approximate values of shock front pressure. Superimposed on any topographic effect would be the normal decrease in shock wave overpressure with distance from GZ, and no studies of these two phenomena occurring simultaneously have been made. Thus, the local slope approach, in addition to being simpler to use, may well be as accurate as any more complex approach.

2. Pressures Behind the Shock Front. How to determine pressures behind the shock front after a wave has passed over a succession of slopes is a subject which has not been previously addressed. That the problem is complex can be seen from Figs. 9 and 10. Clearly, rising slope and falling slope effects are not compensating in many instances. At t/L of just under 0.1 ms/m, for example, on a falling slope of 30 deg. the pressure ratios of shocks with incident pressures ranging from 14 to 173 kPa are all about 0.63, while on a 30 deg. rising slope, the pressure ratios at the same value of t/L range from about 1.3 to 2.2. Furthermore, as is illustrated in Fig. 11, pulse shapes themselves differ at different points on the slope.

In the absence of better information, a quasi-local slope approach was adopted for this program in an attempt to evolve a workable prediction method for predicting shock wave characteristics behind the shock front. As with pressures at the shock front, the effective slope angle at a target relative to the PRP is employed to determine which curve of Figs. 9 and 10 would be used. The value of a L, (which when multiplied by t/L from Figs. 9 and 10 determines actual time) is the distance to the target measured from the first slope change encountered, rather than from the slope change nearest the target. In addition, for stations other than the first encountered, no attempt is made to predict shock wave details between the time of shock front passage, and a time associated

33

with t/L values from Figs. 9 and 10, at which very rapid pressure ratio changes are no longer taking place. Further discussion of this method appears in a later section of this report in which all prediction techniques are evaluated.

III. MODEL CONSIDERATIONS

A. Model Characteristics and Scaling

Since a major purpose of the entire program was to evaluate the adequacy of prediction methods in situations that might actually be encountered in the field, it was decided early in the program to base the model on a "real world" area that is of some interest to tactical planners. The prototype area chosen by BRL is shown in Fig. 14. The full-scale weapon yield of interest was 125 kt; the height of burst was 300 m. In order to enhance the terrain effects on blast, (the better to evaluate methods for predicting these effects) it was decided that the vertical scale of the model based on Fig. 14 would be increased by a factor of five.

Scaling of shock wave phenomena in general depends on the fact that gravity has minimal effect of these phenomena. Ignoring other secondary effects (e.g., viscosity, real gas effects) and assuming that ambient atmospheric conditions over a model and a prototype are the same, the minimal effect of gravity implies that strict geometric scaling will apply, that is, a geometrically scaled model will produce all desired phenomena without relative distortion.* In addition, energy W will scale as the cube of the length scale factor (the ratio between characteristic lengths in prototype and model) or -- equivalently -- the length scale factor between prototype and model equals the cube root of the ratio between explosion energy yield in the two. In the tests with high explosives, the yield ratio is the same as the ratio between charge weights.

In the type of test being considered -- i.e., a burst over a surface -- all lengths, including the burst height h, and distance from ground zero, d scale as $W^{1/3}$. At equal scaled distances from ground zero, (distance divided by $W^{1/3}$), shock pressures will be identical, and all times t, including pressure pulse duration t^+ will scale as $W^{1/3}$. In equation form:

$$p = f_1 (d/W^{1/3})$$

$$t/W^{1/3} = f_2 (d/W^{1/3}) \tag{3a}$$

where d = distance from ground zero

---

* Other explosion phenomena in which gravity is important cannot be scaled in so simple a fashion. For example, the cavity formed in a fluid by the burst of a high explosive charge is gravity dependent. The energy contained in the cavity scales as the fourth power of the length scale factor. (The product of volume and depth is invarient.) But the energy of the explosive scales as the cube of the length scale factor. Thus, there will be distortion; the size of the cavity will change relative to the size of the charge that creates the cavity in two experiments using different charge sizes, all else being equal.
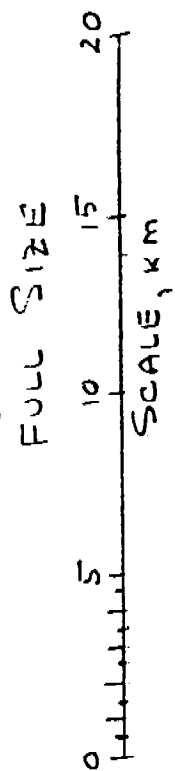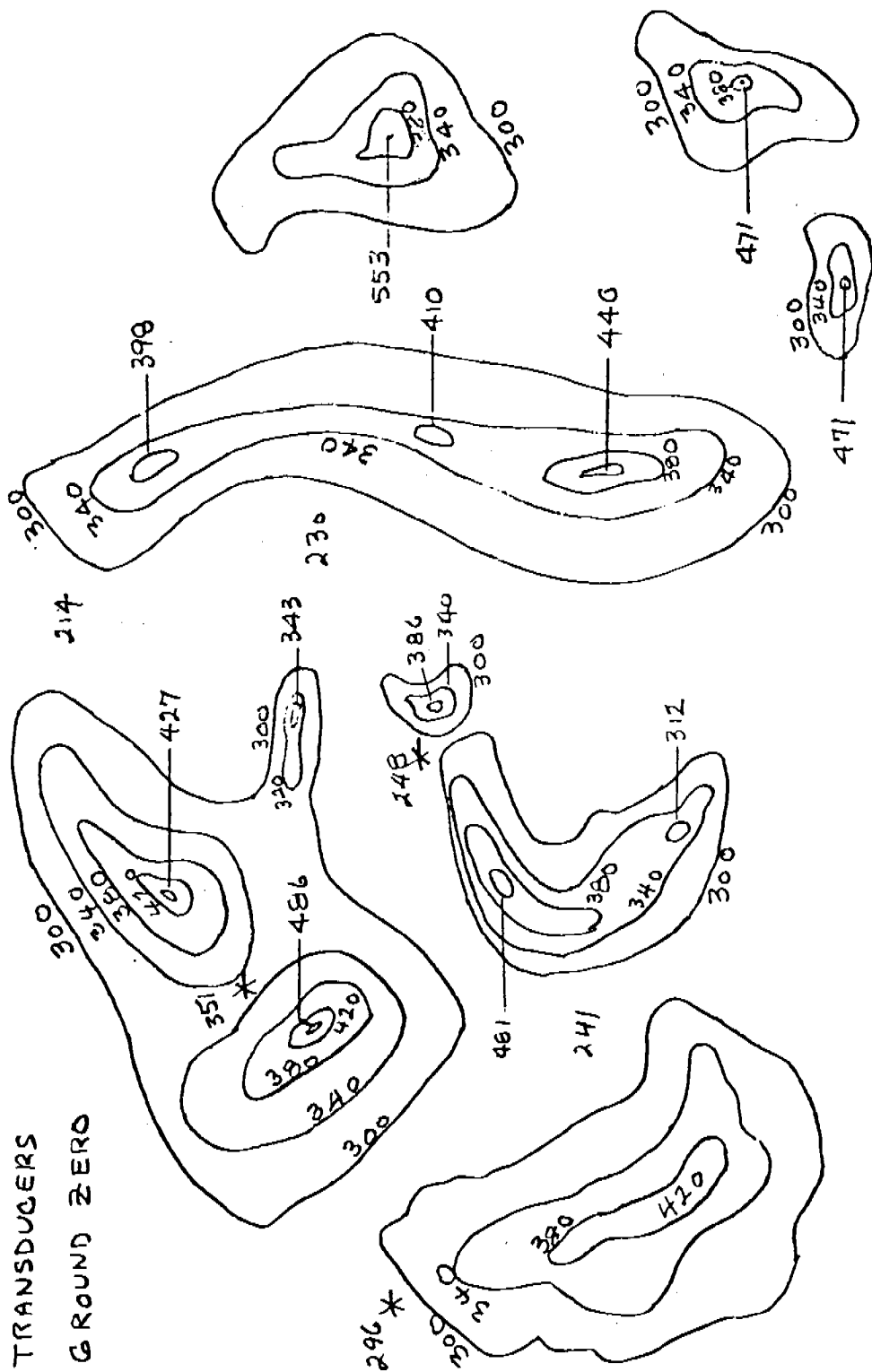
Fig. 14. Full Scale Terrain Contours Provided by BRL.

If the atmospheric pressure (or density) also changes between two experiments, R.G. Sachs showed in Ref. 17 that the relationships still hold, in general, if shock pressure p is replaced by shock strength p/P_0, and the measure of explosive yield W is replaced by P_0/W (now more commonly W/P_0) where P_0 is the ambient pressure. Thus the pressure and time relationships become

$$(p/P_0) = f_1 [d/(W/P_0)^{1/3}]$$

and $\quad [t/(W/P_0)^{1/3}] = f_2 [d/(W/P_0)^{1/3}]$ \hfill (3b)

The quantity $(W/P_0)^{1/3}$ has come to be known as the effective charge weight, since it serves the same function as actual charge weight in Eq. 3a.

Scaling from one nuclear burst condition to another, or from one chemical high explosive condition to another, is straightforward with either Eq. 3a or 3b. Scaling from nuclear explosions to HE explosions, while not as direct, has been accomplished by observing that about one half* of the energy in a nuclear explosion goes into forming blast waves. Thus, the weight of the high explosive charge equivalent to a nuclear burst with an energy yield of one kt $(2 \times 10^6 \text{ lb})$ would be about 10^6 lb or 4.54×10^5 kg.

In the specific case being considered, a nuclear burst with a yield of 125 kt is to be modelled by a high explosive charge weighing one lb or 454 gm. The length scale factor between full-scale and model-scale is the cube root of the ratio of the equivalent HE charge weights, viz $(125 \times 0.454 \times 10^6/0.454)^{1/3}$, or 500. Thus the full-scale burst height of 300 m would become 0.6 m in the model.

Based on these scaling considerations, the model derived from Fig. 14 is shown in Fig. 15. All lengths (vertical as well as horizontal) are in metres; the zero elevation on the model would be the 200 m elevation full-scale. The numbers on Fig. 15 show elevations from this datum, with vertical spacing between contours being 0.4 m. Elevations of high points and low points are also shown.

B. Flat-Terrain Reference Information

The most frequently used measure of the effects of topography on a blast wave at a point on the ground surface is the change in peak overpressure of the incident shock wave, (the wave that would exist at the point if the terrain between the point and ground zero were flat). Changes also occur in pressure behind the peak -- see, for example, Fig. 11 -- and BRL wished to determine whether methods available for predicting these changes were adequate. Thus, information on the characteristics of the entire overpressure pulse over flat terrain was required.

The relationship that will be used in this report between shock front overpressure on flat terrain and distance from ground zero from the burst of a 454 gm

---

* This proportion differs for different weapon types, and heights of burst, and for different high explosives used to model a nuclear blast. It is, however, approximately true for the burst conditions of interest in this study.
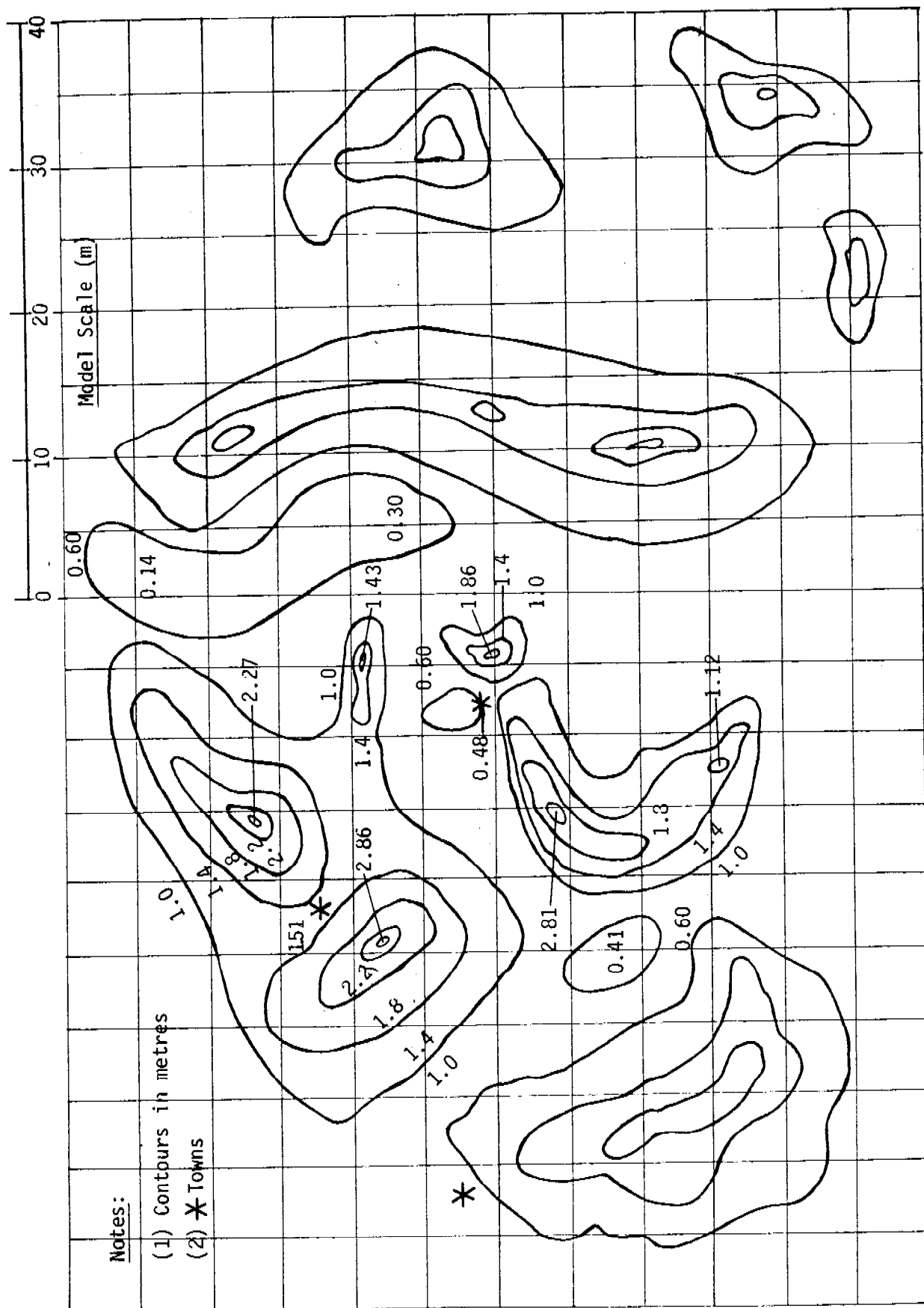
Fig. 15. Contours for Terrain Model (200 m full scale taken as datum).

Notes:

(1) Contours in metres

(2) * Towns

37

charge 0.6 m above the surface, is shown in Fig. 16. Provided by BRL, this relationship is compatible with the height-of-burst (HOB) information in Refs. 19 and 20 derived from charges ranging in weight from 454 gm to 114 kg.*

At the pressure levels of interest in this report, the overpressure pulse from an explosion (nuclear or HE) has been described as a "modified exponential" pulse. Starting at a maximum at the shock front, pressure falls off with time very rapidly at first, then more slowly (as an exponential pulse does). After a certain time, however, dependent largely on explosive yield and distance from the explosion, the overpressure becomes zero. (An exponential pulse would only approach zero, thus the designation of modified exponential.)

The time after the arrival of a shock front at any point on flat terrain that the overpressure falls to zero, is termed the positive pressure phase duration, t^+. The relationship between this parameter and ground range that will be used in this report is plotted on Fig. 16. For ground ranges greater than two metres it is the theorectical value from Von Neumann (Ref. 21); for smaller ground ranges, it is the curve given in Ref. 22 for bursts of hemispherical charges on a surface (which compares very well with that from Ref. 21 for ground ranges greater than two metres). Reported experimental values of durations show wider variation. It is a difficult parameter to measure because pulse overpressure approaches a zero value relatively slowly, and the zero crossing point is often difficult to identify.

If both the overpressure and time after arrival of the pressure pulse at various distances from an explosion are normalized (by dividing pressures within the pulse by shock front overpressure, and time after shock front arrival by positive duration), it will be found, in general, that the higher overpressure pulses (those measured closest to the explosive source) are steeper at early times than lower overpressure pulses.

A relationship between overpressure and normalized time that fairly well represents the pulse from either HE or nuclear explosions and for free-air, on-surface, or above-surface bursts is

$$p(t) = p(o) (1 - \tau) e^{-\alpha\tau} \qquad (4)$$

---

* These HOB curves contain information from a number of different chemical high explosives, the main ones being TNT and Pentolite. While the characteristics of the explosives are by no means identical (TNT, for example, is oxygen deficient, and Pentolite releases some 10% more explosive energy than TNT), differences among the explosives appear to be masked by other experimental variables (including variations from batch to batch of the same explosive). At the scaled burst height used in this project, for example, mean ranges at which 30 to 50 kPa have been measured differ by more than 10% and individual measurements show a still wider variation. Therefore, the term high explosives as used in this report is meant to refer to the general class of high explosives with yields per unit weight about those of TNT or Pentolite.
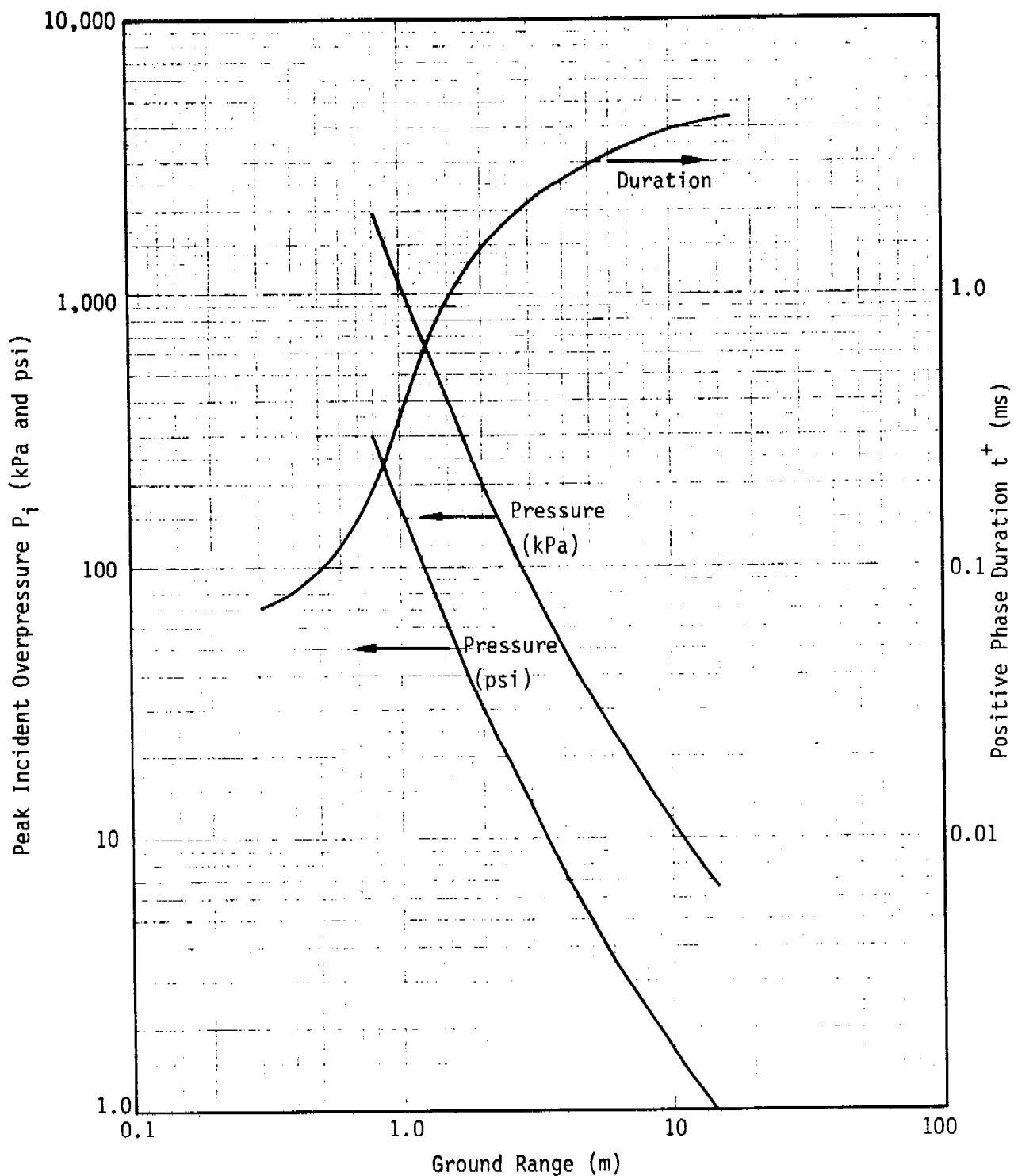
Fig. 16. Peak Incident Overpressure P_i and Positive Phase Duration t^+ vs Ground Range for a Charge Weighing 454 gm (1lb) and a Burst Height of 0.6 m.

where: $p(t)$ = overpressure at any time t after passage of the shock front, thus

               $p(o)$ = shock front overpressure, i.e., pressure at $t = 0$.

               $\tau = t/t^+$

               t = time after arrival of the shock front

               t^+ = positive phase duration

               α = a dimensionless variable dependent on $p(o)$

While this simple relationship is only an approximation of the pulse from an explosive source,* given normal variations from charge to charge, and the difficulty of determining a parameter as important as the duration t^+, Eq. 3 is deemed to be suitable for purposes of this report.

The parameter α in Eq. 4 varies with shock front overpressure $p(o)$ -- or incident overpressure p_i -- and the type of explosive source, principally whether HE or nuclear. Tabulated values in Ref. 23 for TNT (apparently derived from Ref. 24) indicate that:

$$\alpha \simeq 1 \qquad\qquad\qquad\qquad \text{for } p_i \leq 140 \text{ kPa}$$

$$\alpha \simeq 0.04\, p_i^{0.65} \qquad\qquad \text{for } p_i \geq 140 \text{ kPa} \qquad\qquad (5)$$

With a nuclear source, values of α derived from Ref. 18 (as an approximation to the more complex relationship actually used in that report) are:

$$\alpha \simeq 0.14\, p_i^{0.51} \qquad\qquad \text{for } p_i \leq 70 \text{ kPa}$$

$$\alpha \simeq 0.31\, p_i^{0.32} \qquad\qquad \text{for } p_i \geq 70 \text{ kPa} \qquad\qquad (6)$$

For values of p_i between about 40 and 700 kPa, values of α from Eq. 6 are greater than those from Eq. 5, which indicates that the nuclear pulse is generally steeper immediately behind the front than the HE pulse. Below $p_i \simeq 40$ kPa the HE pulse is initially steeper.

Because of the minimum overpressure of interest ($p_i \simeq 7$ kPa) a gauge line extending 14 m from GZ was required for use in the model. Initially 15 stations at fixed distances from GZ were to be used both on flat terrain and on topographic features. (Two stations were added later, at BRL's request, to meet specific requirements.) To minimize the need for gauge location changes, the distances between adjacent stations of the standardized line were made symmetric about the center station (Sta. 8) -- that is, they are the same from either end of the line.

---

* In Ref. 18, for example, the time history of a pulse from a nuclear weapon is given as:

$$p(t) = p(o) \left[a e^{-\alpha\tau} + b e^{-\beta\tau} + c e^{-\gamma\tau} \right] [1 - \tau]$$

where a, b, c, α, β, and γ are functions of incident overpressure.

Table 2 identifies the stations, and gives distances from ground zero as well as between adjacent stations. It also lists predictions of both peak flat terrain overpressures and positive overpressure pulse durations from Fig. 16 for each station.

In Fig. 17 are plots of flat-terrain pulse shapes for each station in Table 2. For clarity, time scales have been expanded at the higher overpressure stations because of the short pulse durations. To provide a sense of how sharply pulse durations actually do change, however, the last parts of pulses from stations nearer ground zero have been superimposed on the plots for Sta. 4 and Sta. 6. It can be seen that the pulse at Sta. 4 is 7.5 times longer than that at Sta. 2, and the pulse at Sta. 6 twice as long as that at Sta. 4 (or 15 times longer than that at Sta. 2).

C. Test Parameters – Burst and Gauge Locations

The criteria used to establish burst and gauge placements reflected the basic purposes of the program: to determine whether currently available prediction techniques are adequate to deal with practical problems that might be encountered in the field. That simple statement led to three corollary criteria:

1. Changes in blast parameters due to terrain should be significant. A change of 20% was adopted as the lower limit of significance.

2. The terrain situations considered should include most (if not all) of the different types of situations that could be encountered. As a minimum, the situations should include effects on blast waves of both rising and falling slopes, successive slopes, contours at an angle to the shock front, location of a measuring point on a slope, and channeling situations.

3. The overpressures considered should be those with which military planners must be concerned. This last criterion tended to put a lower limit on the incident blast pressures of interest. Again, a lower limit of 7 kPa($\sim$1 psi) was adopted.

Plotted on Figs. 18, 19, and 20 is a set of seven GZ locations and eight gauge lines that meet these criteria. Three of the lines (A-2, B-2, and C_a-1) lie along essentially flat terrain; the others traverse various terrain features, and provide the desired variety of blast-terrain interactions. The dots along the gauge lines represent the locations of individual gauge stations identified in Table 2.* Note that gauge lines B-1, C-1, and C-4 have burst locations at both ends (designated as B and B_a, C and C_a, and C and C_b respectively).

---

* Coordinates (including elevations) of each GZ and of each active station on each gauge line are given in Appendix B. The x, y coordinates refer to the co-ordinate system of Figs. 18, 19, and 20.

41

Table 2
Standard Gauge Line Station
Distances, Flat Terrain Pressures, and Duration

Station Number	Distance from GZ (m)	Between Stations (m)	Flat Terrain Overpressure (kPa)	(psi)	Positive Pressure Pulse Duration (ms)
1	0		13,800	2000	-
		0.8			
2	0.8		2,070	300	0.2
		0.4			
3	1.2		690	100	0.6
		0.8			
4	2.0		210	30	1.5
		1.3			
5	3.3		70	10	2.3
		1.7			
6	5.0		33	5	3.0
		1.2			
7	6.2		24	3.5	3.2
		0.8			
8	7.0		21	3	3.4
		0.8			
9	7.8		17	2.5	3.6
		1.2			
10	9.0		14	2	3.8
		1.7			
11	10.7		10	1.5	4.0
		1.3			
12	12.0		9.0	1.3	4.2
		0.8			
13	12.8		8.0	1.2	4.2
		0.4			
14	13.2		7.5	1.1	4.3
		0.8			
15	14.0		7.0	1.0	4.3
Added Stations					
4a	2.6		120	17.4	1.9
5a	4.1		46	6.7	2.7
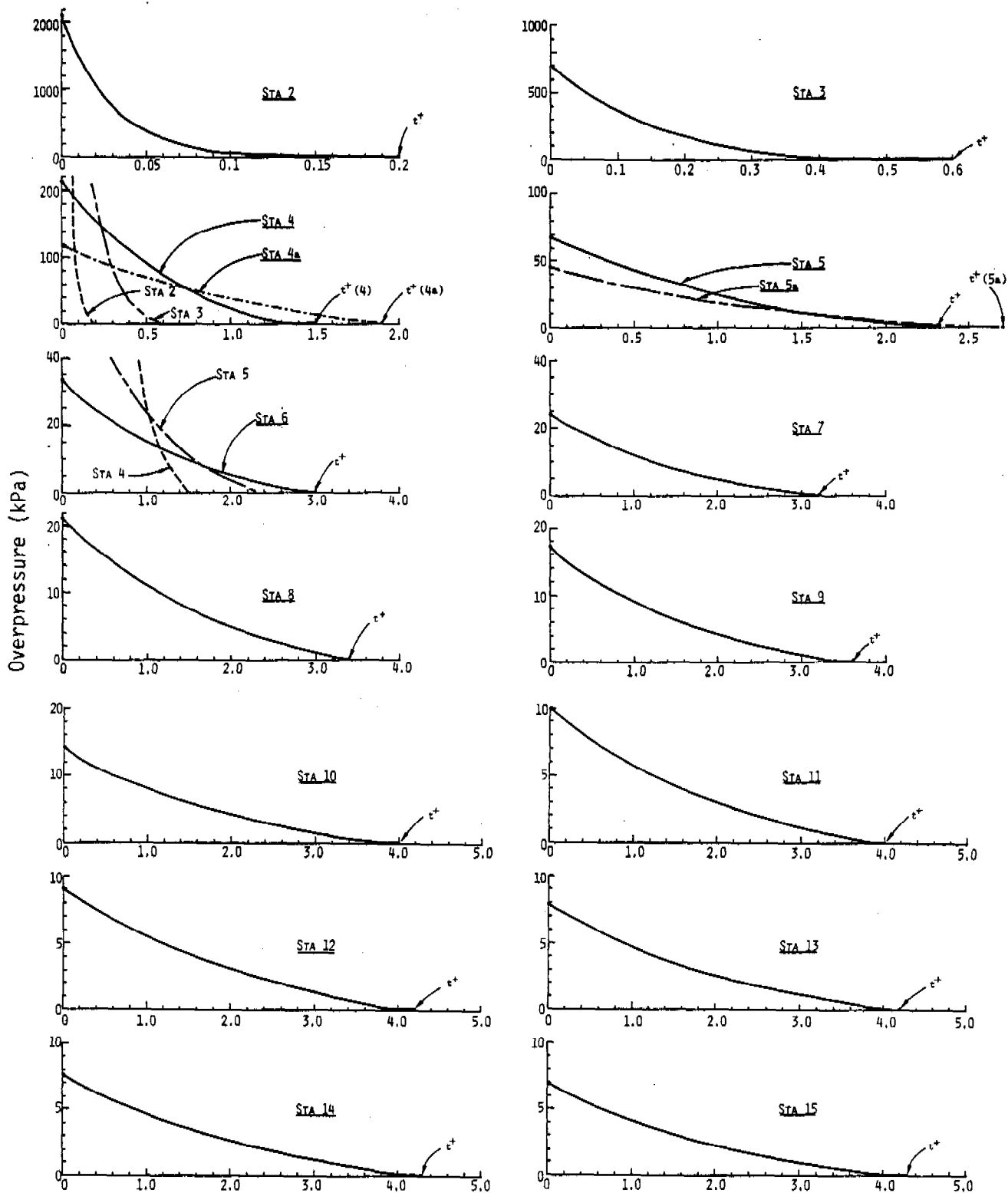
Time After Shock Wave Arrival at the Station (ms)

Fig. 17. Flat Terrain Overpressure Pulses of Sta 2 Through Sta 15.

43

Fig. 18. Plan View, Gauge Lines A-1, A-2, B-1, and B-2, and Ground Zeros A, B, and B_a.

Notes:

(1) Contours in metres

(2) ✱ Towns

◻ = GZ- Elevation

Model Scale (m)

44
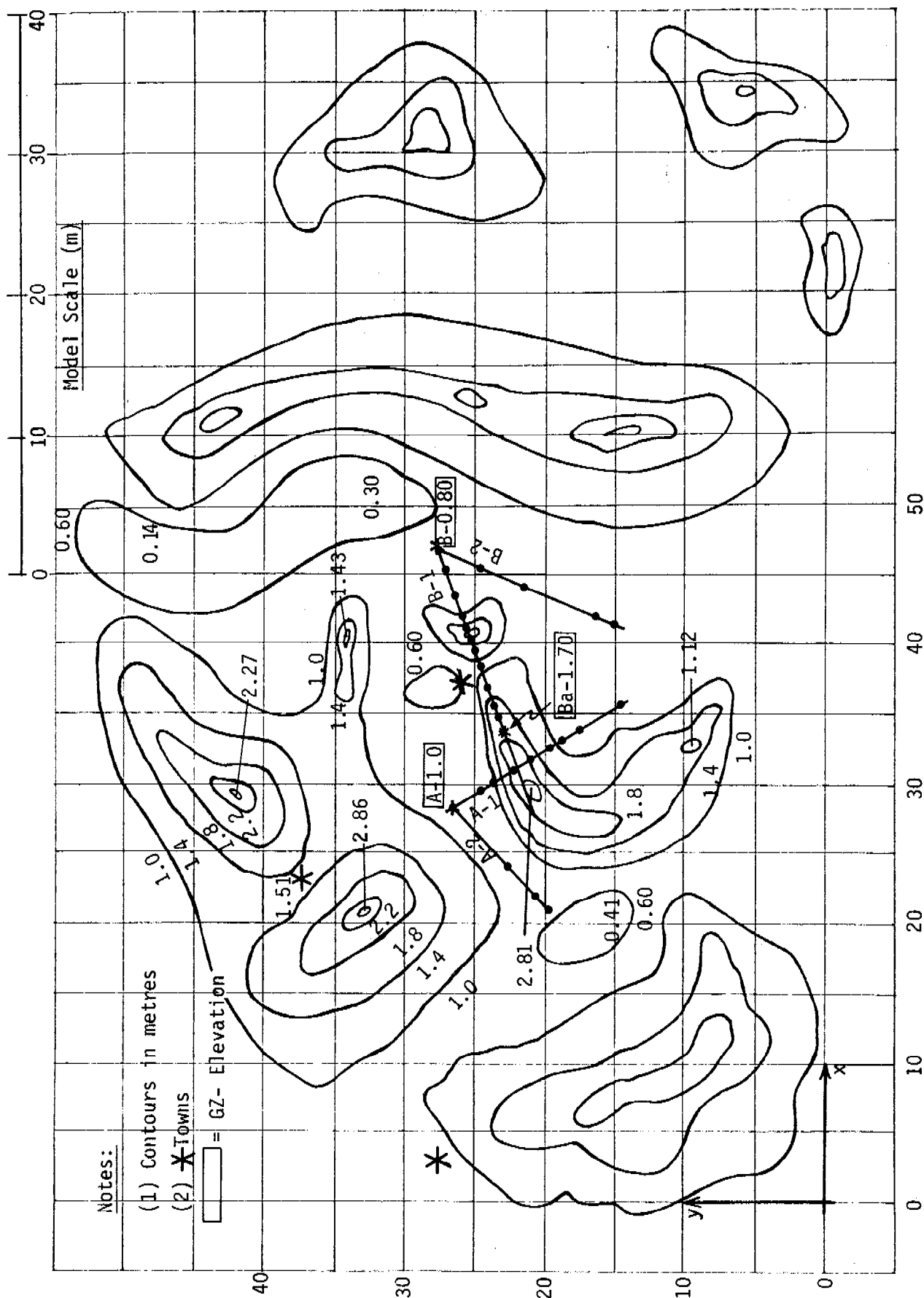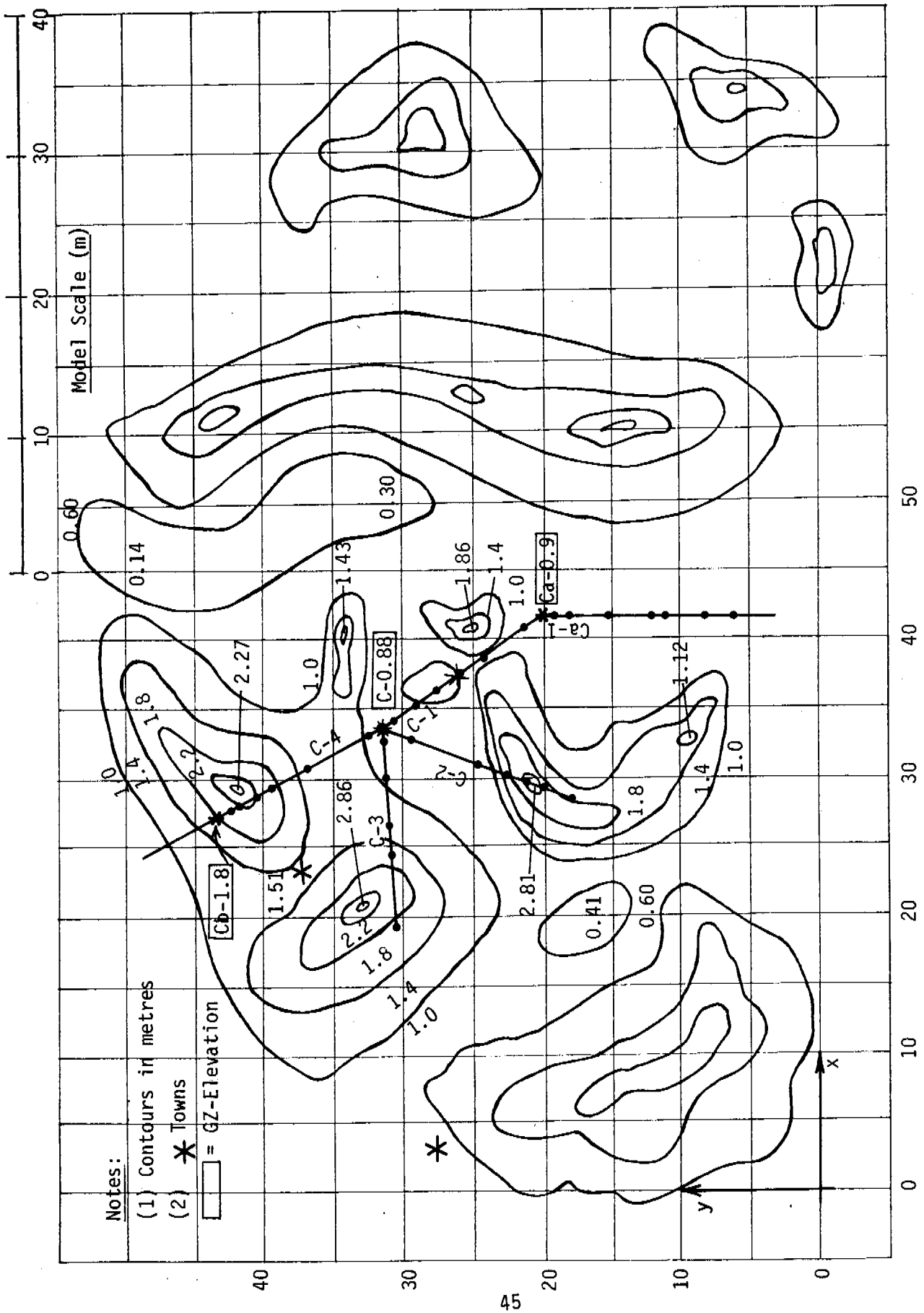
Fig. 19. Plan View, Gauge Lines C-1, C-2, C-3, C-4, and C_a-1, and Ground Zeros C_1, C_a, and C_b.

45

Fig. 20. Plan View, Gauge Lines D-1 and D-2, and Ground Zero D.

46

Table 3 indicates which gauge stations along each gauge line are to be active during a test using the GZ shown at the top of the table. These stations correspond to the dots along the lines in Figs. 18, 19, and 20. The column on the extreme right of Table 3 indicates how many measurements equivalent to flat-terrain measurements would be made at each station location.

In Figs. 21 through 25, profiles along each gauge line are plotted and elevation angles (the modified effective slope angles θ') at each active station location are given. These elevation angles are tabulated in Table 4.

D. Gauge and Recording System Considerations

The basic purpose of the test program is to document the characteristics of the overpressure vs time pulses at ground level in the model, at gauge stations shown in Figs. 18 through 20. As will be seen in the section dealing with predictions, it is anticipated that some overpressure pulses will be marked by pressure spikes of relatively short duration -- about 0.1 ms at a number of stations, as short as 0.04 ms at one particular station. Whether the anticipated short duration transients will be recorded and reported with an acceptable accuracy, depends critically on four elements: first, the response characteristics of the gauges or transducers that will sense the blast wave pressure; second, how these transducers are to be used in the model; third, the system used to record the transducer generated signals; and fourth, the characteristics of the system used to analyze the records. These elements are discussed, in turn, in the following material.

1. Gauge Response. The response characteristics of the transducers planned for use by BRL are well suited to the requirements of this program. The PCB Piezotronics, Inc. series 100 transducers, to be used for lower pressure measurements, employ a quartz sensor, and various models have natural frequencies of between 250 and 500 kHz. The Susquehanna Instruments Model ST-4 transducers to be used for high pressure measurements, employ tourmaline sensors, and have a natural frequency of 1.5 MHz. The specifications for the PCB transducers quote their rise times as 1 μs for the 500 kHz models, and 2 μs for the 250 and 500 kHz models. The Susquehanna specifications merely state that "... high speed reflection shocks can be accurately measured to one microsecond or better." (This appears to be conservative; the rise time should be better than about 0.4 μs.)

2. Gauge Mounting. Given that the transducers have adequate response characteristics and that their function in this test program is to sense ground level pressures, the only requirements that apparently would need be imposed on their placement in the model would be that they be mounted flush with adjacent terrain, and that precautions be taken to avoid generating spurious signals (e.g., from gauge accelerations, cable noise, and the like). Unfortunately, doing so in this program might actually defeat the basic purpose of the program in some instances.

The problem is purely a geometric one. The exposed area of the PCB transducers (i.e., the diaphragms that transmit pressure generated forces to the sensing elements) have a diameter of about 0.55 cm. Shock wave velocities over the pressure

Table 3

Active Gauges for Each
Gauge Line and Ground Zero

(√ Indicates transducer location)

Ground Zero Gauge Line		A		B		Ba	Ca		Cb	C		C		D		Eq. Flat Terrain Measurements
Distance (m)	Station Number	A-1	A-2	B-1	B-2	B-1	C-1	Ca-1	C-4	C-1	C-4	C-2	C-3	D-1	D-2	
0	1	√-----	√							√-----	√	√-----	√	√-----	√	4
0.8	2									√		√		√		3
1.2	3	√		√		√	√		√	√		√		√		3
2.0	4	√		√	√	√	√	√		√		√		√	√	4
3.3	5	√		√		√	√	√	√	√		√		√		3
5.0	6	√		√		√	√		√	√	√	√		√	√	3
6.2	7	√	√	√		√	√	√	√	√	√	√		√		2
7.0	8	√		√	√	√	√	√	√	√	√	√		√		2
7.8	9	√		√		√	√		√	√	√					1
9.0	10	√	√	√	√	√	√	√		√		√	√	√		1
10.7	11	√		√	√	√	√			√						1
12	12			√	√	√	√			√						1
12.8	13			√						√						1
13.2	14															0
14.0	15	√		√	√	√	√			√		√	√	√	√	2
2.6	4a														√	
4.1	5a	√														
Total Active Channels per GZ		13		13		6	12		6	12		12		13		

α= 31.0° ⑤ ⑤ₐ
β= 9.7° ⑥
γ= 24.2° ⑦ ⑧
δ= 15.6° ⑨

Ground Range from GZ "A" Along Line A-1 (m).

α =19.3° ⑥
β =41.2° ⑦
γ =36.3° ⑧
δ =21.3° ⑨
ε =14.0° ⑩ ⑪
ζ = 5.3° ⑫ ⑬

Ground Range from GZ "B" Along Line B-1 (m).
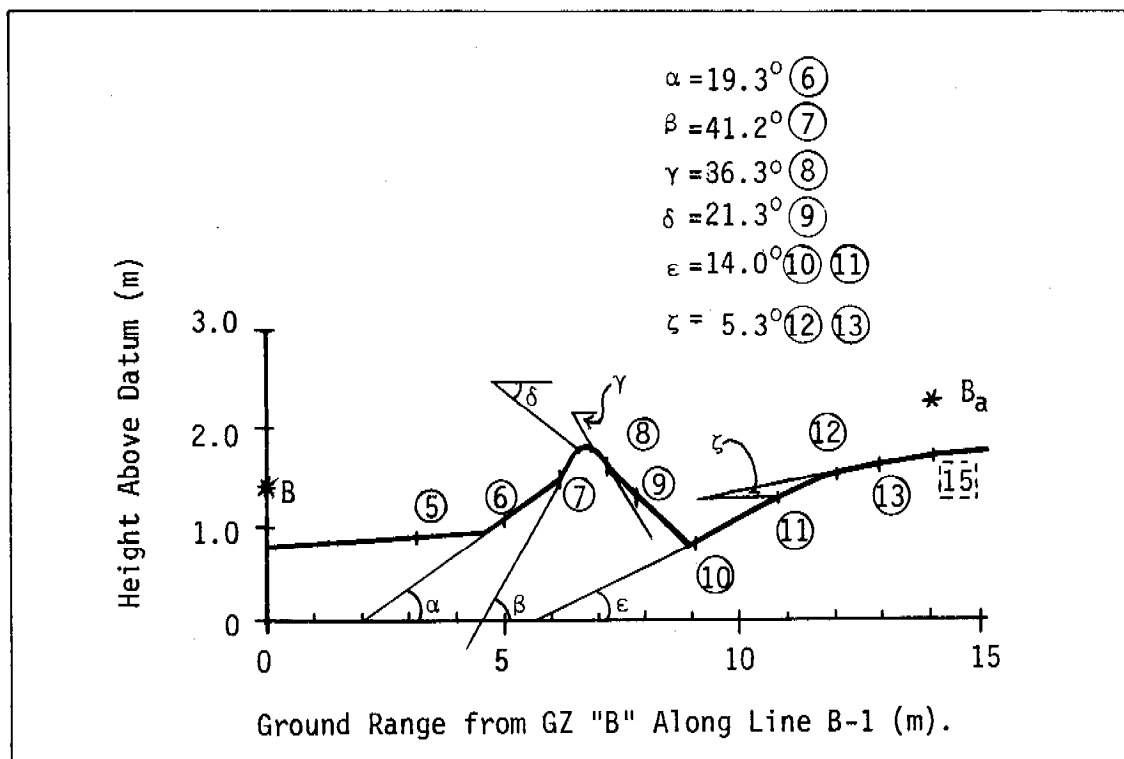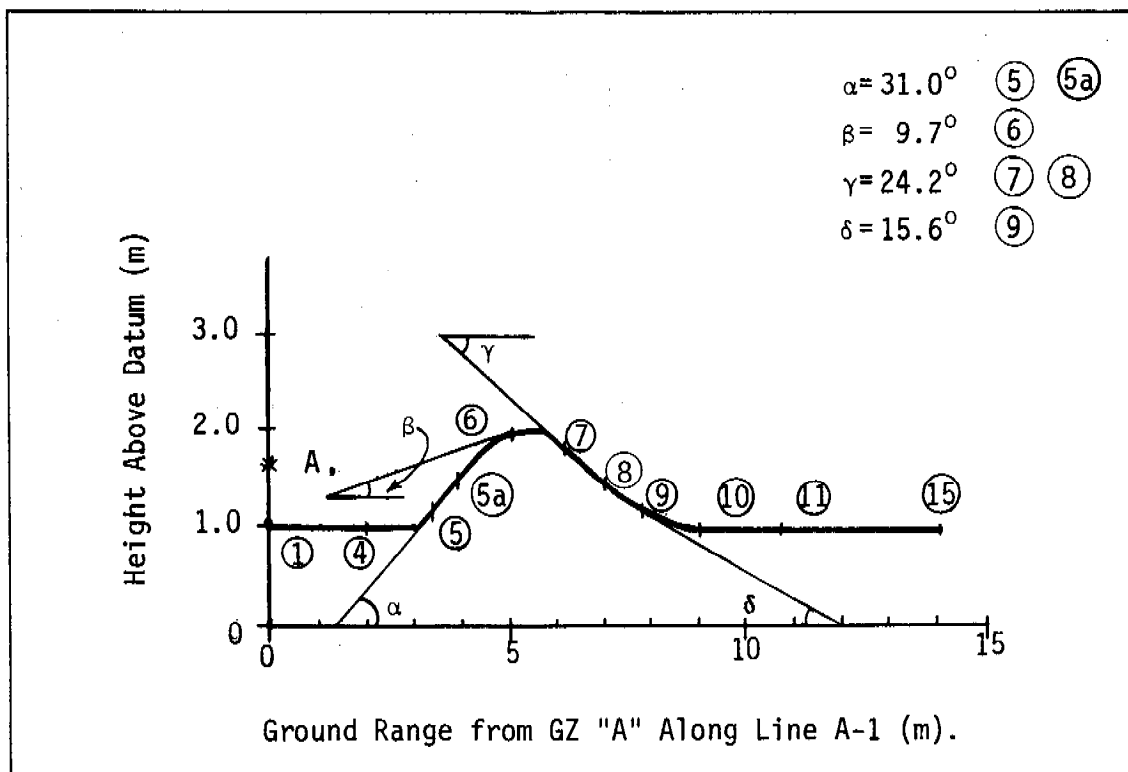
Fig. 21. Profiles of Terrain Along Gauge Lines A-1 and B-1.

α = 6.4° ③ ⑤ ⑥
β = 14.8° ⑧
γ = 21.2°
δ = 4.0° ⑩
ε = 10.4°

Note: Sta ⑩ is Sta ⑩ of line B-1 and Sta ⑮ of line D-1.

α = 28.8° ⑩
β = 24.0° ⑪
γ = 56.0° ⑫
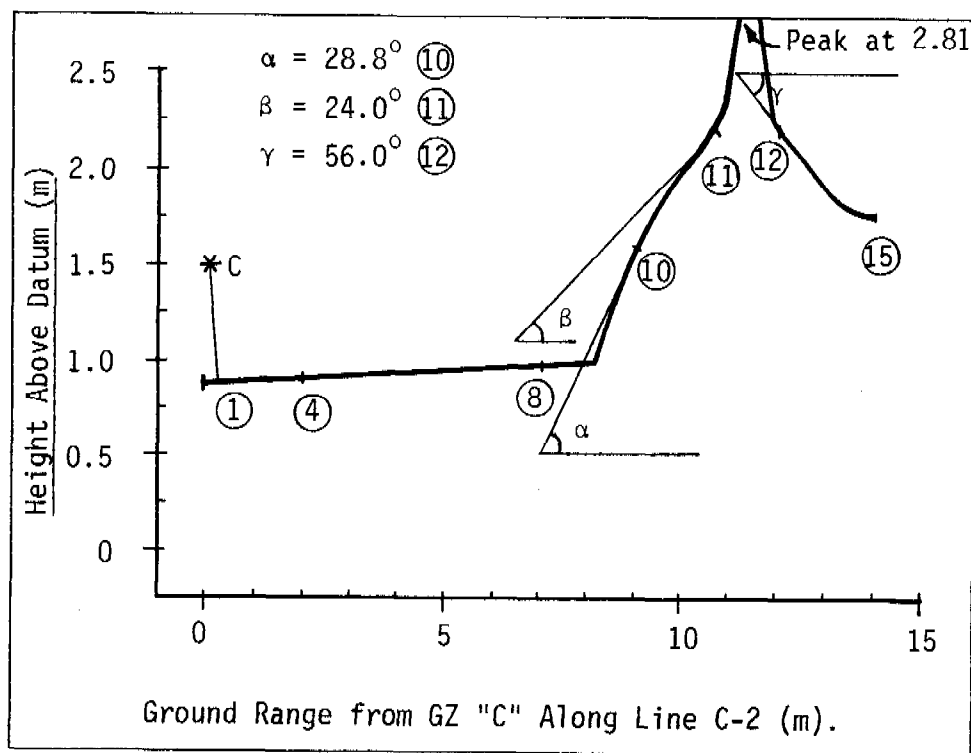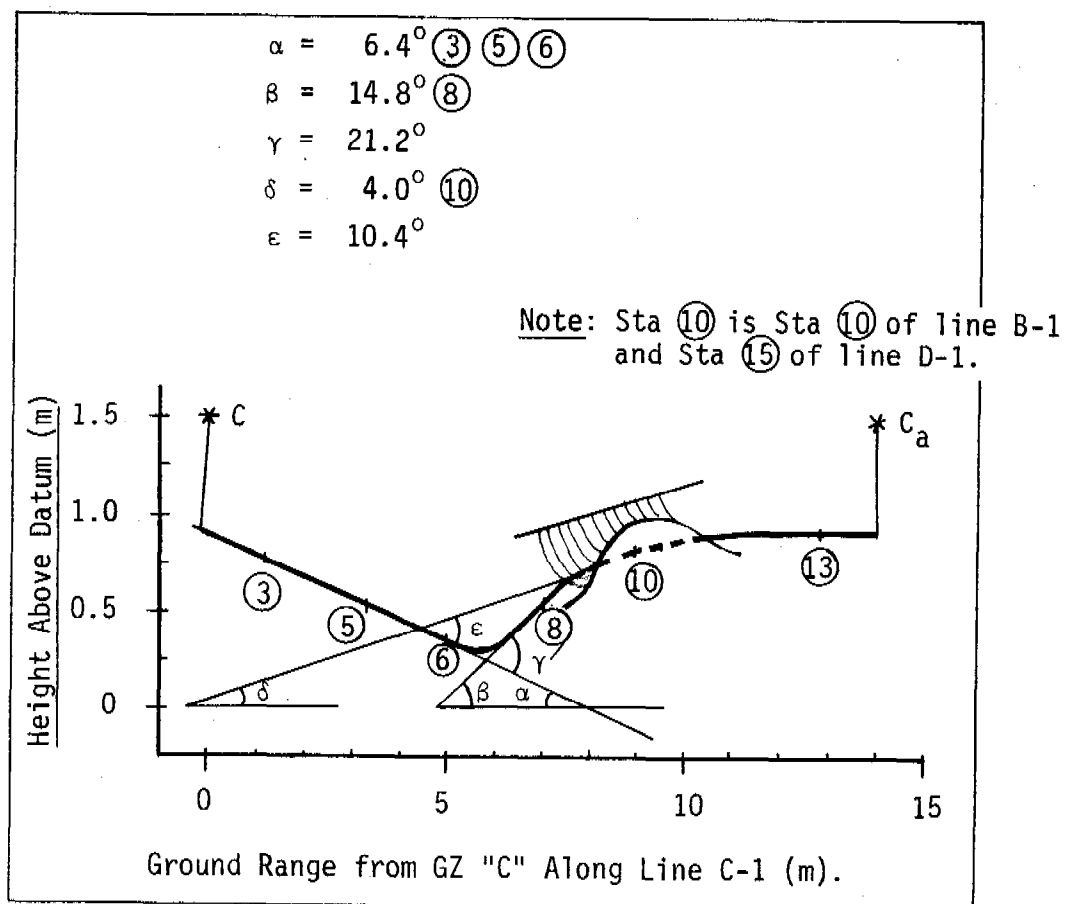
Fig. 22. Profiles of Terrain Along Gauge Lines C-1 and C-2.
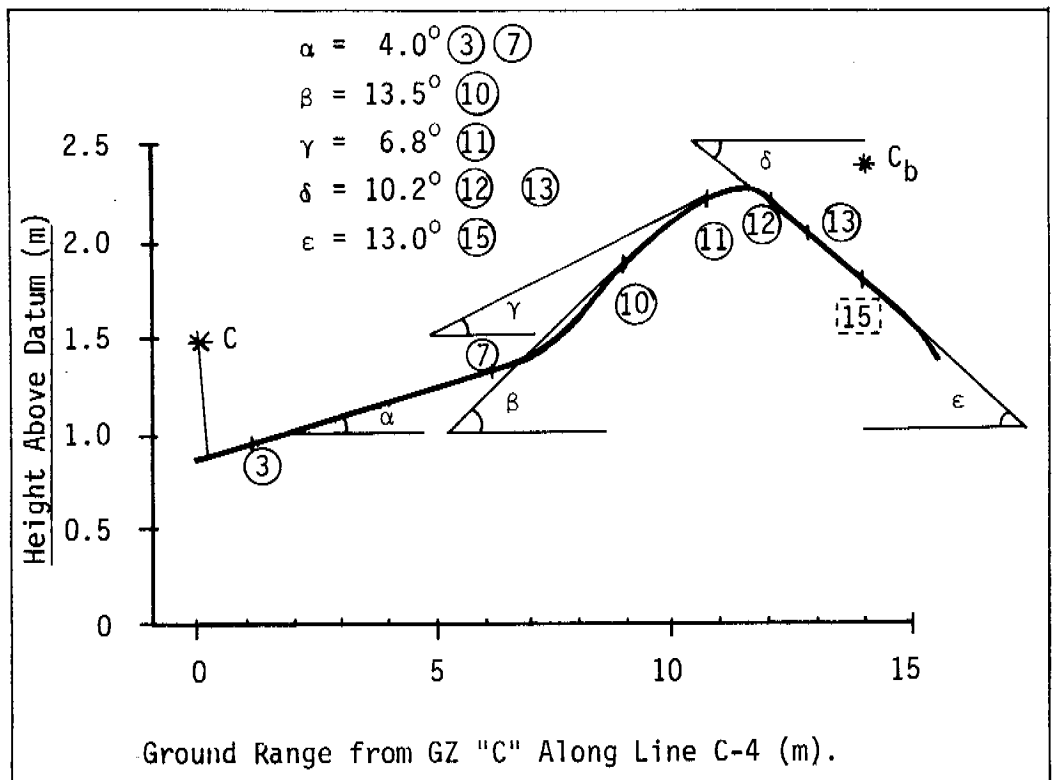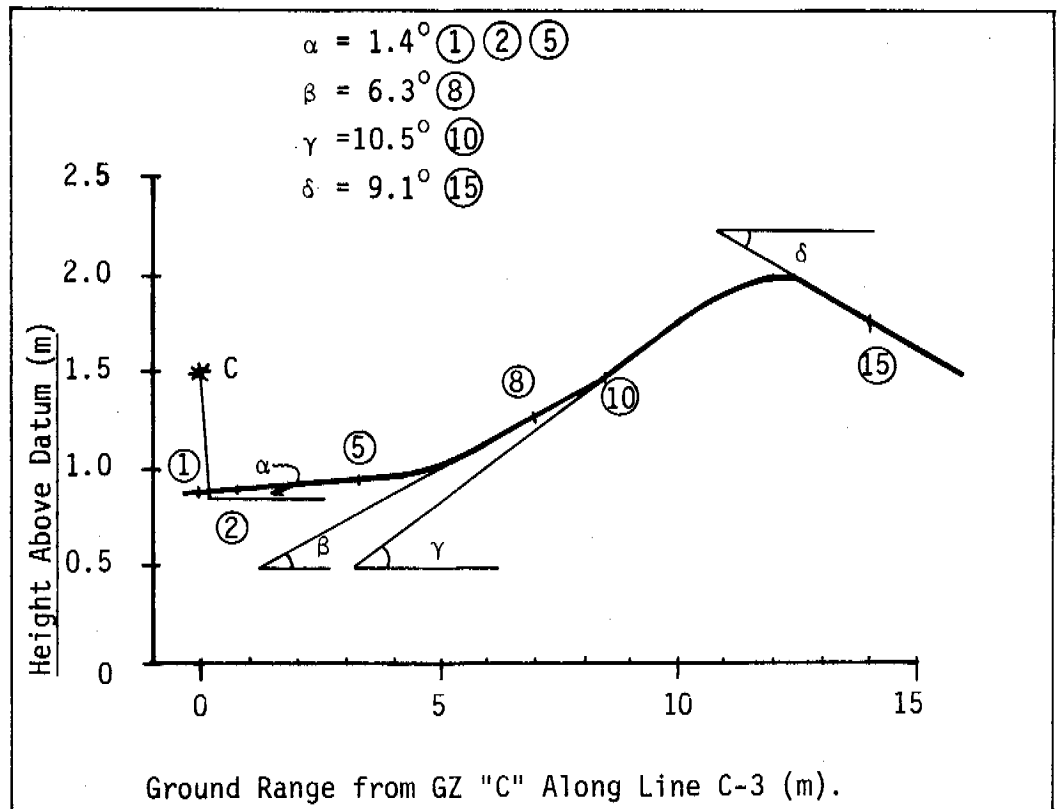
Fig. 23. Profiles of Terrain Along Gauge Lines C-3 and C-4.
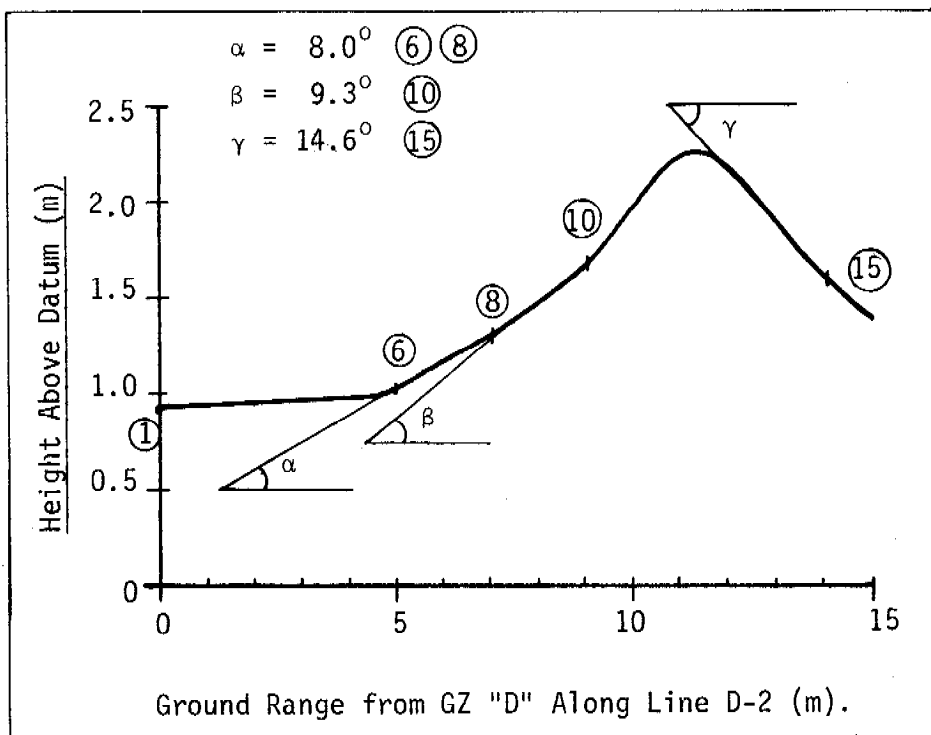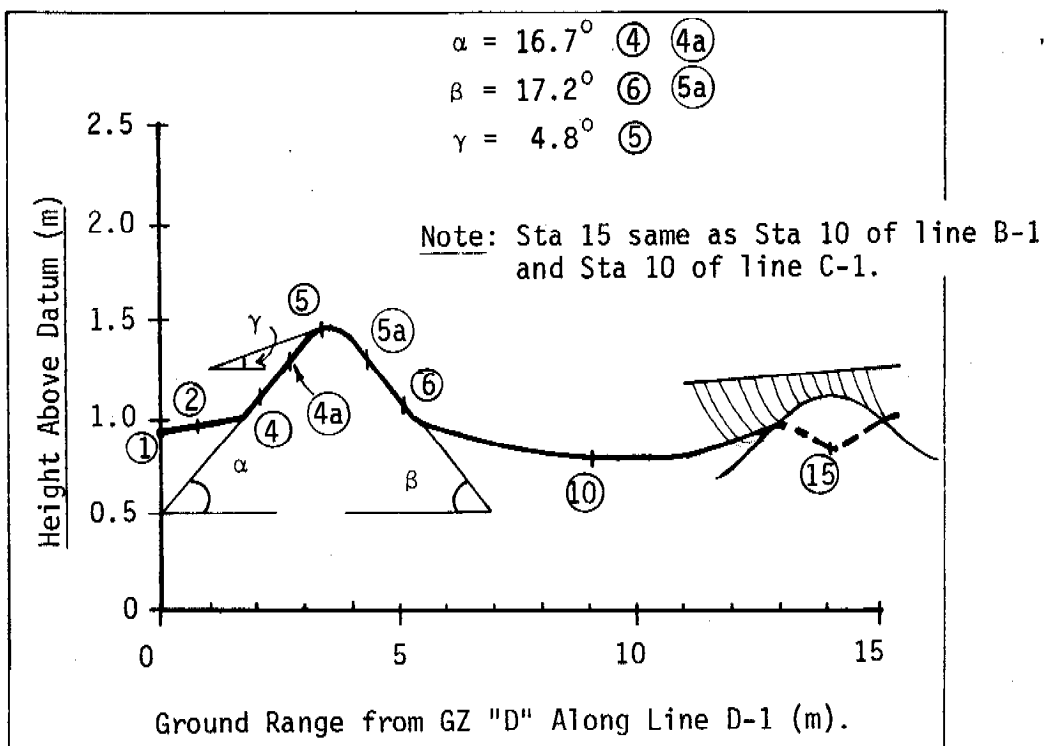
Fig. 24. Profiles of Terrain Along Gauge Lines D-1 and D-2.

52
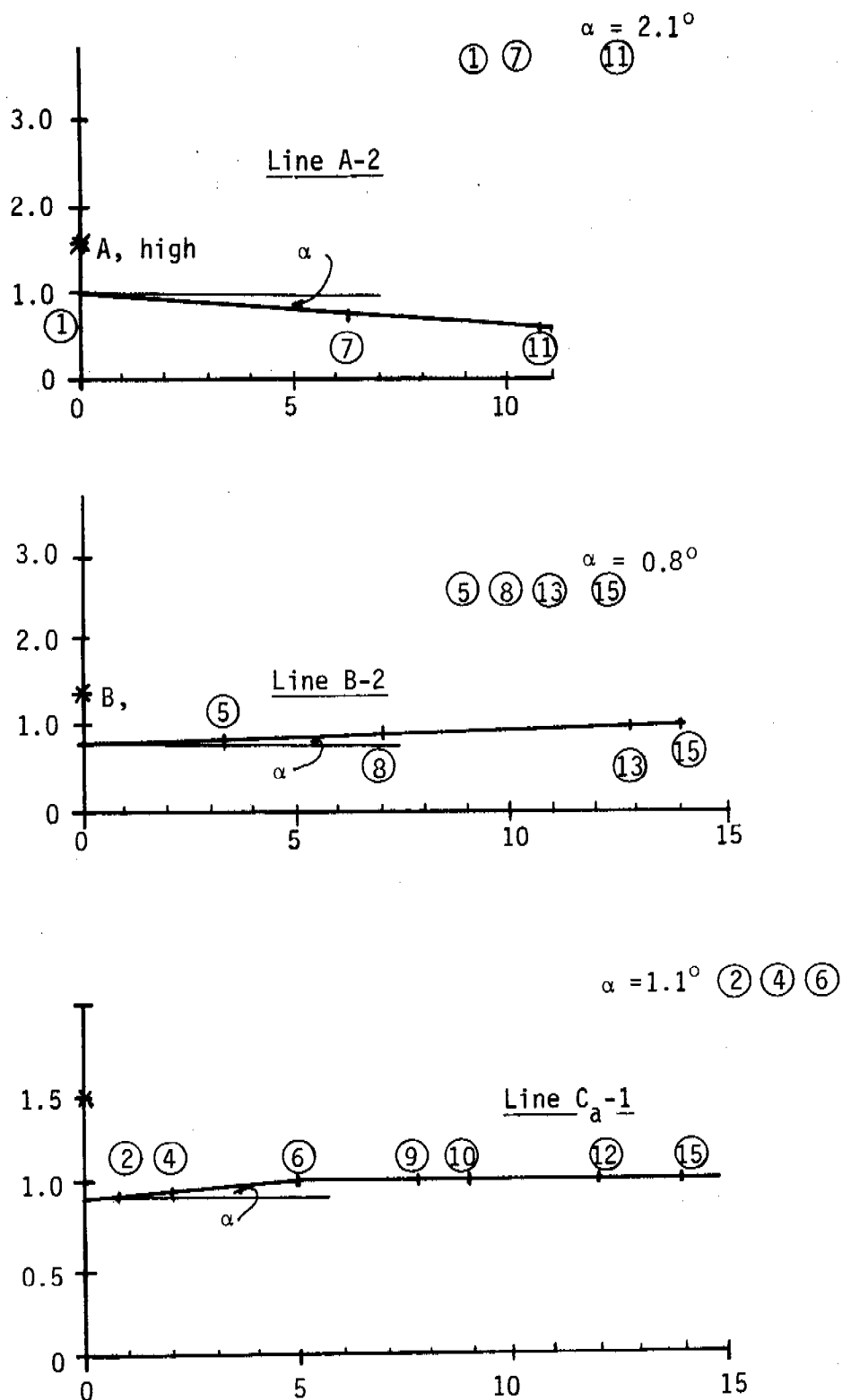
Fig. 25. Flat Terrain Monitoring Lines A-2, B-2, and C_a-1.

Table 4

Elevation (Modified Effective Slope) Angles at
Stations Along Terrain Gauge Line*
(degrees)

Gauge Line	A-1	B-1	C-1	C-2	C-3	C-4	D-1	D-2
Station Number								
1	0			0.7	1.4		2.3	0.7
2					1.4		2.3	
3		1.4	-6.4			4.0		
4	0			0.7			16.7	0.7
5	31.0	1.4	-6.4		1.4		4.8	
6	9.7	19.3	-6.4				-17.2	8.0
7	-24.2	41.2				4.0		
8	-24.2	-36.3	14.8	0.7	6.3			8.0
9	-15.6	-21.3						
10	0	14.0	4.0	28.8	10.5	13.5	0	9.3
11	0	14.0		14.6		6.8		
12		5.3		-16.7		-10.2		
13			0			-10.2		
14								
15	0			0	-9.1		0	-14.6
4a							16.7	
5a	31.0						-17.2	

* These angles are measured along each gauge line. They are not slope angles (i.e., elevation angles θs drawn normal to a contour as in Fig. 1), nor are they Effective Slope Angles θ as defined in Eq. 1a and Fig. 2. They are the angle θ' given in Eq. 1b, and are very nearly equal to θ_s as shown in Table 1.

54

range of interest (where the PCB transducer would be used), range from about 340 to 600 m/s. Thus, the time required for the shock front to cross the sensitive area of the transducers range from about 9 to 16 µs. (In the specific case in which a transient duration of 40 µs is anticipated, the crossing time would be about 14 µs, i.e., about 1/3 the duration of the transient.)

If enough were known about the transducers (viz, their sensitivities with only part of their diaphragms subjected to pressure) and the velocity of the shock wave itself, the characteristics of a transient could be derived or recon-structed from a record. But there would always be some uncertainty, at least because an element used in the reconstruction -- shock front velocity -- depends on a quantity to be derived -- shock front pressure.

For this reason, it is recommended that where short-time transients are ex-pected, an attempt be made to record head-on pressure at the shock front, from which actual shock-front pressure can be derived by use of the Rankine Hugonoit relationships for the shock front. An above-surface mounting block into which one of the PCB transducers could be placed in a head-on orientation would be small enough that any effects of its presence would not be detected at other stations. Such effects are well dissipated within about 10 block heights, and the minimum distance between adjacent stations is 40 cm (between Sta. 2 and 3, and 13 and 14, see Table 2). With duplicate test conditions, a head-on measure-ment might be made during one test to document the shock front, and a side-on measurement made during a second test to document the remainder of the pulse.

3. Recording System. The recording system used to record the signals gen-erated by the transducers, must, of course, have response characteristics com-patible with quantity to be recorded. A typical magnetic tape system when operated in a standard FM record mode, has a maximum band width of about 0 to 20 kHz (one db down), though an extended mode increases this to about 0 to 80 kHz (e.g., Honeywell Model 7610). A direct recording mode is also available which changes the maximum band width to about 0.4 to 700 kHz. Other recording systems (e.g., cathode ray oscilloscopes) can increase the high frequency response still further.

4. Data Analysis System. If the data analysis system incorporates some form of sampling at a fixed time rate, care must be taken that the system does not, in effect, act as a relatively low band-pass filter, which could very well modify (or totally eliminate) important pulse characteristics. If the recording system incorporates an analog mode, it is strongly recommended that this be played back and re-recorded for visual inspection at a proper speed. Visual examination is mandatory in any analysis system with inadequate (or borderline) sampling rate.

IV. PREDICTIONS

A. General Considerations

Predicted shapes of the overpressure vs time pulses at those stations along

55

the 11 gauge lines -- 52 stations in all -- where overpressure pulses should
be modified to a significant degree by the topography of the model in Fig. 15,
are given in Appendix A (along with the flat-terrain pulse at each station for
comparison). For reasons to be discussed in the next section, where appropriate, predictions have been made of shock front pressures using both the Whitham
theory curves (Figs. 5 and 6) and the curves based on small charge studies
(Figs. 7 and 8). The shapes of later parts of the pulses were derived from
Figs. 9 and 10.* Critical elements of the predicted pulse (e.g., shock front
pressures, durations) are tabulated in Appendix B.

In each set of traces (i.e., for stations along a particular gauge line
using a particular GZ) predictions for the first station to experience any
topographic effects are differentiated from those for stations further from GZ.
(This is because predictions of pressures behind the shock front at these later
stations were made with untried methods.) At each first station, the combination
of shock front prediction made with the Whitham theory curves (Figs. 5 and 6),
and later time predictions made with Figs. 9 and 10, is drawn as a solid line.
At each more distant station that combination of predictions is drawn as a dashed
line to indicate increased uncertainty. At all stations, however, where shock
front predictions were made with the small charge curves of Figs. 7 and 8, the
initial part of that pulse is shown as a dotted line.

After finding shock front overpressures, a pressure ratio behind the front
was found from Figs. 9 and 10 using a low value of t/L (between 0.1 and 0.3).
Actual time was then calculated by multiplying the value by L, the distance from
the initial slope changes. Pressure in the incident pulse at that time was found
from the plot of incident pressure vs time (Fig. 17), and actual pressure at
that time was calculated by multiplying incident pressure by the pressure ratio
from Figs. 9 and 10. Curves were then drawn connecting shock front pressures
with the pressure-time point calculated as described. Simple curves or straight
lines were employed to connect these two points except with stations on falling
slopes for which shock front pressures were derived from the Whitham theory
curve, Fig. 6. In those cases, an initially sharply rising curve was employed
to indicate the possibility of a rapid, early-time rise in pressure from shock
front values. The reason for doing this is discussed more fully in the next
section of this report.

B. Discussion of Results

The general natures of the predicted pressure-time pulses were as expected:
shock front pressures increased on rising slopes, and decreased on falling
slopes, and the greater the slope angle the greater the change from incident
pressure. The characteristics of some of the prediction changes, however, are
of some interest.

For example, some of the pulses at stations on rising slopes are of very
short duration. Sta 6 along line B-1 with GZ "B", and Sta 10 along line C-2
with "C" (reproduced in Fig. 26) are particularly noteworthy in that regard.
At both stations, the spike is 23-24 kPa high based on Whitham theory (about
11-13 kPa high based on small charge results). At Sta 10, the spike duration

---

* Special methods were used for Sta 11 and 12 of Line C-2. See Table B-2.
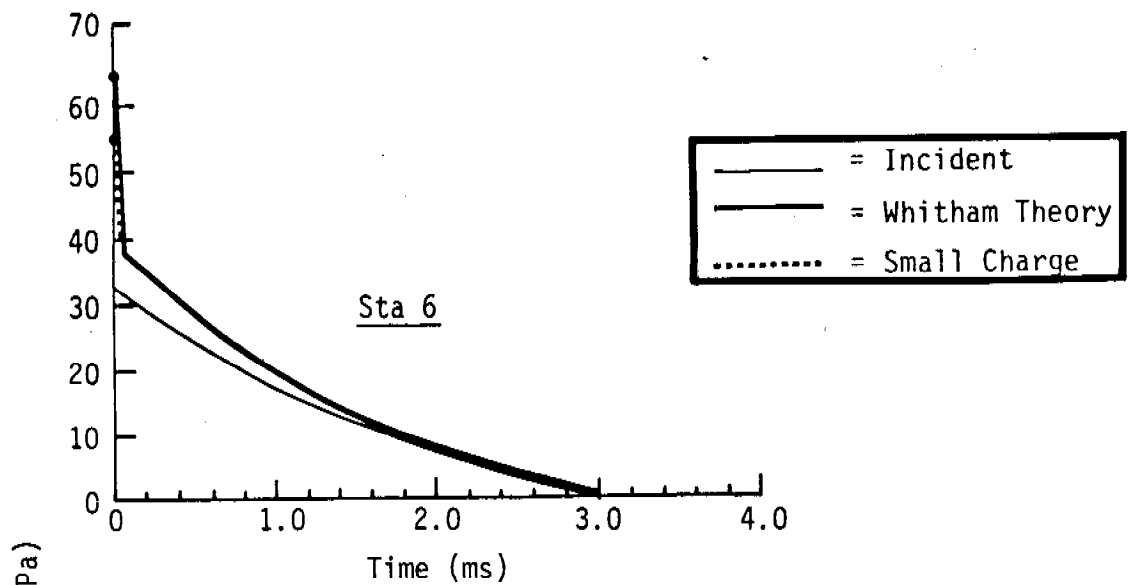
A. Overpressures along Line B-1 from a Burst over GZ "B".
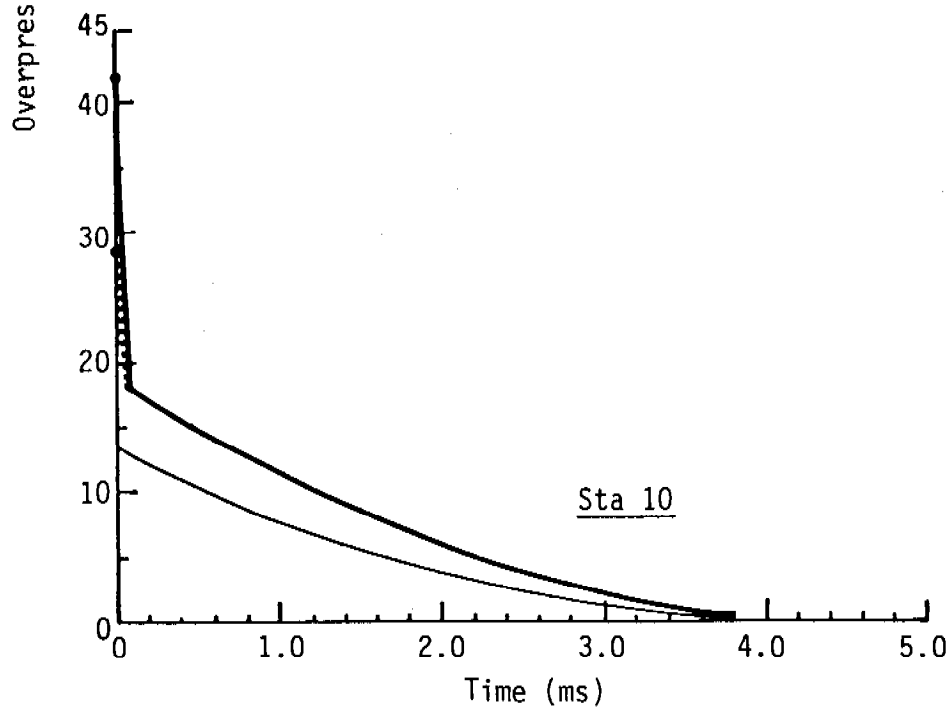
B. Overpressures along Line C-2 from a Burst over GZ "C".

Fig. 26. Pulse Shapes on Rising Slopes Showing Short Duration Pressure Spikes.

is about 0.08 ms, at Sta. 6, it is about 0.04 ms.

Measurements on negative slopes may also display sharp pressure changes if Whitham theory for pressure of the shock front holds. At stations such as No. 8 along line A-1 with GZ "A", No. 12 along line C-2 with GZ "C", and No. 15 along line D-2 with GZ "D" (all reproduced Fig. 27), shock-front pressure predictions from Whitham theory are 1/3 to 1/2 of those based on measurements with small charges. As discussed more fully in the next section of this report, this would imply very rapidly rising pressure close to the shock front.

Finally, note should be made of the effects of channeling on the pulses along lines C-1 and D-1. Fig. 12 indicated that this valley would produce a pressure ratio of 1.25, that is, a 25% increase in overpressure. In the case of Sta. 10 along line C-1 with GZ "C" this was superimposed on a 70% increase (Whitham theory) due to rising slope effects to produce an overall increase of over 110% in shock front overpressure. (The overall increase, using small charge based shock front predictions, is about 80%.) In the case of Sta 15 along line D-1 with GZ "D", the effect of channeling was simply to increase the incident pulse by 25%. Predicted pulses at both stations are reproduced in Fig. 28.

V.   APPRAISAL OF PREDICTION METHODS
AND
SOURCES OF NEW INFORMATION

Among the more important findings of this effort to investigate and apply techniques for predicting terrain effects on blast, were: that there are unresolved conflicts between two approaches, both of which had, at one time or another, been recommended for use in the field; that there could be some question about the accuracy of some of the available prediction curves; and that, for certain terrain situations, no techniques for predicting terrain effects had been developed. Since one of BRL's major purposes in undertaking the overall program was to uncover such deficiencies (if they existed) this phase of the program could be considered a success.

In this section of the report the causes of these findings as they apply to predictions of pressures both at the shock front and behind the front are discussed first, followed by a brief discussion of ways in which needed additional information could be acquired.

A.   Shock Front Predictions

In Section II, two different sets of curves are given for predicting the effects of both rising and falling slopes: one from an approximate theory due to Whitham (Figs. 5 and 6); and one based on measurements with small charges (Figs. 7 and 8). The Whitham theory curves are more extensive than those from small charge tests, though both sets generally cover the overpressure range of interest. For the most part, Whitham theory predictions for rising slopes are higher, and for falling slopes are lower than the small charge predictions. As can be seen in Figs. 29 and 30, for certain conditions,

58

Legend:

——— = Incident

– – – = Whitham Theory

········ = Small Charge
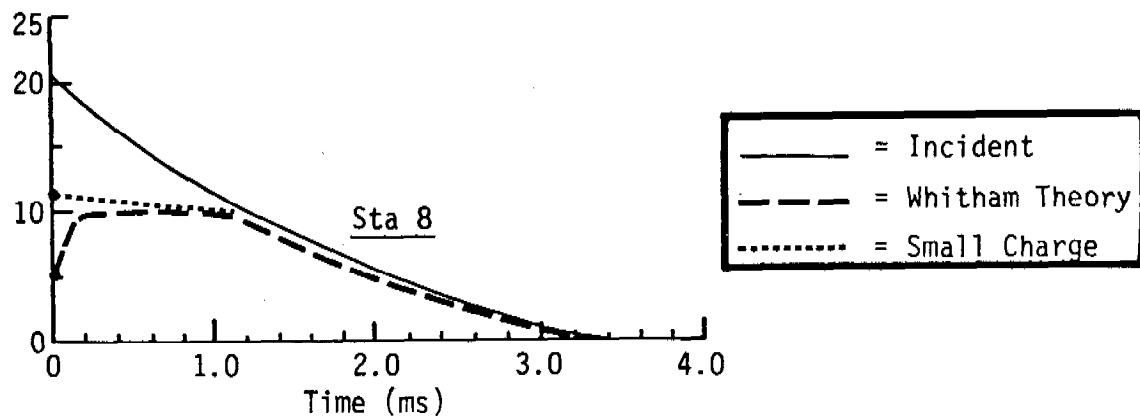
A. Overpressures along Line A-1 from a Burst over GZ "A".
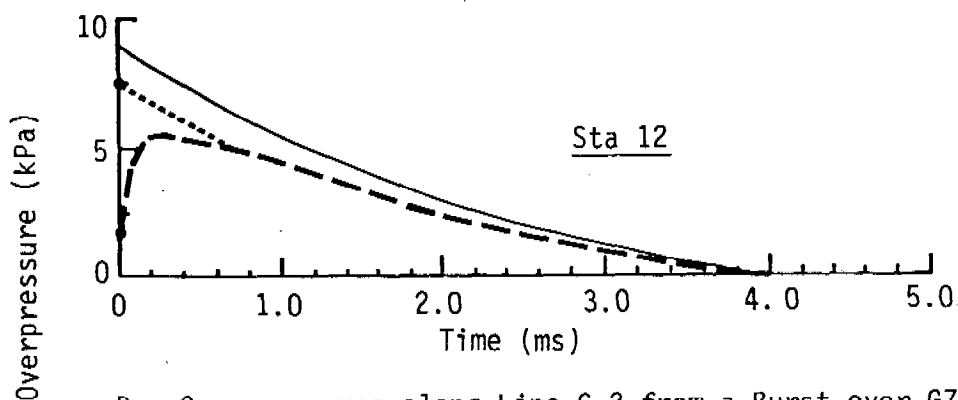
B. Overpressures along Line C-2 from a Burst over GZ "C".
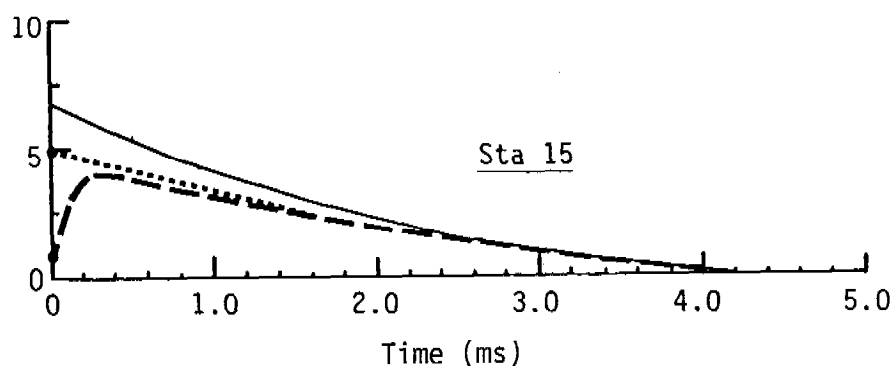
C. Overpressures along Line D-2 from a Burst over GZ "D".

Fig. 27. Pulse Shapes on Falling Slopes.
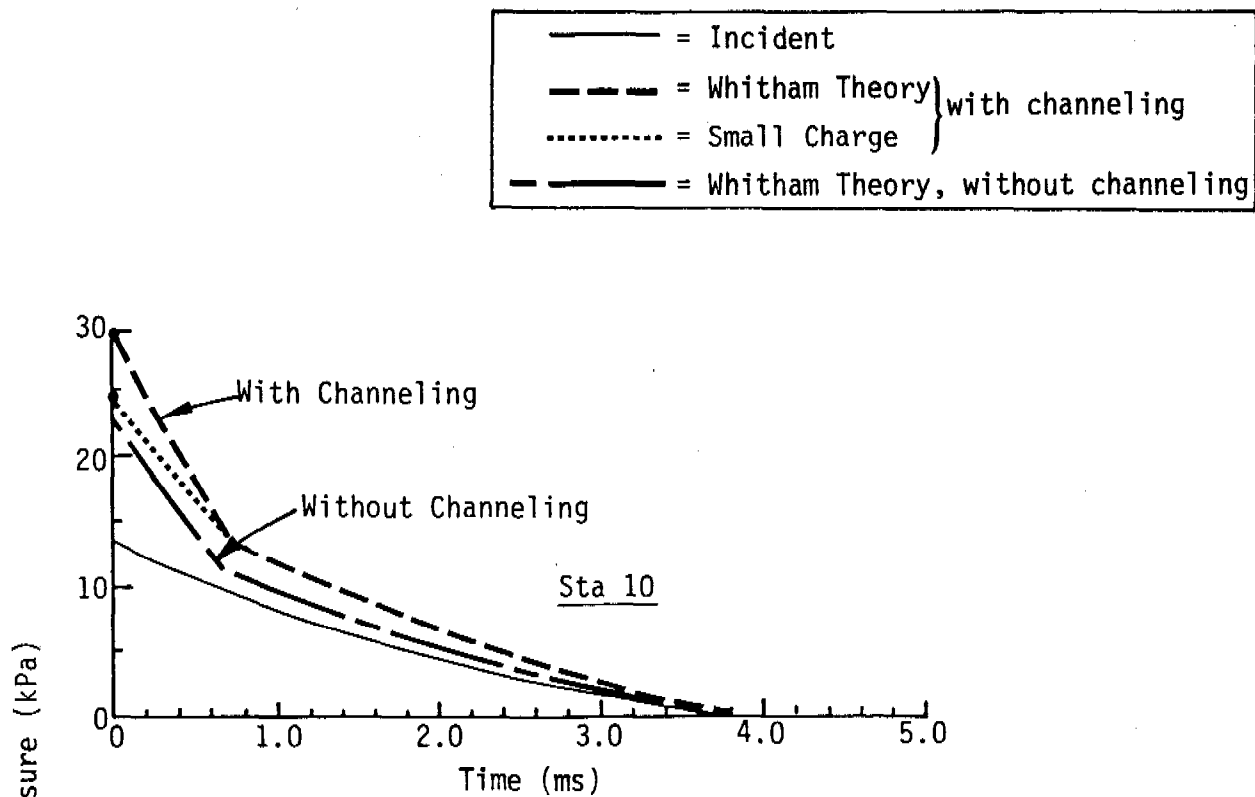
Legend:

——————— = Incident

— — — — = Whitham Theory ⎫ with channeling
·············· = Small Charge ⎭

— — = Whitham Theory, without channeling

With Channeling

Without Channeling

Sta 10

Overpressure (kPa)

Time (ms)

A. Overpressures along Line C-1 from a Burst over GZ "C".

With Channeling

Sta 15

Without Channeling

Time (ms)
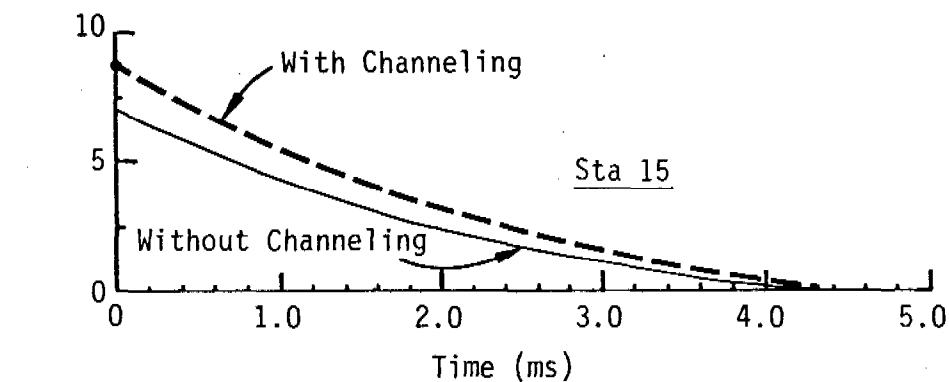
B. Overpressures along Line D-1 from a Burst over GZ "D".

Fig. 28. Effects of Channeling.
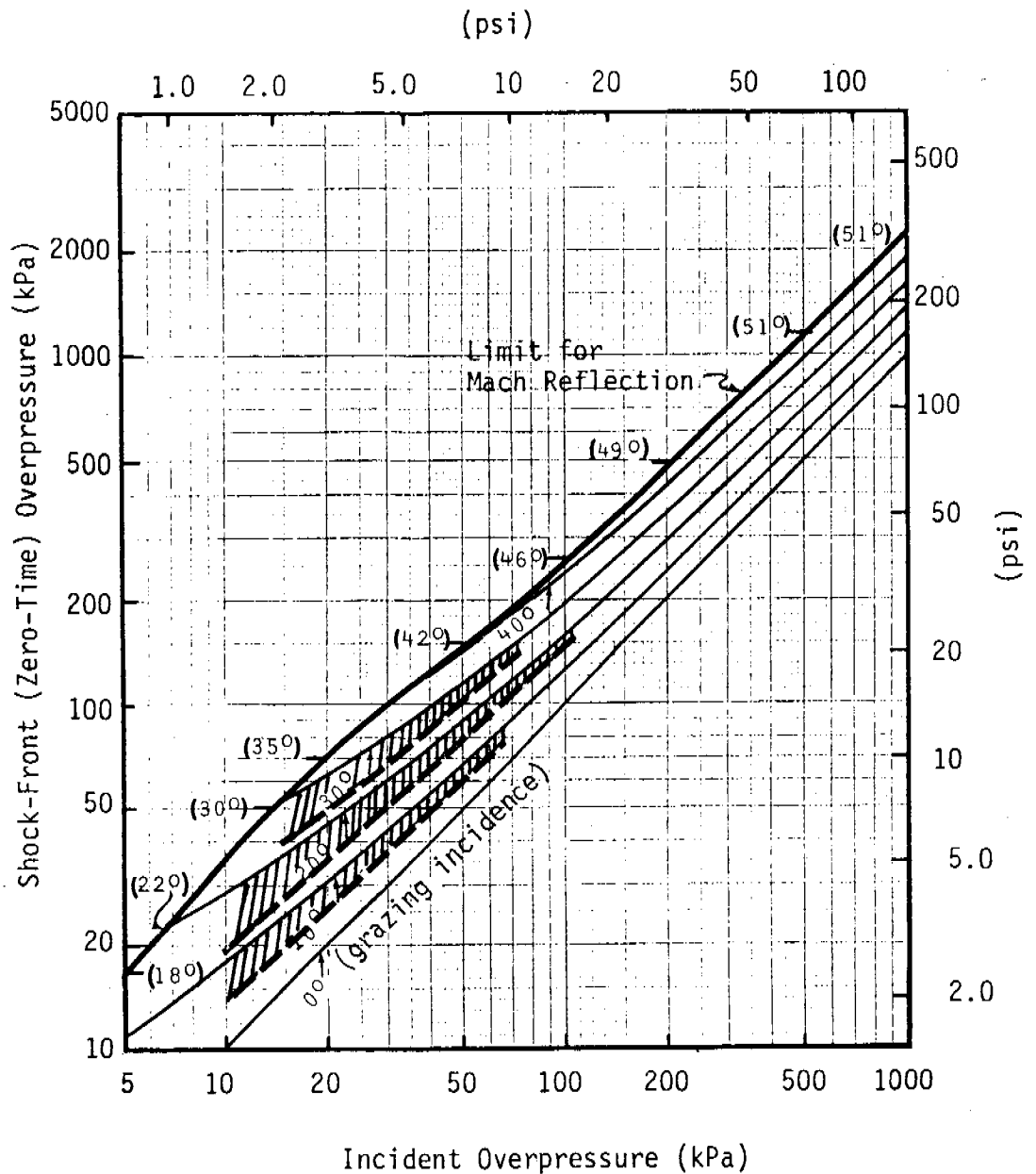
Fig. 29. Overpressure at the Shock Front on a Rising Slope (Reflected Overpressure) vs Peak Incident Overpressure for Shock Waves Undergoing Mach Reflection. From Whitam Theory and Small Charge Tests.

Note: Numbers in parenthesis identify extreme (limit) slope angles along the "Limit for Mach Reflection" line. Other numbers on the figures identify the slope angles to which each curve applies.

Solid lines are Whitham Theory; dashed lines are from small charge tests. Shaded areas show differences.
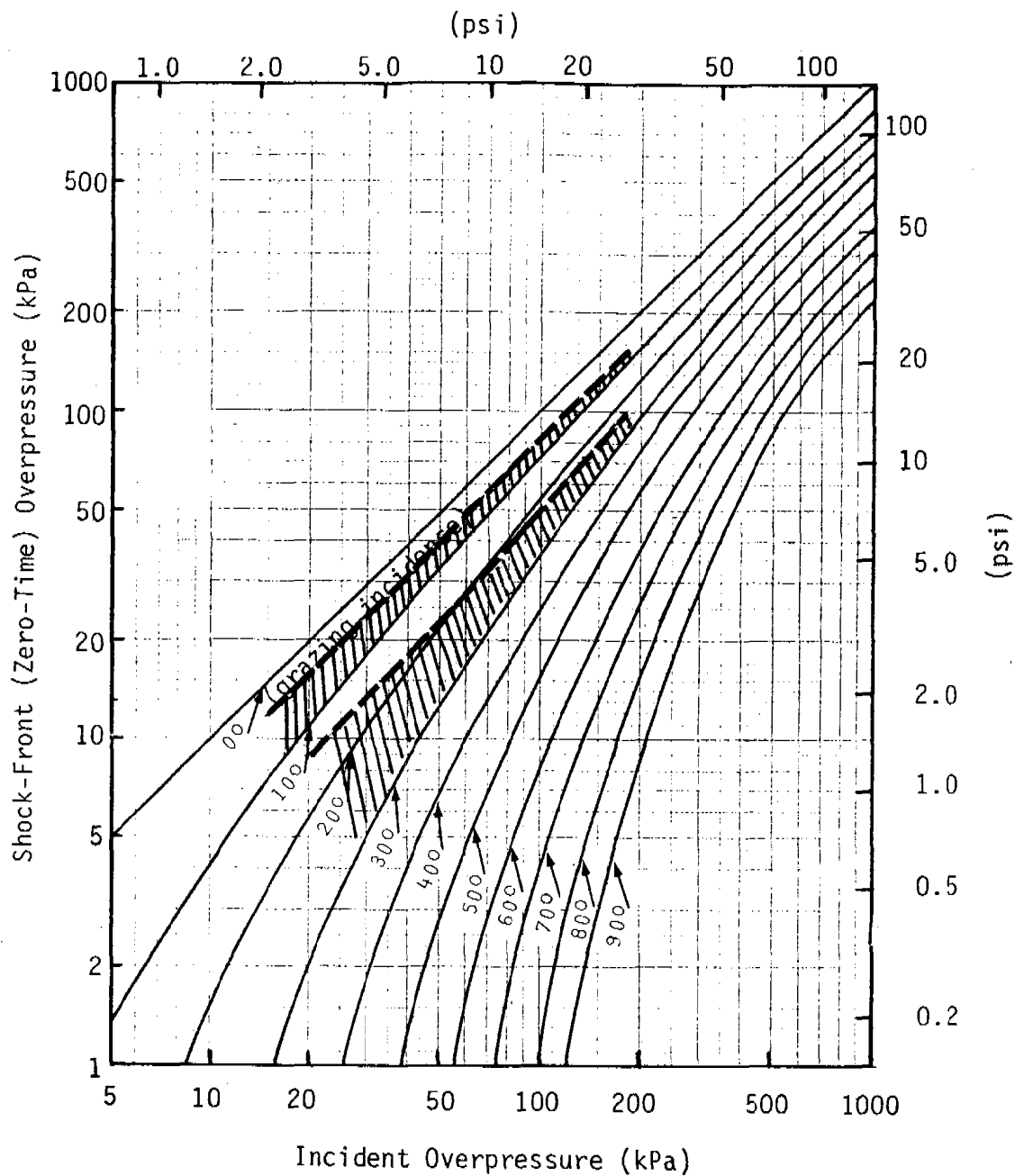
Fig. 30. Overpressure at the Shock Front on a <u>Falling Slope</u> (Diffracted Over-pressure) vs Peak Incident Overpressure. <u>From Whitham Theory</u> and Small Charge Tests.

Note: Numbers on the Figure identify the slope angles to which each curve applies.

Solid Lines are Whitham Theory; dashed lines are from small charge tests. Shaded areas show differences.

differences in predictions of shock front pressure can be substantial.

As already noted, many years ago it was recommended that the Whitham theory curves replace the small charge curves, because of both their theoretical basis, and the excellent agreement of predictions with shock tube measurements shown in Fig. 3. Upon review, however, whether there is adequate justification for this action is open to question, especially over the pressure region of interest (taken to be that for collateral damage, and damage to exposed material and equipment other than tanks, i.e., between about 10 and 100 kPa.

On the one hand, while the agreement between Whitham theory and shock tube experiment shown in Fig. 3 is very good, the comparisons only extend down to shock strengths of about one, that is, to incident overpressure of about 100 kPa -- at the upper end of the range of interest. On the other hand, the measurements made with small charges were concentrated at overpressures between about 10 and 200 kPa, that is, covering the entire range of interest. Thus, in this range, there is experimental evidence of shock front overpressure levels which do not agree with Whitham theory predictions.

It is possible, however, that differences between the two sets of curves could be due to limitations inherent in the small charge test program, and thus that the conflicts between the two sources are only apparent rather than real. As can be seen in Fig. 10, and perhaps more graphically in Fig. 26, blast pulses on rising slopes can be characterized by pressure spikes at the shock front of very short duration. While the basic recording system used in the small charge studies was adequate to record such spikes, some rounding of the recorded pulse was inevitable (because of the time required for the shock front to pass over the sensitive area of the gauges used), and some subjective interpretation of the shock wave records was required (because each gauge displayed different overshoot characteristics). In addition, the recording system, which was based on photographic recording of a single sweep of a cathode ray oscilloscope (CRO), could have masked some very short-time phenomena. Thus, reported shock front pressures on rising slopes from the small charge studies might be lower than they should have been, and curves based on this information would lead to low predictions of pressure.

In a similar fashion, with falling slopes, the point at which maximum shock front pressure is attained can be very difficult to locate, if -- immediately after shock passage -- pressures rise rapidly. The finite time required for shock front passage over the gauge, and the method used to record the trace would both tend to mask the point. Thus, again because of gauge characteristics and recording system limitations, reported shock front pressures from the small charge studies might be higher than they should have been, and curves based on that information would lead to high predictions of pressure.

B. Pressure Behind the Shock Front

The prediction curves for pressures behind the shock front on falling slopes (Fig. 10) suffer from many of the same uncertainties as the curves for overpressures at the shock front. They were derived from tests with small

charges recorded in such a way that subtle changes between incident pressures (also from measurements) and pressures on a slope might be difficult to find. The prediction curves for pressures on rising slopes (Fig. 9) do not, in general, have the same shortcomings; they were derived from White's shock tube tests, which employed optical interferometric techniques instead of pressure transducers for determining shock strengths. The values at t/L = 0 for these curves, however, (that is, the values at the shock front) were derived directly from the small charge tests, and near that value of t/L, the curves should have increased uncertainty. Thus, there is some question about the overall accuracy of the falling slope curves, and about values near the shock front of the rising slope curves.

In addition, as pointed out in Section II, there exists no simple technique to account for the effects of successive slopes on pressures behind the shock front, as exists for pressures at the shock front, where the local slope concept appears to work quite well. The quasi-local slope approach first used in this report to make predictions, is essentially an attempt to solve the problem by avoiding it, on the basic ground that further refinement is not likely to be warrented.

What this approach does, for stations on slopes other than the first encountered, is to delimit a portion of the pressure-time pulse immediately after passage of the shock front, during which predictions are just not attempted. The time length of this excluded portion of the pulse is based on the distance to a station in question from the first slope change that a shock wave encounters. Actual time after shock front passage is calculated by multiplying particular t/L values used with Figs. 9 and 10 by a length L. Use of a value of L based on the first slope change encountered in essence defines the portion of the pulse over which the influence of the first slope change is manifest. Other slope changes located between the first encountered and a particular measuring station will, at any given value of t/L, influence the pulse at shorter actual times, but no attempt is made to identify these influences.

This technique has not been used before. Whether it yields reasonable results should be determined by the test program because of the very wide variety of topographic conditions built into the program.

C. Acquisition of Additional Information

It is anticipated that many of the conflicts and inaccuracies just discussed can be resolved by the experimental phase of the overall program. As noted earlier, however, that phase could have some of the same experimental problems as those that led to the conflicts and inaccuracies in the first place, that is, transducer geometry and recording system frequency response might limit the accuracy of measurement of some of the short-time transients, and shock front pressures. (Transients are predicted to be as short as 40 μs; time required for the shock front to pass over the sensitive area of a gauge will be from 9 to 16 μs.) Ways of overcoming some of these experimental difficulties are discussed earlier in this report.

64

It is possible, however, that the experimental program could not resolve all conflicts to the accuracy desired, and additional work to do so would be required. A program to acquire the necessary new information could benefit both from lessons learned during the earlier program, and from advances in analytical capabilities made since their completion.

For example, the earlier programs showed that information from two-dimensional analyses and tests could be applied to the basic three-dimensional situation inherent in the terrain effects problem, i.e., shock wave expanding spherically in free air encountering and propagating over assymetric topography. Therefore, much relevant information could be derived from two-dimensional approaches, namely, carefully thought out computer analyses, and shock tube programs. The latter would extend and improve White's and Bleakney's work, now some 30 years old (Refs. 11 and 26). Such programs could well be followed with additional high-explosive tests in either two-dimensional, or three-dimensional geometries, possibly with larger charges than will be employed in this program, as was done some years ago (Ref. 27).

VI. REFERENCES

1. Merrit, M., "Some Measurements of Terrain Effects on Blast Waves (U)", Operation BUSTER-JANGLE, WT-301, 12 February 1952, Secret-RD.

2. Todd, "A Scale-Model Study of the Effects of Symmetric Ridges on Blast Overpressures", SC-3335 (TR), May 3, 1954. Confidential.

3. Willoughby, Kaplan, Condit, "Effects of Topography on Shock Waves In Air", BRC, AFSWC TR-57-9, August 1956.

4. Kaplan, K., "Effects of Topography in High Shock Strength Regions", URS Corporation, Burlingame, January 1965.

5. Willoughby, Fitch, Condit, and Ketler, "Effects of Topography on Shock Waves in Air", BRD-54-6A1, Interim Report, January 1954-July 1954, pp 57-65. Secret.

6. "Effects of Rough and Sloping Terrain on Air Blast Phenomena", Operation PLUMBBOB- Projects 1.8a and 1.8c, WT-1407, September 15, 1960. Confidential FRD.

7. "Nuclear Weapons Blast Phenomena", DASA 1200, Vol. II.

8. Wallace, N.R., "Effects of Topography on Dynamic Pressure", URS B170-10, DASA-1323, URS Corporation, Burlingame, California, 1961.

9. Arave, R.J. and N.R. Wallace, "Dyanamic Pressure from Blast Waves: Methods for Predicting the Effects of Terrain", DASA-1732, URS 649-6 Final Report, URS Corporation, Burlingame, California, February 1966.

10. Whitham, G.B., "A New Approach to Problems of Shock Dynamics", J. Fluid Mech., Vol. 2, 1957, p 145.

11. White, "An Experimental Survey of the Mach Reflection of Shock Waves", Princeton, U., Dept. of Physics, Tech. Report II-10, August 21, 1951.

12. Wilton, C., K. Kaplan, and N.R. Wallace, "Study of Channeling of Air Blast Waves", DASA-1605, URS 170-19, prepared for Defense Atomic Support Agency by URS Corporation, Burlingame, California, December 1964.

13. Kaplan, K., "Techniques for Predicting the Effects of Topography on Air Blast in Real Terrain", URS 649-7, Final Report, URS Corporation, Burlingame, January 1967.

14. _____, "Capabilities of Nuclear Weapons", (EM-1) Defense Nuclear Agency, Washington, D.C.

15. Brode, H.L., "Nuclear Blast Wave Calculations Including Thermal Losses", RM-2076, The Rand Corporation, December 1957 (S).

16. Polachek, H., and R.J. Seeger, "Regular Reflection of Shocks in Ideal Gases" Navy Department, 12 February 1944.

17. Sachs, R.G., "Dependence of Blast on Ambient Pressure & Temperature", BRL 466, May 1944.

18. Brode, H.L., "A Review of Nuclear Explosion Phenomena Pertinent to Protective Construction", The RAND Corporation, Santa Monica, CA, May 1964.

19. _____, Nuclear Weapons Blast Phenomena (DASA-1200) Vol. IV, "Simulation of Nuclear Air Blast Phenomena With High Explosives (U)", Defense Nuclear Agency, Washington, D.C., 31 July 1973.

20. Reisler, R.E., "H.E. Height-of-Burst Blast at Moderate to Low Overpressures", In Draft, to be published as a BRL Memorandum Report.

21. Von Neumann, J. "Oblique Reflection of Shocks", Navy Department Bureau of Ordinance Explosives Research Report No. 12, Oct. 12, 1943.

22. _____, "Structures to Resist the Effects of Accidental Explosions", Departments of the Army (TM5-1300), the Navy (NAVFAC P-397), and the Air Force (AFM 88-22), June 1969.

23. Kinney, G.F., "Explosive Shocks in Air", The MacMillan Co., New York, 1962.

24. Brode, H.L., "A Calculation of the Blast Wave from a Spherical Charge of TNT", The RAND Corporation, Santa Monica, CA, 21 Aug. 1957.

25. Kaplan, K., N.R. Wallace, and A.B. Willoughby, "Effects of Topography and Shielding", Prepared as Sections 5.1 and 5.2 for the Publication Nuclear Weapons Blast Phenomena (U), DASA-1200, 1959.

26. Bleakney, W., "The Diffraction of Shock Waves Around Obstacles and the Transient Loading of Structures", Technical Report II-3, Princeton University, Department of Physics, 16 March 1950.

27. Keefer, J.H. and J.D. Day, "Terrain Effects on Blast Wave Parameters", BRL Report No. 1319, Apr 1966, Aberdeen Proving Ground, Maryland.

Appendix A
PREDICTED OVERPRESSURE vs TIME PULSES

        Included in this appendix are predicted pulses for all stations which
should experience terrain effects along the gauge lines originating from
the eight ground zeros shown in Figs. 18, 19, and 20, and tabulated in Table 3.
For each ground zero, a sketch (from Figs. 21 through 24) and a key identifies
the origin of the predicted curves. For the first station on each slope, pulses
starting with Whitham theory predictions at the shock front are shown as solid
lines; for all other stations, because of increased uncertainties, they are
shown as dashed lines. At all stations, pulses starting with shock front
predictions based on small charge studies are shown as dotted lines.
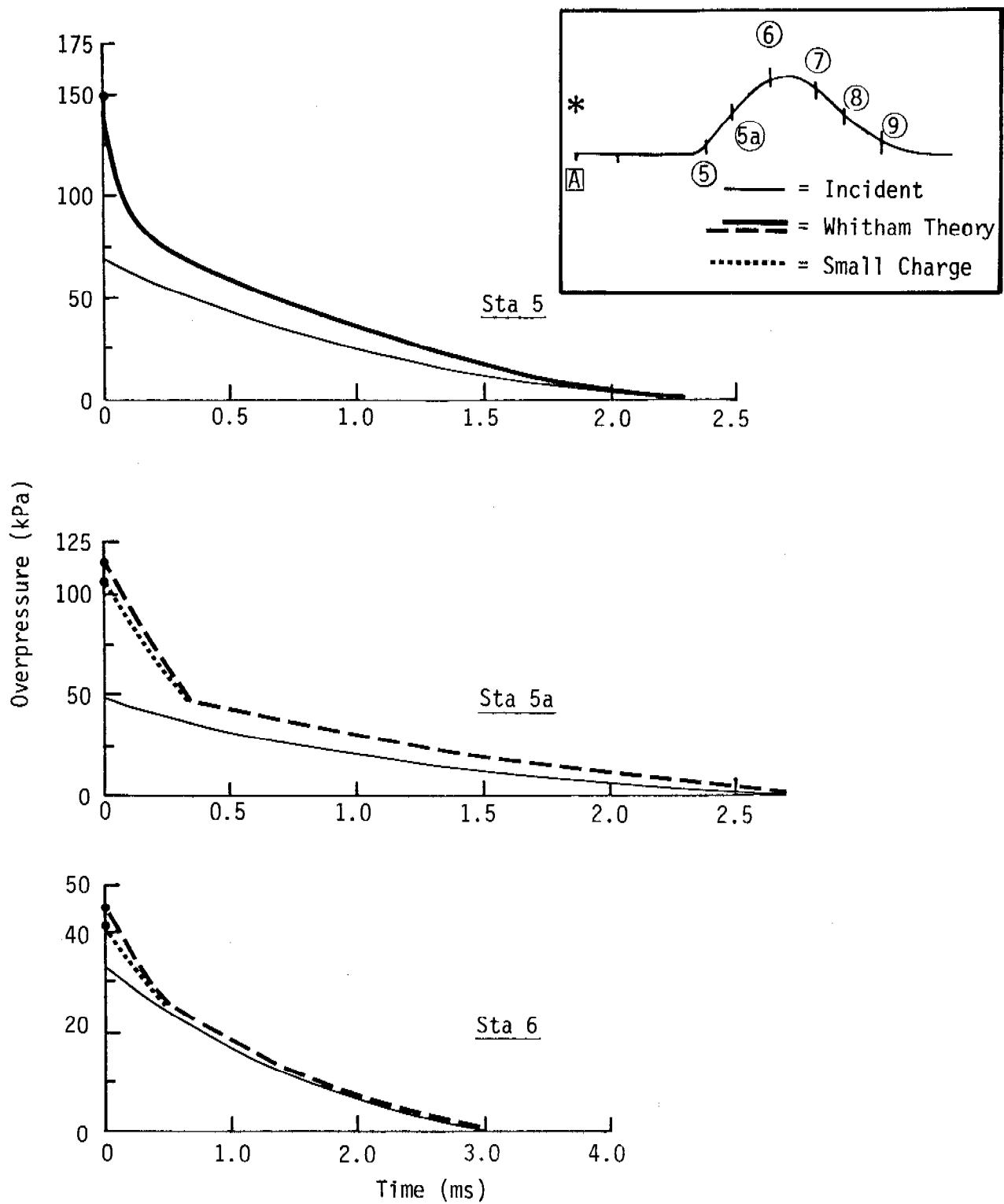
Fig. A-1a.   Overpressures along Line A-1 from a Burst over GZ "A".
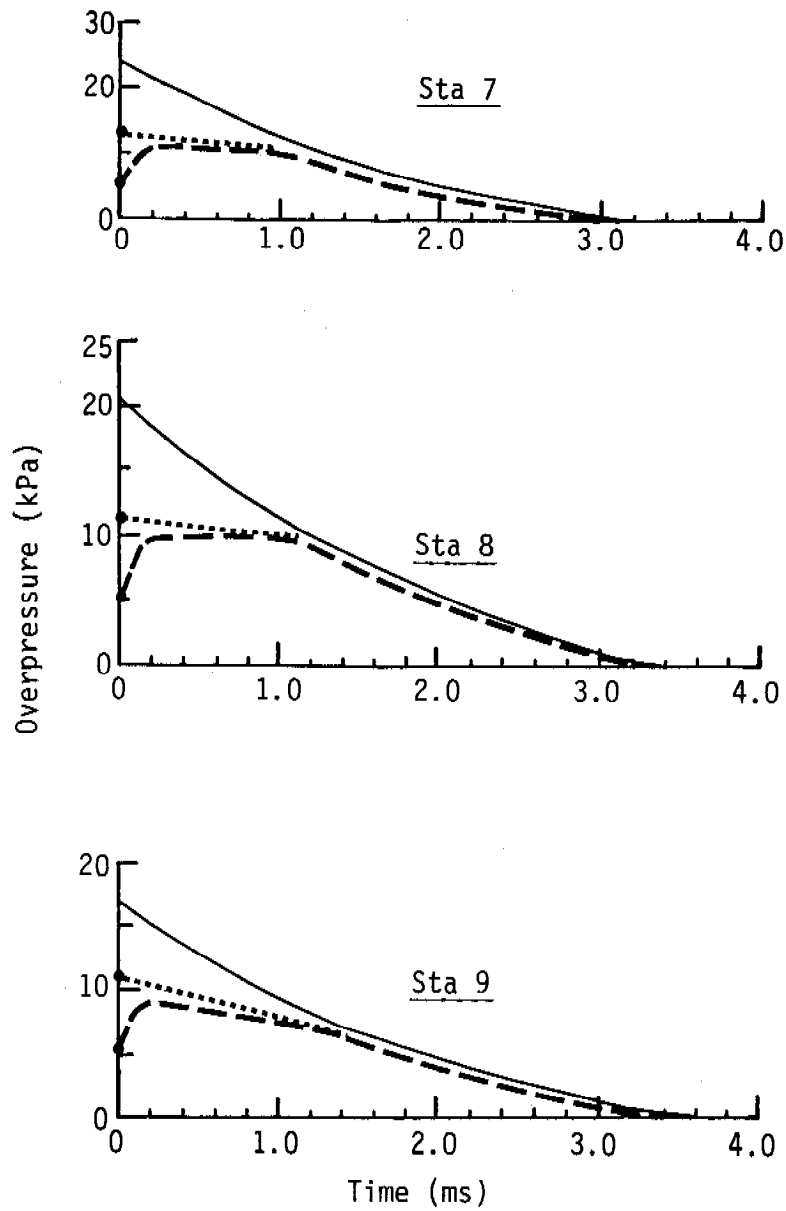
Fig. A-1b. Overpressures along Line A-1 from a Burst over GZ "A" (cont'd).

Fig. A-2a. Overpressures along Line B-1 from a Burst over GZ "B".

Sta 6

Sta 7
(Regular Reflection)

Sta 8

Sta 9

Overpressure (kPa)

Time (ms)

—— = Incident
– – – = Whitham Theory
········ = Small Charge
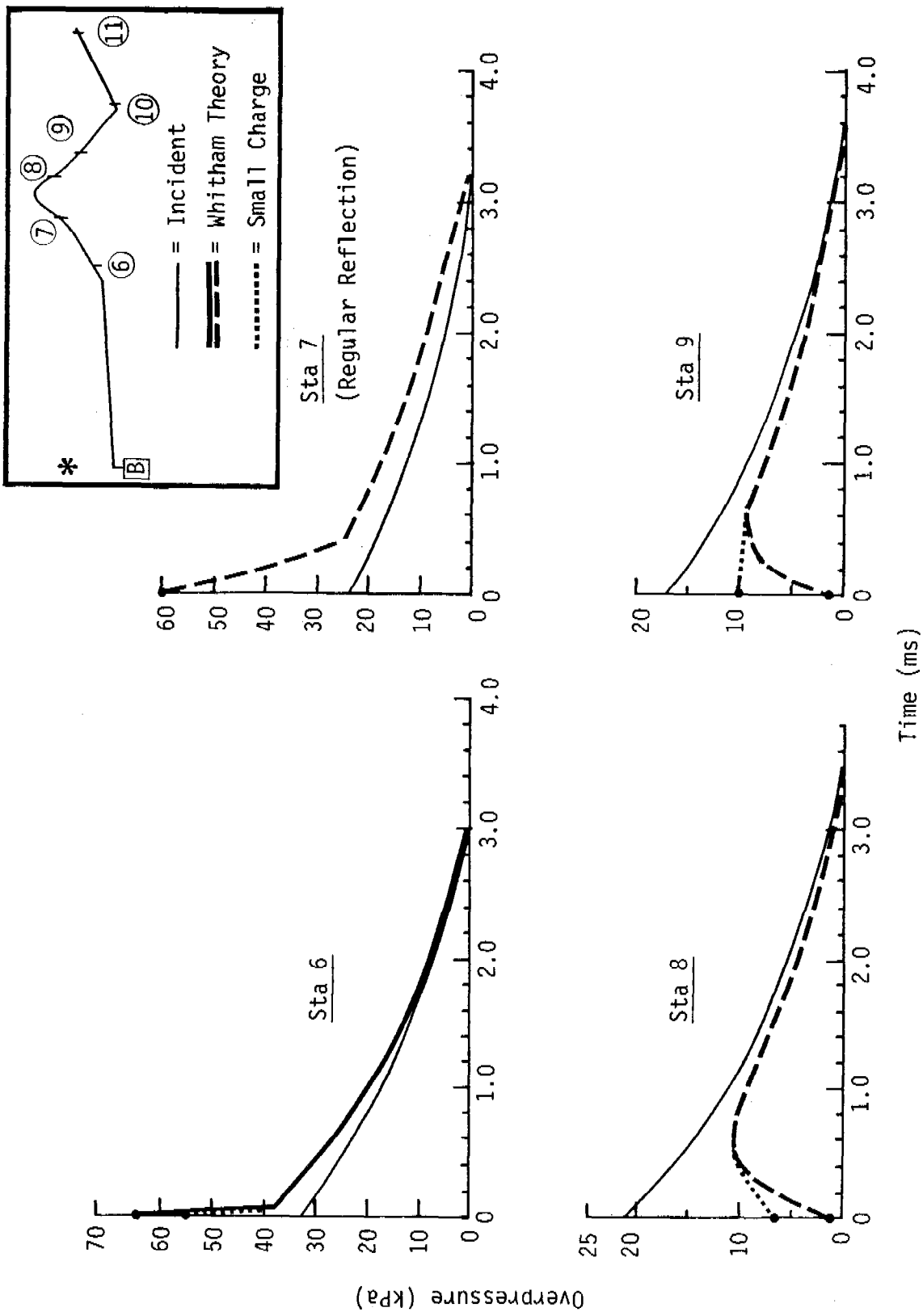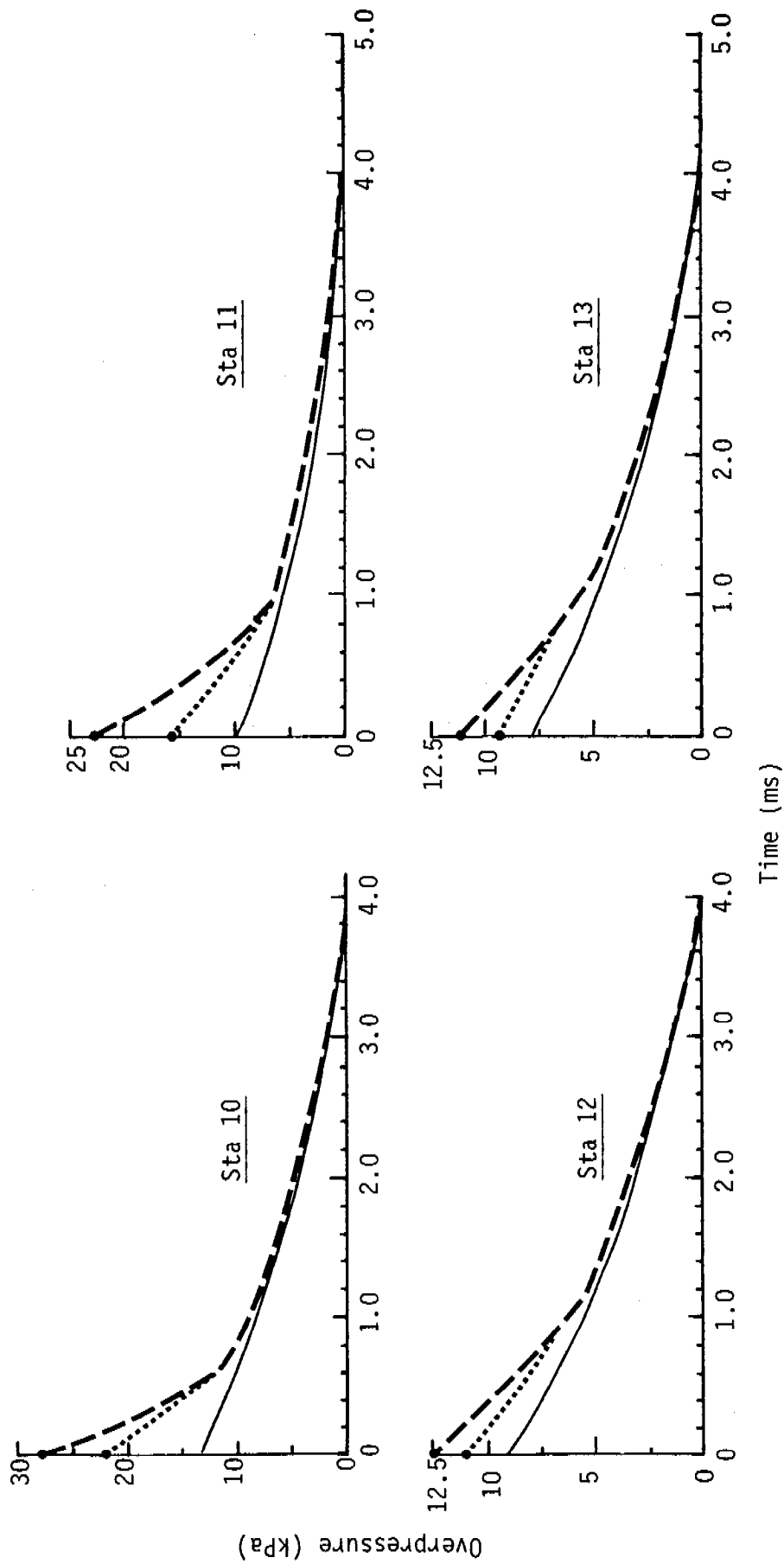
Fig. A-2b. Overpressures along Line B-1 from a Burst over GZ "B" (cont'd).

73
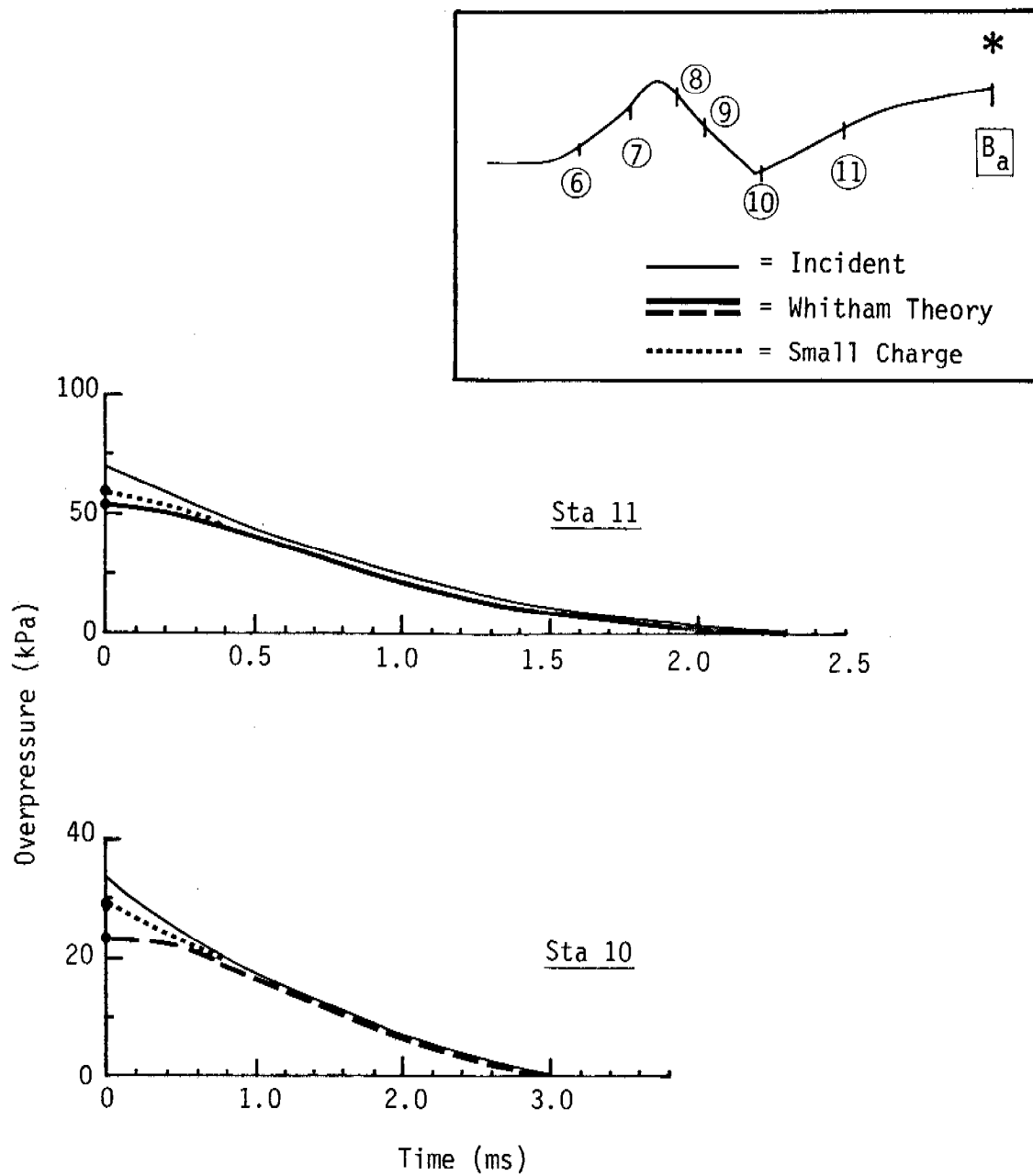
Fig. A-3a. Overpressures along Line B-1 from a Burst over GZ "B_a".
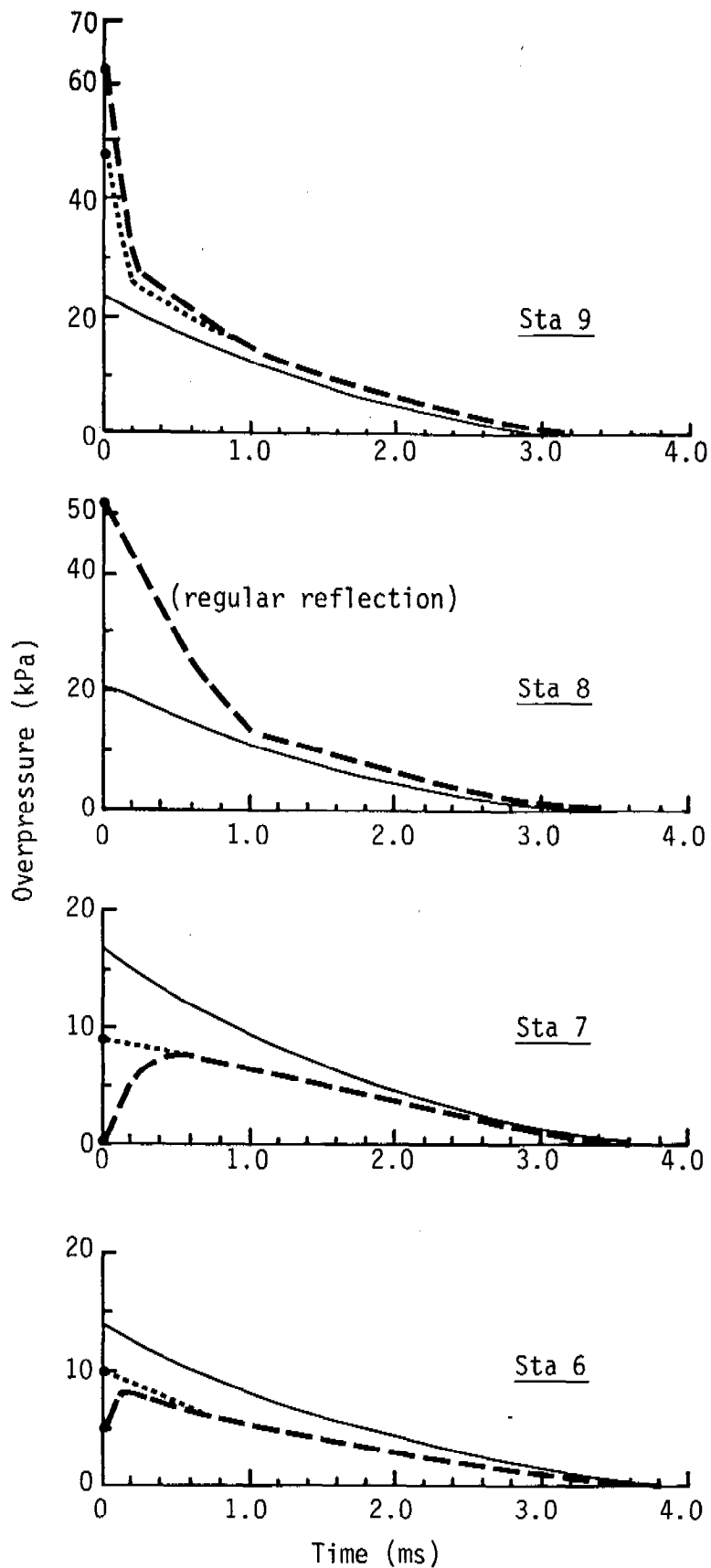
Fig. A-3b. Overpressures along Line B-1 from a Burst over GZ "B$_a$" (cont'd).
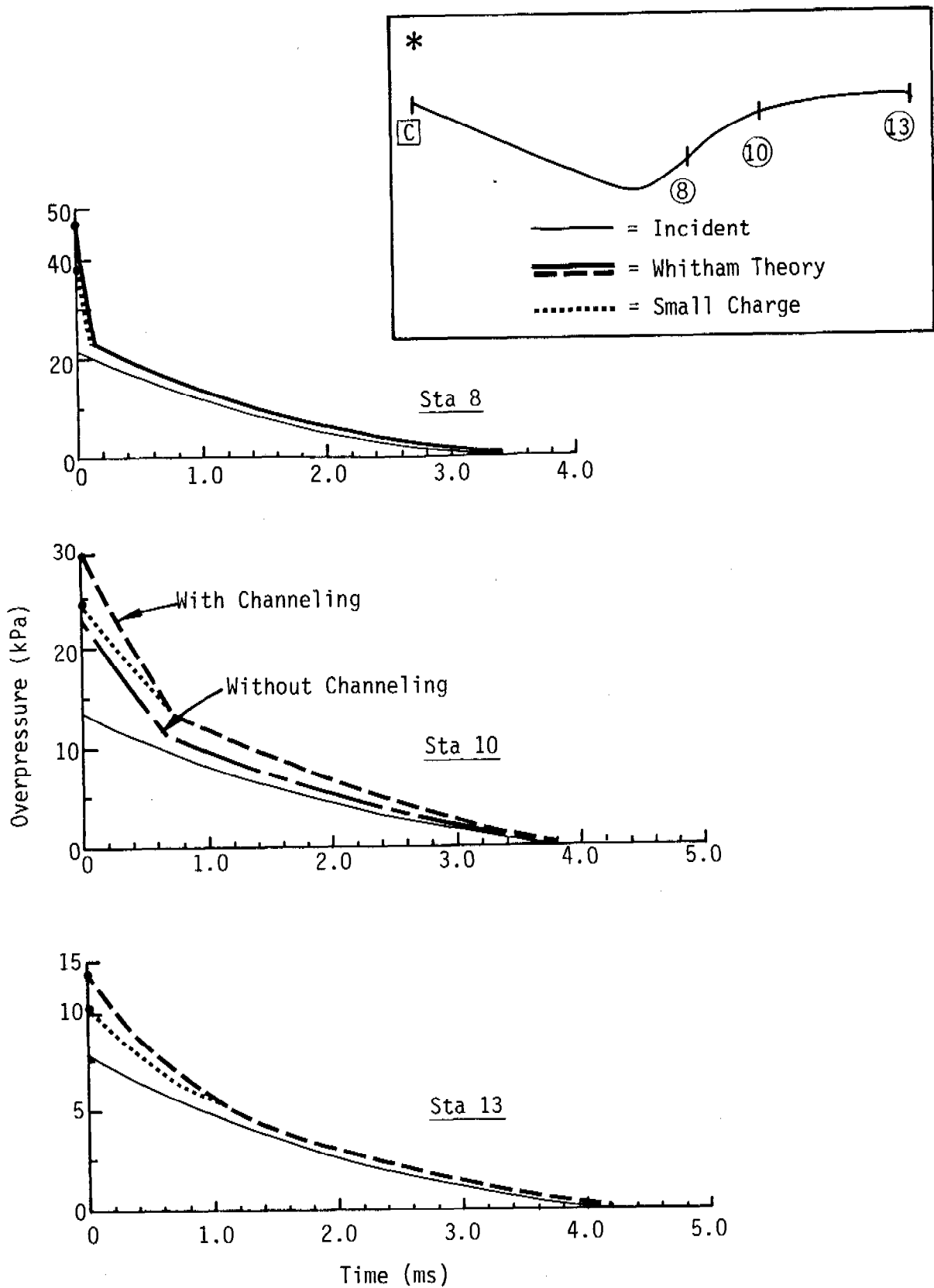
Fig. A-4. Overpressures along Line C-1 from a Burst over GZ "C".
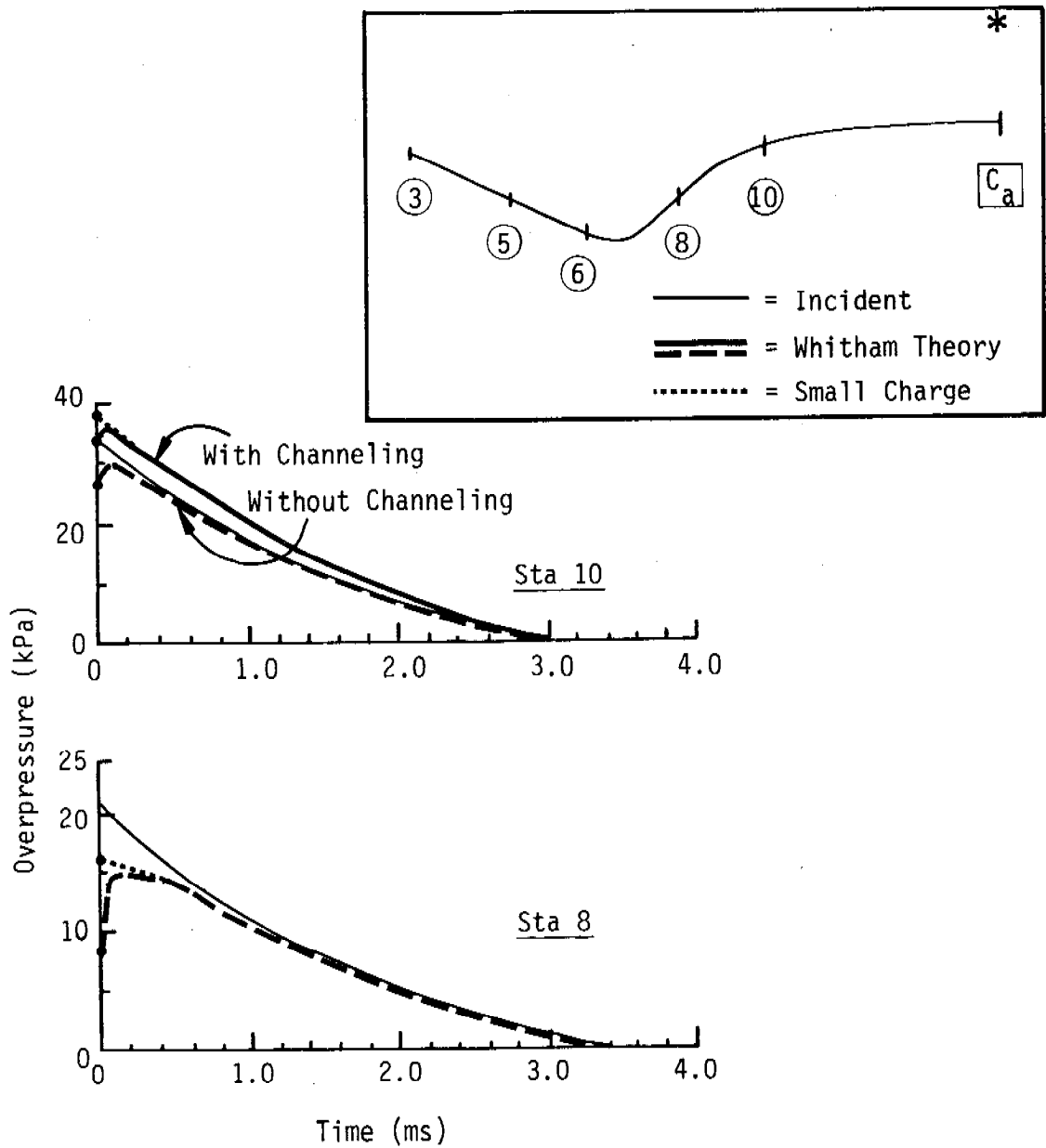
Fig. A-5a. Overpressures along Line C-1 from a Burst over GZ "C_a".
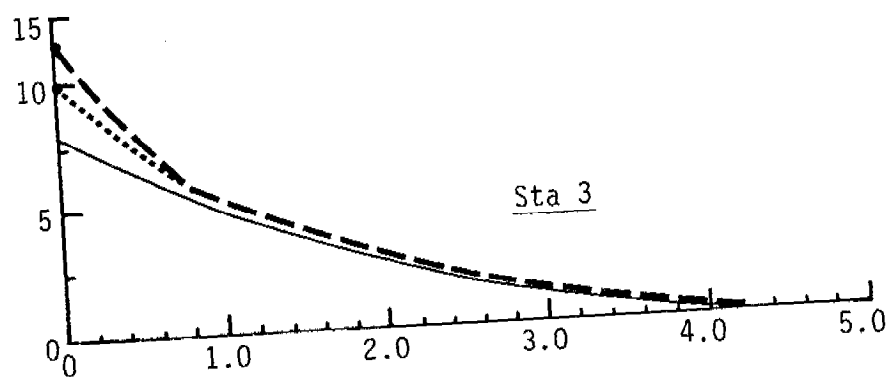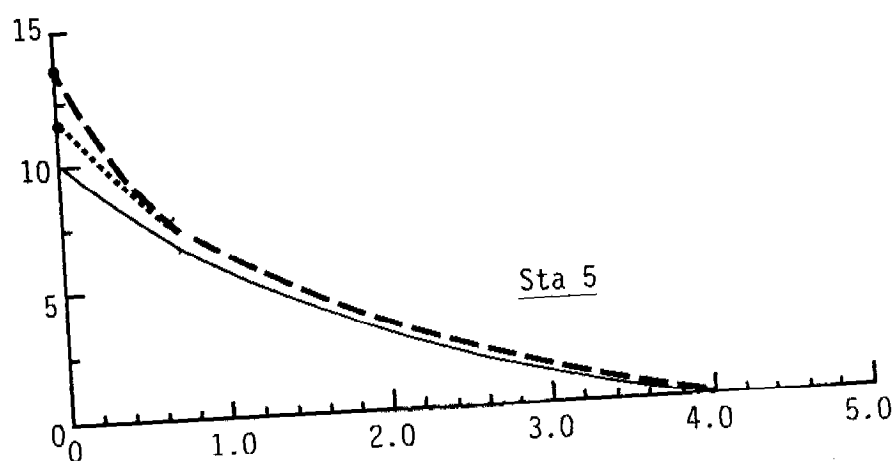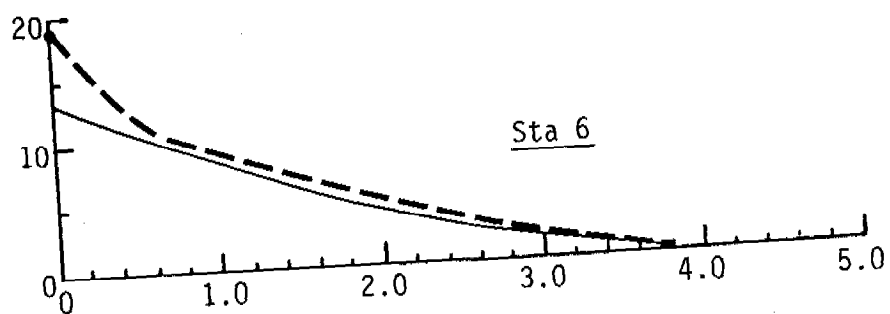
Fig. A-5b. Overpressures along Line C-1 from a Burst over GZ "C_a" (cont'd).
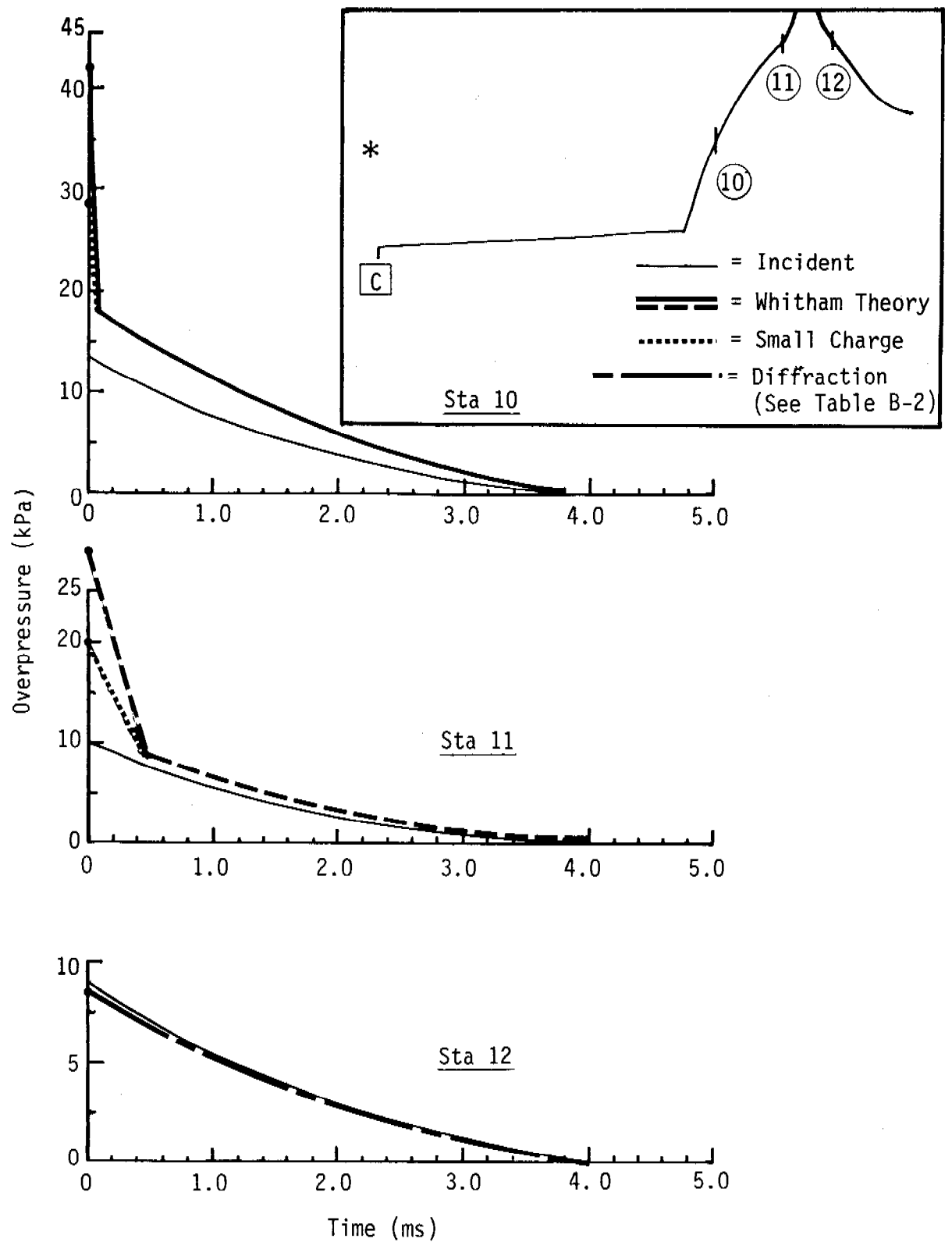
Fig. A-6. Overpressures along Line C-2 from a Burst over GZ "C".
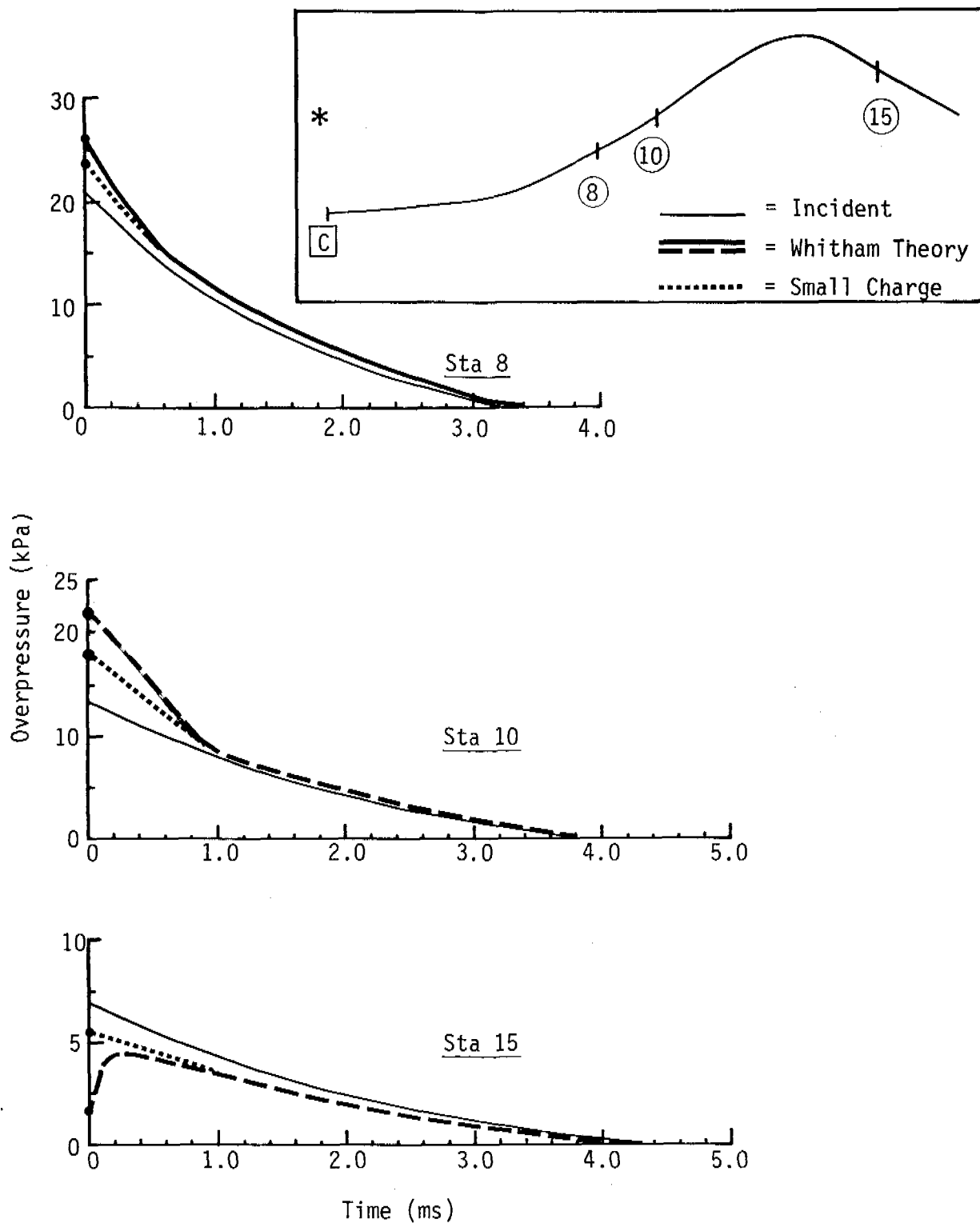
Fig. A-7. Overpressures along Line C-3 from a Burst over GZ "C".
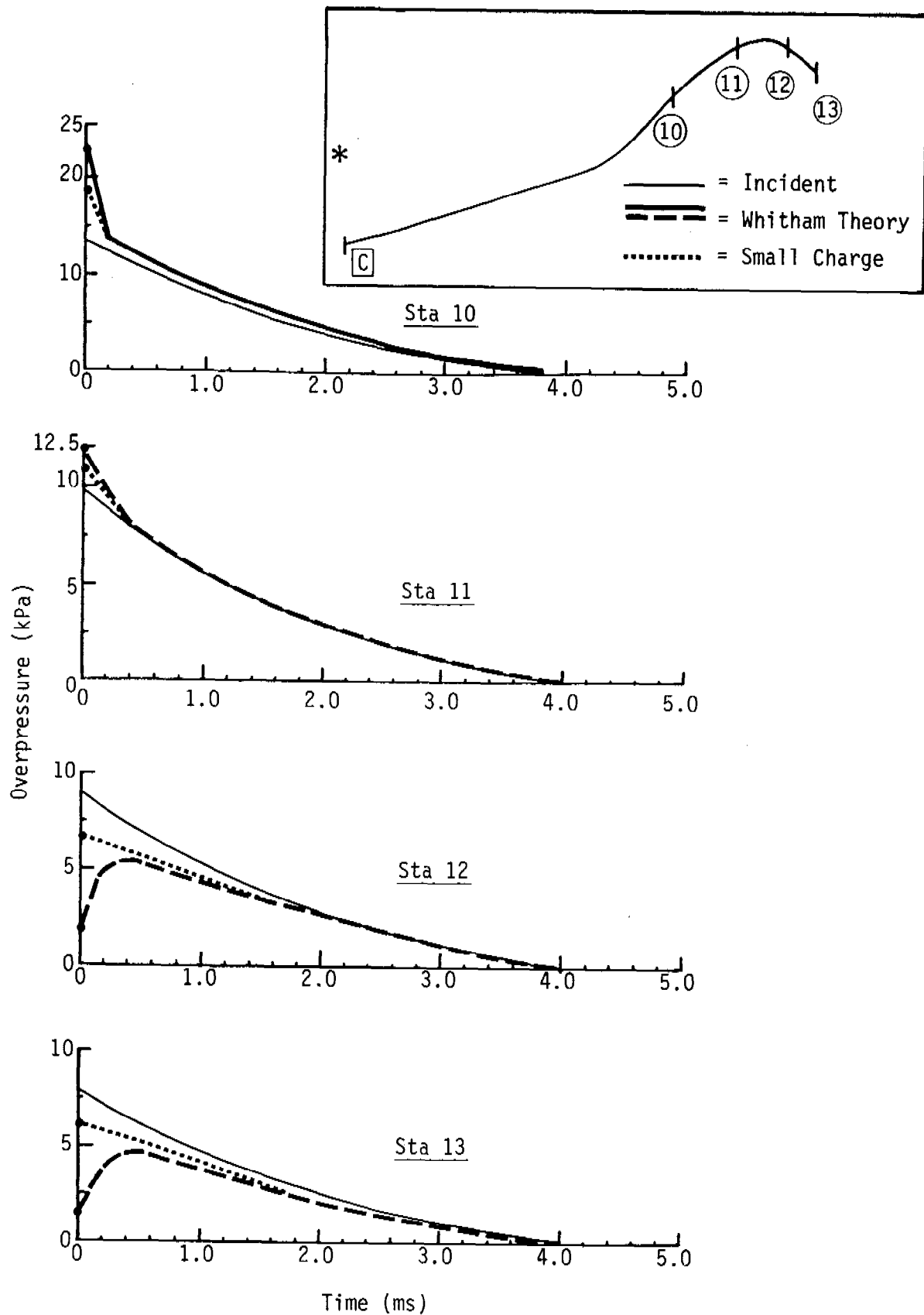
Fig. A-8. Overpressures along Line C-4 from a Blast over GZ "C".
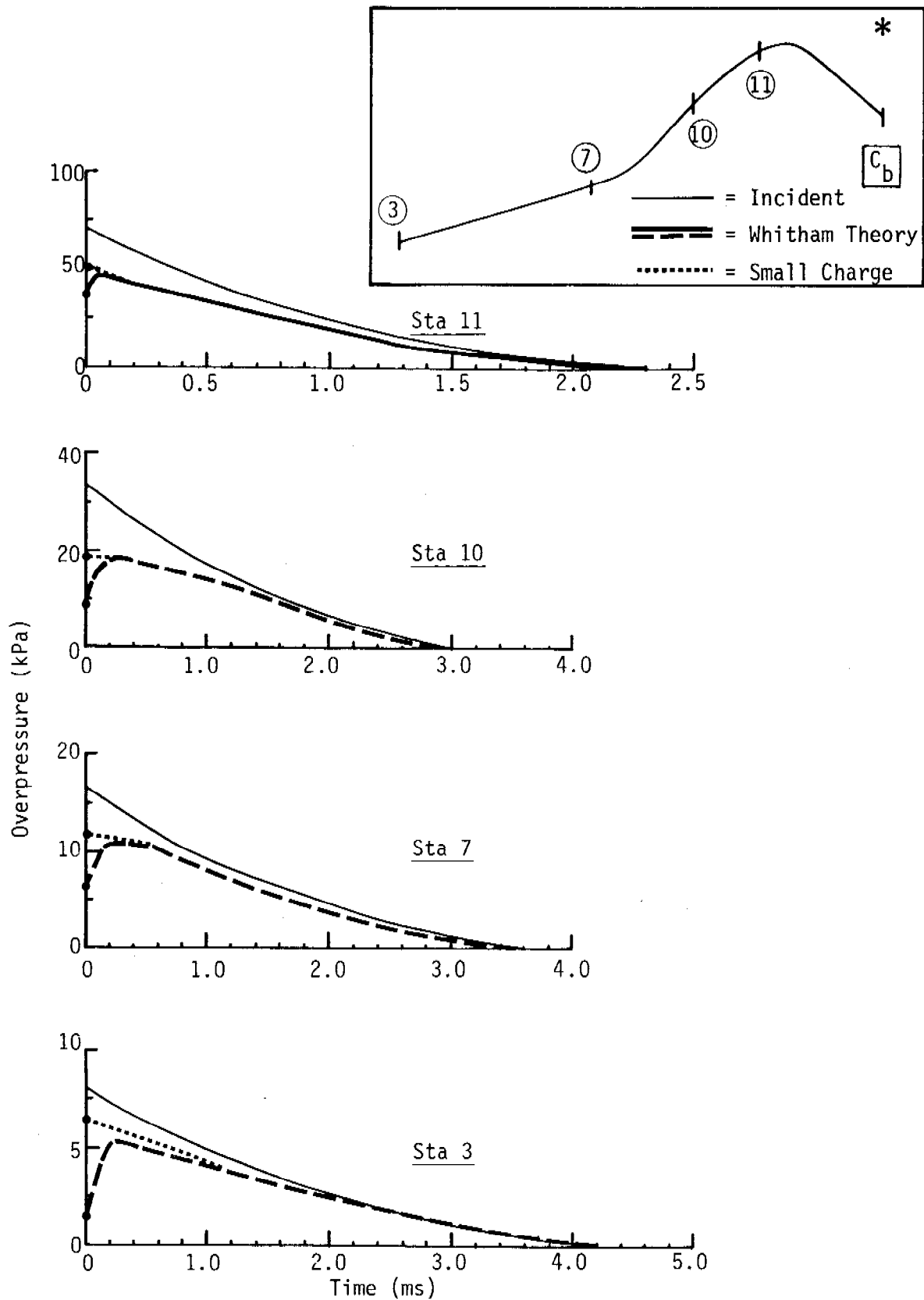
Fig. A-9. Overpressures along Line C-4 from a Burst over GZ "C_b".
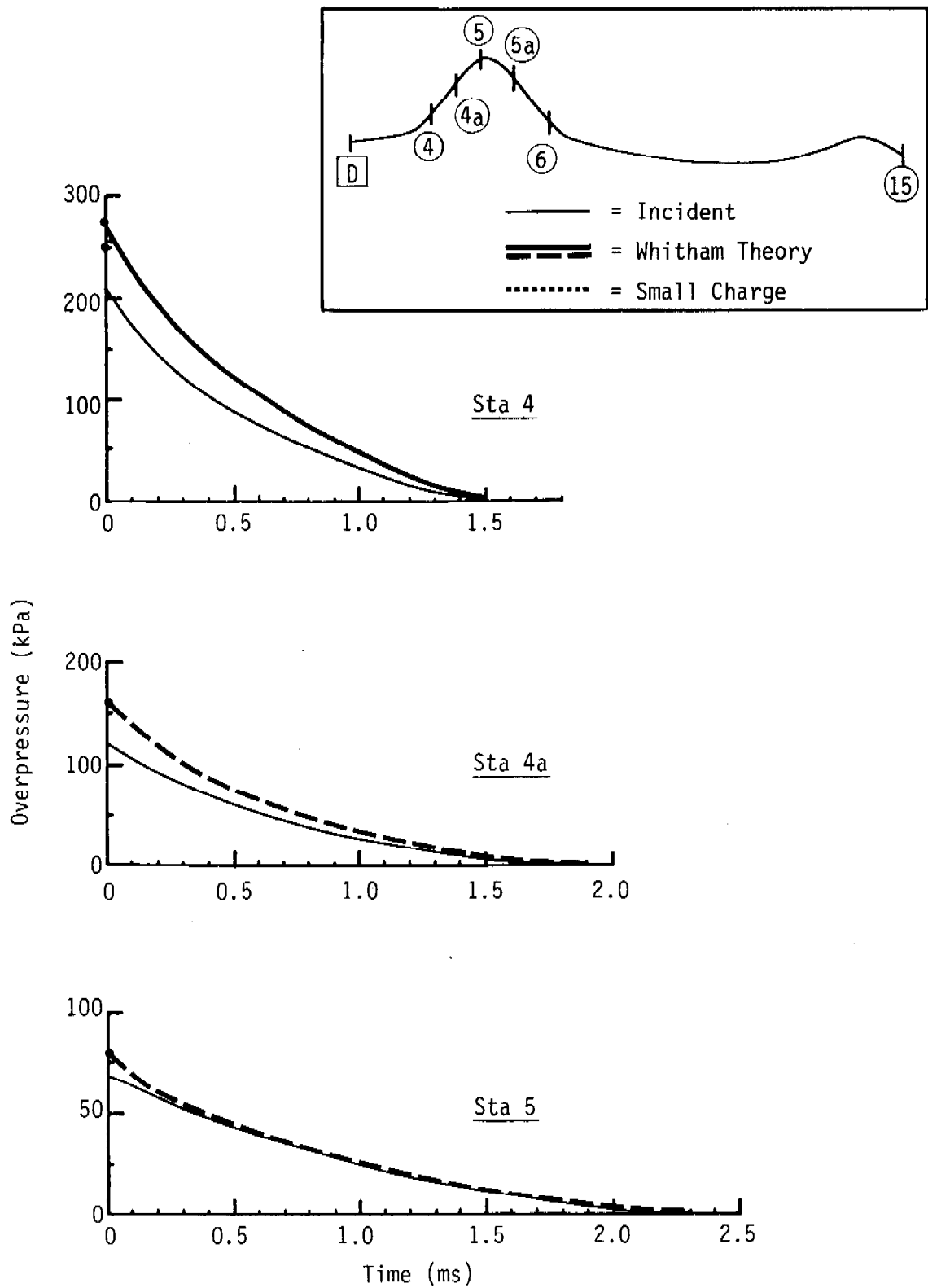
Fig. A-10a.   Overpressures along Line D-1 from a Burst over GZ "D".
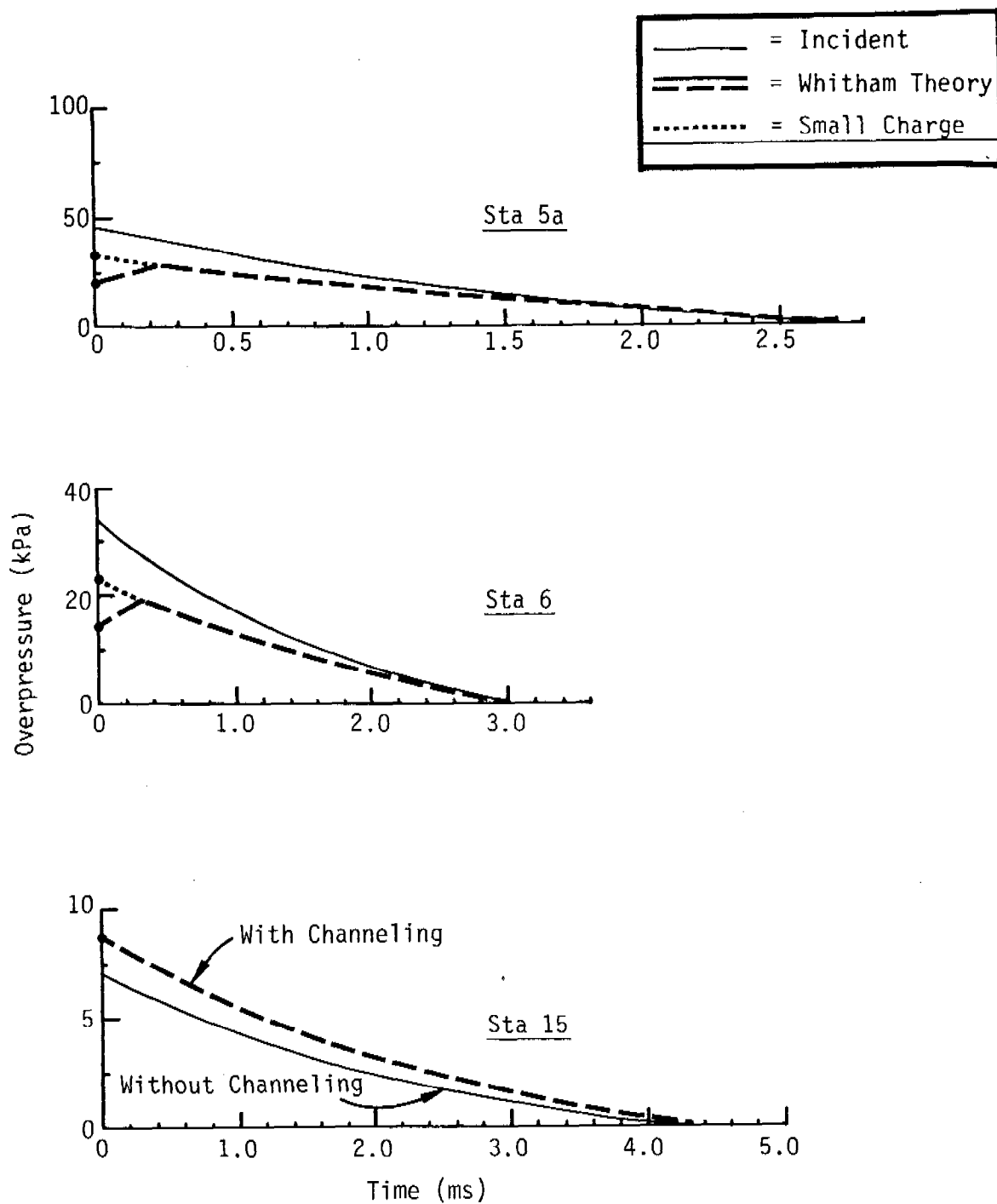
Fig. A-10b. Overpressures along Line D-1 from a Burst over GZ "D".
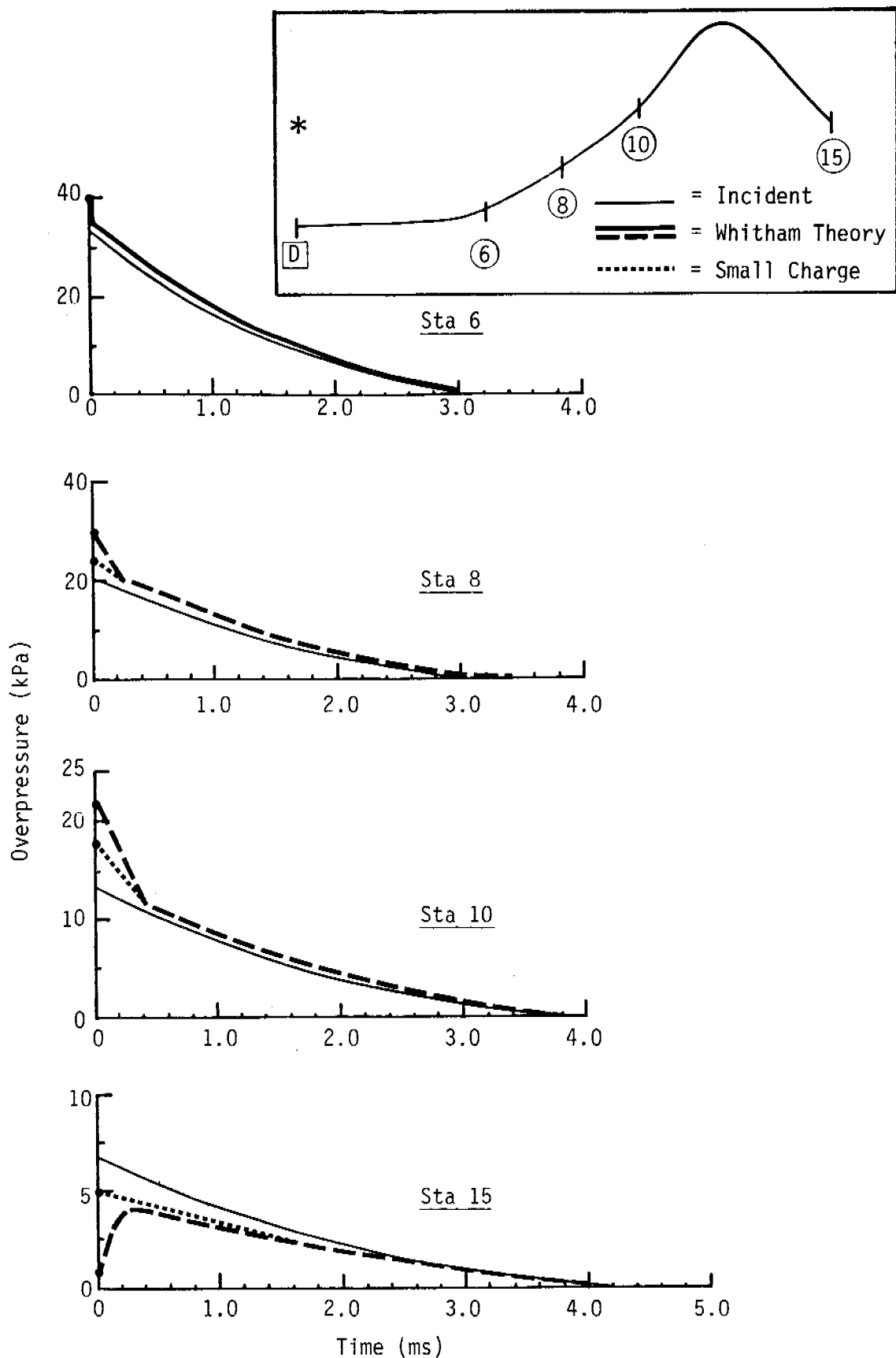
Fig. A-11. Overpressures along Line D-2 from a Burst over GZ "D".

Appendix B
TEST PROGRAM INFORMATION

Table B-1

Coordinates* of Ground Zeros
and Pressure Gauges

Gauge line →	A-1			A-2			B-1		
Coordinate Sta. No.	x	y	z	x	y	z	x	y	z
1	28.5	26.3	1.0	28.5	26.3	1.0	46.8	27.5	0.80
2							45.5	26.8	0.80
3							43.6	26.2	0.85
4	29.6	24.7	1.0				42.2	25.8	1.0
5	30.2	23.5	1.1				41.0	25.2	1.5
6	31.0	22.3	1.95	24.0	22.3	0.78	40.3	25.0	1.60
7	31.8	21.0	1.85				39.6	24.8	1.25
8	32.2	20.3	1.4	22.0	20.3	0.67	38.5	24.0	0.80
9	32.7	19.5	1.20	20.8	19.3	0.60	37.0	23.9	1.30
10	33.2	18.8	1.0				35.5	23.2	1.5
11	34.0	17.5	1.0				34.9	22.9	1.6
12							33.5	22.5	1.7
13									
14									
15	35.9	14.5	1.0						

Added Station

5a   30.6   23.1   1.6

* x,y coordinates are based on the coordinate system of Fig. 18,19, and 20. The z coordinate gives station elevation.

Table B-1 (cont.)

Coordinates* of Ground Zeros
and Pressure Gauges

Gauge line	B-2			C_1			C_2		
Coordinate	x	y	z	x	y	z	x	y	z
Sta. No.									
1	46.8	27.5	0.8	33.2	31.2	0.88	33.2	31.2	0.88
2									
3				33.8	30.3	0.77			
4							32.6	29.7	0.90
5	45.5	24.5	0.84	35.3	28.6	0.54			
6				36.3	27.2	0.35			
7									
8	44.2	21.2	0.90	37.5	25.7	0.55	31.2	24.6	0.98
9									
10				38.5	24.0	0.80	30.4	22.7	1.60
11							29.8	21.2	2.20
12							29.3	20.2	2.20
13	42.0	16.2	0.98	40.8	21.0	0.90			
14									
15	41.5	15.0	1.0	41.5	20.0	0.90	28.5	18.2	1.75

* x, y coordinates are based on the coordinate system of Fig. 18, 19, and 20. The z coordinate gives station elevation.

Table B-1 (cont.)
Coordinates of Ground Zeros
and Pressure Gauges

Gauge line →	C-3			C-4			C_a-1		
Coordinate	x	y	z	x	y	z	x	y	z
Sta. No.									
1	33.2	31.2	0.88	33.2	31.2	0.88	41.5	20.0	0.90
2	32.5	31.2	0.90				41.5	19.2	0.92
3				32.8	32.2	0.95			
4							41.5	18.0	0.94
5	30.0	31.1	0.95						
6							41.5	15.0	1.0
7				30.4	37.0	1.32			
8	26.5	30.8	1.27						
9							41.5	12.2	1.0
10	24.5	30.7	1.57	29.0	39.0	1.90	41.5	11.0	1.0
11				28.3	40.4	2.20			
12				27.8	41.5	2.20	41.5	8.0	1.0
13				27.3	42.3	2.05			
14									
15	19.2	30.4	1.78	26.7	43.3	1.80	41.5	6.0	1.0

* x, y coordinates are based on the coordinate system of Fig. 18, 19, and 20. The z coordinate gives station elevation.

Table B-1 (cont.)

Coordinates* of Ground Zeros
and Pressure Gauges

Gauge line ⟶	D-1			D-2		
Coordinate	x	y	z	x	y	z
Sta. No.						
1	39.4	37.5	0.95	39.4	37.5	0.95
2	39.4	36.9	0.97			
3						
4	39.3	35.5	1.10			
5	39.3	34.4	1.45			
6	39.2	32.8	1.10	34.9	40.0	1.03
7						
8				32.9	40.8	1.30
9						
10	39.0	28.6	0.80	31.2	41.5	1.68
11						
12						
13						
14						
15	38.5	24.0	0.80	26.6	43.9	1.62

Added Stations

	x	y	z
4a	39.3	34.9	1.3
5a	39.3	33.6	1.3

* x, y coordinates are based on the coordinate system of Fig. 18, 19, and 20. The z coordinate gives station elevation.

Table B-2

Overpressure Pulses: Critical Pressures and Times

Sta No.	p_i (kPa)	t^+ (ms)	A-1 p(o) WT (kPa)	A-1 p(o) SC (kPa)	A-1 p(t) (kPa)	A-1 t (ms)	B-1 p(o) WT (kPa)	B-1 p(o) SC (kPa)	B-1 p(t) (kPa)	B-1 t (ms)	C-1 p(o) WT (kPa)	C-1 p(o) SC (kPa)	C-1 p(t) (kPa)	C-1 t (ms)	C-2 p(o) WT (kPa)	C-2 p(o) SC (kPa)	C-2 p(t) (kPa)	C-2 t (ms)
			GZ 'A' Line A-1				GZ 'B' Line B-1				GZ 'C' Line C-1				GZ 'C' Line C-2			
1	13,800	-	p_i		-	-											-	-
2	2,070	0.20																
3	690	0.60																
4	210	1.5	p_i		-	-												
4a	120	1.9																
5	70	2.3	150	150	91	0.12	p_i		-	-	p_i		-	-	p_i		-	-
5a	46	2.7	120	110	47	0.33					p_i		-	-				
6	33	3.0	45	42	28	0.40	63	53	41	0.04	p_i		-	-				
7	24	3.2	5.2	13	10	0.96	60(R)		25	0.40	p_i		-	-				
8	21	3.4	4.2	11.5	8.1	1.2	1.0	7.0	12	0.48	48	39	23	0.12	p_i		-	-
9	17	3.6	5.2	11.5	6.0	1.4	1.1	10	9.2	0.64								
10	14	3.8	p_i		-		28	22	10	0.66	30(C)	25(C)	14(C)	0.64	42	29	18	0.08
11	10	4.0	p_i		-		23	16	6.6	0.92					30*	20*	8.0*	0.50
12	9.0	4.2					13	11	5.5	1.1	12	10	4.1	1.4		8.7*	6.5*	0.76
13	8.3	4.2					11	10	4.7	1.2								
14	7.6	4.3																
15	6.9	4.3	p_i		-	-									p_i		-	-

Key:
p_i = Peak (shock front) pressure on flat terrain
p(o) = Zero-time (shock front) pressure on topographic feature
t = Time after shock front passage
p(t)= Pressure in pulse at time t

t^+ = Positive overpressure phase duration
WT = Pressures derived from Whitham Theory
SC = Pressures derived from small charge studies
(C) = Channeling

* These stations are at the foot of a very steep, conical feature with a very narrow base (diameter ~1m). Pressures at Station 11 drop rapidly to near incident values. Pressures at Station 12 should be close to incident values throughout the pulse.

Table B-2 (cont.)

Overpressure Pulses: Critical Pressures and Times

Sta No.	p_i (kPa)	t^+ (ms)	GZ 'C' Line C-3 p(o) WT (kPa)	GZ 'C' Line C-3 p(o) SC (kPa)	GZ 'C' Line C-3 p(t) (kPa)	GZ 'C' Line C-3 t (ms)	GZ 'C' Line C-4 p(o) WT (kPa)	GZ 'C' Line C-4 p(o) SC (kPa)	GZ 'C' Line C-4 p(t) (kPa)	GZ 'C' Line C-4 t (ms)	GZ 'D' Line D-1 p(o) WT (kPa)	GZ 'D' Line D-1 p(o) SC (kPa)	GZ 'D' Line D-1 p(t) (kPa)	GZ 'D' Line D-1 t (ms)	GZ 'D' Line D-2 p(o) WT (kPa)	GZ 'D' Line D-2 p(o) SC (kPa)	GZ 'D' Line D-2 p(t) (kPa)	GZ 'D' Line D-2 t (ms)
1	13,800	-	-	p_i	-	-		p_i	-	-							-	-
2	2,070	0.20		p_i	-	-						p_i	-	-		p_i		
3	690	0.60						p_i	-	-		p_i	-	-				
4	210	1.5									280	250	263	0.03				
4a	120	1.9									170	160	140	0.09				
5	70	2.3		p_i							80	78	60	0.16				
5a	46	2.7			-	-					23	32	29	0.24				
6	33	3.0									15	23	19	0.33	42	40	35	0.04
7	24	3.2						p_i	-	-								
8	21	3.4	26	24	15	0.56									29	25	20	0.24
9	17	3.6																
10	14	3.8	22	18	8.8	0.96	23	19	14	0.20	p_i		-	-	22	18	12	0.44
11	10	4.0					12	12	8.0	0.37								
12	9.0	4.2					2.2	6.6	3.8	1.5								
13	8.3	4.2					1.9	6.1	2.9	1.7								
14	7.6	4.3																
15	6.9	4.3	2.0	5.5	3.7	0.98						8.7(C)	-	-	1.1	5.0	2.9	1.4

Key: p_i = Peak (shock front) pressure on flat terrain
p(o)= Zero-time (shock front) pressure on topographic feature
t = Time after shock front passage
p(t)= Pressure in pulse at time t

t^+ = Positive overpressure phase duration
WT = Pressures derived from Whitham Theory
SC = Pressures derived from small charge studies
(C)= Channeling

94

Table B-2 (cont.)

Overpressure Pulses: Critical Pressures and Time*

Sta No.	p_i (kPa)	t^+ (ms)	GZ 'B$_a$' Line B-1 p(o) WT (kPa)	GZ 'B$_a$' Line B-1 p(o) SC (kPa)	GZ 'B$_a$' Line B-1 p(t) (kPa)	GZ 'B$_a$' Line B-1 t (ms)	GZ C$_a$' Line C-1 p(o) WT (kPa)	GZ C$_a$' Line C-1 p(o) SC (kPa)	GZ C$_a$' Line C-1 p(t) (kPa)	GZ C$_a$' Line C-1 t (ms)	GZ 'C$_b$' Line C-4 p(o) WT (kPa)	GZ 'C$_b$' Line C-4 p(o) SC (kPa)	GZ 'C$_b$' Line C-4 p(t) (kPa)	GZ 'C$_b$' Line C-4 t (ms)
1	6.9	4.3												
2	7.6	4.3												
3	8.3	4.2					12	10	5.5	0.94	1.8	6.3	4.0	1.1
4	9.0	4.2												
5	10	4.0	p_i		-	-	14	12	7.2	0.73				
6	14	3.8	5.0	10	6.1	0.68	18	17	11	0.56				
7	17	3.6	<1	7.5	7.8	0.56					6.4	12	11	0.56
8	21	3.4		52(R)	14	0.96	8.5	16	14	0.47				
9	24	3.2	62	48	18	0.80								
10	33	3.0	23	29	19	0.78	34(C)	38(C)	34(C)	0.21	9	19	19	0.28
11	70	2.3	55	60	48	0.33					40	52	45	0.11
12	210	1.5	p_i		-	-	p_i		-	-	p_i		-	-
13	690	0.6	p_i		-	-					p_f		-	-
14	2,070	0.2												
15	13,800	-												

Key: p_i = Peak (shock front) pressure on flat terrain
p(o) = Zero-time (shock front) pressure on topographic feature
t = Time after shock front passage
p(t) = Pressure in pulse at time t

t^+ = Positive overpressure phase duration
WT = Pressures derived from Whitham Theory
SC = Pressures derived from small charge studies
(C) = Channeling

* Note that for these ground zeros, values of p_i increase, and of t^+ decrease as Station numbers increase.

LIST OF SYMBOLS

d	Distance from ground zero	Eq. 3
K	Variable in Whitham Theory	Eq. 2
L	Distance from point of slope change	Fig. 9,10
M	Mach number	Eq. 2
p	Overpressure	Eq. 3
p_i	Peak (shock front) overpressure on flat terrain	Fig. 16
$p(t)$	Overpressure at time t	Eq. 4
$p(o)$	Zero time (shock front) overpressure	Eq. 4
P_o	Ambient pressure	Eq. 3
t	Time after passage of shock front	Fig. 9,10
t^+	Positive phase overpressure duration	Fig. 16
w	Whitham function	Eq. 2
W	Charge weight or energy yield	Eq. 3
α	A dimensionless variable in Eq. 4	Eq. 4,5,6
γ	Ratio of specific heats of a gas at constant pressure and volume	Eq. 2
θ	Effective slope angle	Eq. 1a
θ'	Modified effective slope angle	Eq. 1b
θ_s	Slope angle; the angle of steepest assent	Eq. 1a
μ	Variable in Whitham Theory	Eq. 2
ϕ	Azimuth angle; the angle between the direction of shock wave propagation and a perpendicular to the slope contours	Fig. 2
τ	t/t^+	Eq. 4

DISTRIBUTION LIST

No. of Copies	Organization	No. of Copies	Organization
12	Commander Defense Documentation Center ATTN: DDC-TCA Cameron Station Alexandria, VA 22314	1	Commander US Army Materiel Development and Readiness Command ATTN: DRCDMA-ST 5001 Eisenhower Avenue Alexandria, VA 22333
4	Director of Defense Research & Engineering ATTN: DD/TWP DD/S&SS DD/T&SS AD/SW Washington, DC 20301	1	Commander US Army Aviation Research and Development Command ATTN: DRSAV-E 12th and Spruce Streets St. Louis, MO 63166
6	Director Defense Nuclear Agency ATTN: STTL (Tech Lib, 2 cys) SPAS, Mr. J. Moulton DDST, Mr. P. H. Haas SPSS, Mr. T. Kennedy SPAS, Mr. D. Kohler Washington, DC 20305	1	Director US Army Air Mobility Research and Development Laboratory Ames Research Center Moffett Field, CA 94035
3	Director Defense Advanced Research Projects Agency ATTN: Tech Lib NMRO PMO 1400 Wilson Boulevard Arlington, VA 22209	2	Commander US Army Electronics Command ATTN: DRSEL-RD DRSEL-TL, R. Freiberg Fort Monmouth, NJ 07703
		2	Commander US Army Missile Research and Development Command ATTN: DRDMI-R DRDMI-S, Ch Scientist Redstone Arsenal, AL 35809
2	Commander Field Command, DNA ATTN: FCPR Mr. Noel Gantick Kirtland AFB, NM 87115	2	Commander US Army Tank Automotive Research & Development Cmd ATTN: DRDTA-RWL DRDTA-RHT, LT P. Hasek Warren, MI 48090
2	Department of Defense Explosives Safety Board ATTN: R. Perkins Dr. Tom Zaker Room GS-270, Forrestal Bldg. Washington, DC 20314	2	Commander US Army Mobility Equipment Research & Development Cmd ATTN: Tech Docu Cen, Bldg. 315 DRSME-RZT Fort Belvoir, VA 22060

DISTRIBUTION LIST

No. of Copies	Organization	No. of Copies	Organization
1	Commander US Army Armament Materiel Readiness Command ATTN: SARRI-LR, B. Morris DRSAR-LEP-L, Tech Lib Rock Island, IL 61202	3	Commander US Army Nuclear Agency ATTN: ATCN-W, CPT M. Bowling CDINS-E Technical Library 7500 Backlick Rd, Bldg. 2073 Springfield, VA 22150
2	Commander US Army Armament Research and Development Command ATTN: P. Angelotti Mr. Demitrack Dover, NJ 07801	3	Director US Army Advanced BMD Technology Center ATTN: Mr. B. E. Kelley Mr. M. Capps Mr. Marcus Whitfield P. O. Box 1500 Huntsville, AL 35807
5	Commander US Army Harry Diamond Labs ATTN: DRXDO-TI DRXDO-TI/012 DRXDO-NP, F. Wimenitz DRXDO-NP, J. Gaul DRXDO-NP, J. Gwaltney 2800 Powder Mill Road Adelphi, MD 20783	1	Commander US Army Ballistic Missile Defense Program Office ATTN: DACS-SAE-S, J. Shea 5001 Eisenhower Avenue Alexandria, VA 22333
1	Director US Army TRADOC Systems Analysis Activity ATTN: ATAA-SL, Tech Lib White Sands Missile Range NM 88002	1	Commander US Army Ballistic Missile Defense Systems Command ATTN: SSC-DH, H. Solomonson P. O. Box 1500 Huntsville, AL 35807
1	Director US Army Materials and Mechanics Research Center ATTN: Tech Lib Watertown, MA 02172	1	HQDA (DAMA-AR, NCB Div) Washington, DC 20310
1	Commander US Army Foreign Science and Technology Center ATTN: Rsch & Data Branch 220 7th Street, NE Charlottesville, VA 22901	2	Commander US Army Engineer Waterways Experiment Station ATTN: Library W. Flateau P. O. Box 631 Vicksburg, MS 39180

No. of Copies	Organization

3	Chief of Naval Research
	Department of the Navy
	ATTN: T. Quinn, Code 464
	   Technical Library
	   J.L. Warner, Code 464
	Washington, DC 20360

2	Commander
	US Naval Ship Engineering Ctr
	ATTN: J. R. Sullivan
	   NSEC 6105-G
	   Technical Library
	Hyattsville, MD 20782

3	Commander
	US Naval Surface Weapons Ctr
	ATTN: Code 1224, Navy Nuclear
	   Programs Office
	   Code 241, J. Petes
	   Code 730, Tech Lib
	Silver Spring, MD 20910

1	Commander US Naval Weapons Evaluation Facility ATTN: Document Control Kirtland AFB, NM 87117
1	Commander US Naval Civil Engineering Lab ATTN: Dr. W. A. Shaw, Code L31 Port Hueneme, CA 93041

3	Commander
	US Naval Research Laboratory
	ATTN: M. Persechino
	   G. Cooperstein
	   Tech Lib, Code 2027
	Washington, DC 20375

1	Commander Charleston Navy Shipyard ATTN: H. Shuler Charleston, SC 29451

No. of Copies	Organization
1	HQ USAFSC (DLCAW, Tech Lib) Andrews AFB Washington, DC 20331
1	AFOSR (OAR) Bolling AFB, DC 20332
1	RADC (Docu Lib, EMTLD) Griffiss AFB, NY 13440
4	AFWL (CA, Dr. A. Guenther; DYT, Charles Needham; DYT, MAJ G. Ganong; S. Melzer) Kirtland AFB, NM 87117
1	AFCRL (F. Doherty) L. G. Hanscom Field Bedford, MA 01730
2	SAMSO (CPT T. Edwards; Library) P. O. Box 92960 Los Angeles, CA 90009
3	AFTAC (K. Rosenlof; R. McBryde; G. Leies) Patrick AFB, FL 32925
2	AFML (G. Schmitt, MAS; D. Schmidt) Wright-Patterson AFB, OH 45433
1	Department of the Interior US Geological Survey ATTN: Dr. D. Roddy 601 East Cedar Avenue Flagstaff, AZ 86001
2	Energy Research & Development Administration Dept of Military Applications ATTN: R&D Branch Library Branch, G-043 Washington, DC 20545

DISTRIBUTION LIST

No. of Copies	Organization	No. of Copies	Organization
1	Director National Aeronautics and Space Administration ATTN: Code 04.000 Langley Research Center Langley Station Hampton, VA 23365	1	AVCO-Everett Research Lab ATTN: Technical Library 2385 Revere Beach Parkway Everett, MA 02149
1	Director NASA Scientific and Technical Information Facility ATTN: SAK/DL P.O. Box 8757 Baltimore/Washington International Airport, MD 21240	1	Battelle Memorial Institute ATTN: Technical Library 505 King Avenue Columbus, OH 43201
2	Director Los Alamos Scientific Lab ATTN: Dr. J. Taylor Technical Library P.O. Box 1663 Los Alamos, NM 87544	1	Bell Telephone Laboratories ATTN: Mr. E. Witt Whippany Road Whippany, NJ 07981
		1	John A. Blume and Associates ATTN: Dr. John A. Blume Sheraton - Palace Hotel 100 Jessie Street San Francisco, CA 94105
1	National Academy of Sciences ATTN: Dr. Donald Groves 2101 Constitution Avenue, NW Washington, DC 20418	1	Calspan Corporation ATTN: Library P.O. Box 235 Buffalo, NY 14221
1	Agbabian Associates ATTN: Dr. J. Malthan 250 N. Nash Street El Segundo, CA 90245	1	Effects Technology, Inc. ATTN: E. Anderson 5383 Holister Avenue Santa Barbara, CA 93105
		1	General Electric Co., TEMPO ATTN: DASIAC 816 State Street, Drawer QQ Santa Barbara, CA 93102

1	AVCO Government Products Group
	ATTN: Dr. W. Bade
	201 Lowell Street
	Wilmington, MA 01887
		3	General Electric Co., TEMPO
			ATTN: Dr. Craig Hudson
			      Dr. Lynn Kennedy
			      Mr. Gerald L.E. Perry
			7800 Marble Ave, NE, Suite 5
			Albuquerque, NM 87110

DISTRIBUTION LIST

No. of Copies	Organization	No. of Copies	Organization
1	Hughes Aircraft Company Systems Development Laboratory ATTN: Dr. A. Puckett Centinela and Teale Streets Culver City, CA 92032	1	Maxwell Laboratories, Inc. ATTN: A. Kolb 9244 Balboa Avenue San Diego, CA 92123
1	Ion Physics Corporation ATTN: Technical Library South Bedford Street Burlington, MA 01803	1	McDonnell Douglas Astronautics Corporation ATTN: Technical Library 5301 Bolsa Avenue Huntington Beach, CA 92647
1	Kaman Sciences Corporation ATTN: Dr. D. Sachs 1500 Garden of the Gods Road Colorado Springs, CO 80907	1	Philco Ford Corporation Aeronutronic Division ATTN: L. K. Goodwin Newport Beach, CA 92663
1	Kaman Avidyne, Division of Kaman Sciences ATTN: Dr. J. Ray Ruetenik 83 2nd Avenue, NW Industrial Park Burlington, MA 01803	2	Physics International Company ATTN: Document Control F. Sauer 2700 Merced Street San Leandro, CA 94577
1	KTECH Corporation ATTN: Dr. Donald V. Keeler 911 Pennsylvania NE Albuquerque, NM 87110	1	R&D Associates ATTN: Tech Library P.O. Box 9695 Marina del Rey, CA 90291
1	Lockheed Missiles & Space Company, Inc. Division of Lockheed Aircraft Corporation ATTN: J. Nickell P.O. Box 504 Sunnyvale, CA 94088	4	Sandia Laboratories ATTN: Dr. C. Broyles Dr. D. McCloskey Mr. Jack W. Reed Dr. J. Kennedy Albuquerque, NM 87115
2	Lovelace Foundation ATTN: Dr. D. Richmond Dr. R. Fletcher 4800 Gibson Blvd., SE Albuquerque, NM 87108	2	Science Applications, Inc. ATTN: Mr. J. W. Miller Dr. John Cockayne 8400 West Park Drive McLean, VA 22101
1	Martin Marietta Aerospace Orlando Division ATTN: A. Ossin P.O. Box 5837 Orlando, FL 32805	5	Scientific Service, Inc. ATTN: Kenneth Kaplan 1536 Maple Street Redwood City, CA 94063

DISTRIBUTION LIST

No. of Copies	Organization
1	Shock Hydrodynamics, Inc. ATTN: L. Zernow 4710-16 Vineland Avenue N. Hollywood, CA 91602
1	Systems, Science & Software ATTN: H. E. Read P. O. Box 1620 La Jolla, CA 92036
2	Teledyne-Brown Engineering ATTN: Dr. M. Batel Dr. R. Patrick Research Park Huntsville, AL 35807
1	Union Carbide Corporation Oak Ridge National Laboratory ATTN: J. Auxier P. O. Box X Oak Ridge, TN 37830
1	URS Research Company ATTN: Technical Library 155 Bovet Road San Mateo, CA 94002
1	Denver Research Institute University of Denver ATTN: Mr. John Wisotski P. O. Box 10127 Denver, CO 80210
1	Director Applied Physics Laboratory The Johns Hopkins University Johns Hopkins Road Laurel, MD 20810
1	Massachusetts Institute of Technology Aerophysics Laboratory Cambridge, MA 02139

No. of Copies	Organization
1	Northwestern Michigan College ATTN: Prof. D. C. Kennard,Jr. Traverse City, MI 49684
1	Spectron Development Labs ATTN: C. W. Busch 3303 Harbor Blvd. Suite G-3 Costa Mesa, CA 92626
1	Southwest Research Insitute ATTN: Dr. W. Baker 8500 Culebra Road San Antonio, TX 78206
1	Stevens Institute of Tech Dept of Elec Engineering ATTN: Prof. R. Geldmacher Castle Point Station Hoboken, NJ 07039
1	Syracuse University Department of Physics ATTN: Prof. C. Bachman Syracuse, NY 13201
1	Temple University Department of Physics ATTN: Prof. T. Korneff Philadelphia, PA 19122
1	Research Institute of Temple University ATTN: Technical Library Philadelphia, PA 19144
1	Texas Tech University Dept of Civil Engineering ATTN: Mr. Joseph E. Minor Lubbock, TX 79409
1	University of Arkansas Department of Physics ATTN: Prof. O. Zinke Fayetteville, AR 72701

DISTRIBUTION LIST